Graphene oxide platforms decorated with porphyrinoids and gold nanoparticles for optical detection of H_2O_2

João Carlos Teixeira Louro

Thesis to obtain the Master of Science Degree in

Bioengineering and Nanosystems

Supervisor: Doctor Suzana Maria de Andrade Sousa Paiva

Examination Committee

Chairperson: Professor Luís Joaquim Pina da Fonseca

Supervisor: Doctor Suzana Maria de Andrade Sousa Paiva

Members of Committee:

Doctor Pedro Miguel Neves Ribeiro Paulo

Doctor Vanda Isabel Roldão Canelas Vaz Serra

November 2016

Graphene oxide platforms decorated with porphyrinoids and gold nanoparticles for optical detection of H_2O_2

João Carlos Teixeira Louro

Thesis to obtain the Master of Science Degree in

Bioengineering and Nanosystems

Supervisor: Doctor Suzana Maria de Andrade Sousa Paiva

Examination Committee

Chairperson: Professor Luís Joaquim Pina da Fonseca

Supervisor: Doctor Suzana Maria de Andrade Sousa Paiva

Members of Committee:

Doctor Pedro Miguel Neves Ribeiro Paulo

Doctor Vanda Isabel Roldão Canelas Vaz Serra

November 2016

Acknowledgements

First of all, I would like to gratefully thank the Molecular Photochemistry group in the person of its coordinator, Professor Sílvia Costa, the opportunity to select this topic and develop my master thesis there with all the available support. I can't let go without acknowledging also all the members of the group as well as my colleagues with whom I shared the working place with and that provided me occasional support.

Regarding technical support, I thank the Bioinorganic Chemistry group for the availability of their apparatus, namely the pH meter, the Circular Dichroism Spectrometer and the spectrophotometer. I also thank Professor Luís Filipe Santos for the RAMAN spectra as well as Professor Luís Fonseca for the Horseradish Peroxidase enzyme used in this research.

Last but not least, I acknowledge and gratefully thank my supervisor Doctor Suzana Andrade for all the orientation and constant availability along this period of more than a year that included the project and the thesis. Without her exceptional support the work wouldn't certainly come this far.

Abstract

The main goal of this dissertation was to analyze the possibility of optical detection of hydrogen peroxide using platforms of graphene oxide with gold nanoparticles and porphyrinoids. Graphene sheets and carbon nanotubes facilitate collection and transportation of electrons which can be used to grow metal nanoparticles (MNP) on their high surface area. To achieve this goal several experimental steps were followed. In the beginning a study of self-assembling of electron donor molecules like porphyrins and phthalocyanines were performed. This evaluated the conditions of assembling with a cationic polymer (polyethylenimine) and a polysaccharide (chitosan). The presence of the polymers was thought to facilitate the dispersion of the carbon material in aqueous solution as well as to improve the interaction with metal nanoparticles thus potentiating a synergistic effect of this nanohybrid material.

The characterization of the nanohybrid systems was carried out by spectroscopic (UV-Vis absorption; steady-state and time resolved fluorescence) and microscopic techniques (Fluorescence Lifetime Imaging Microscopy and Transmission Electron Microscopy). The spectroscopic studies identified phenomena of aggregation, quenching and strong interactions with the polymer under given conditions. The sensing experiments were performed using spectrophotometry with tetramethylbenzidine, with the assembled system acting as a catalyst in its reaction of oxidation in the presence of hydrogen peroxide. After an optimization of concentration and proportion of tetramethylbenzidine and hydrogen peroxide, the system revealed sensitivity to hydrogen peroxide in the range of 5 to 100 µM.

Keywords

Sensor; Graphene; Nanoparticles; Porphyrinoids; Aggregation; Spectrophotometry.

Resumo

O principal objetivo desta dissertação foi analisar a possibilidade de deteção ótica de peróxido de hidrogénio usando plataformas de óxido de grafeno com nanopartículas de ouro e porfirinóides. Folhas de grafeno e nanotubos de carbono facilitam a recolha e transporte de eletrões podendo ser usado para crescer as nanopartículas de metal (MNP) na sua área de elevada área superficial. Para alcançar este objetivo seguiram-se várias etapas experimentais. Inicialmente, realizaram-se estudos de auto-agregação de moléculas doadoras de eletrões como porfirinas e ftalocianinas. Isto avaliou as condições de agregação com um polímero catiónico (polietilenimina) e um polissacarídeo (quitosano). A presença dos polímeros foi pensada para facilitar a dispersão do material em solução aquosa, bem como para melhorar a interação com nanopartículas metálicas, potenciando assim um efeito sinérgico deste material nanohíbrido.

A caracterização dos sistemas compósito foi realizada por técnicas espectroscópicas (absorção UV-Vis; fluorescência em estado estacionário e transiente) e técnicas microscópicas (microscopia de tempos de vida de fluorescência e microscopia eletrónica de transmissão). Os estudos espectroscópicos identificaram fenómenos de agregação, extinção de fluorescência e interações fortes com os polímeros sob dadas condições. As experiências espectrofotométricas de *sensing* foram realizadas com tetrametilbenzidina, com o sistema composto agindo como um catalisador na sua reação de oxidação na presença de peróxido de hidrogénio. Depois da otimização da concentração e proporção de tetrametilbenzidina e peróxido de hidrogénio, o sistema revelou sensibilidade ao peróxido de hidrogénio na gama de 5 a 100 µM.

Palavras-chave

Sensor; Grafeno; Nanopartículas; Porfirinóides; Agregação; Espectrofotometria.

Table of Contents

List of Figures

List of Tables

List of Abbreviations and Symbols

a.u.	Arbitrary units
AlPcS4	Aluminum phthalocyanine tetrasulfonate
AuNP	Gold Nanoparticles
Chi	Chitosan
DMF	N,N-Dymethylformamide
FLIM	Fluorescence Lifetime Imaging Microscopy
GO	Graphene Oxide
HRP	Horseradish Peroxidase
MEF	Metal Enhanced Fluorescence
PEI	Polyethylenimine
SPR	Surface Plasmon Ressonance
TMB	3,3',5,5'-Tetramethylbenzidine
TCSPC	Time-correlated Single photon counting
TEM	Transmission Electron Microscopy
TSPP	*Meso-tetrakis* (p-sulfonatophenyl) porphyrin
UV-Vis	Ultraviolet-visible region
λ_{exc}	Excitation wavelength
τ	Fluorescence lifetime
E_m, E_j	Extinction coefficients of monomer and aggregate
$[J]$	Concentration of formed aggregate
k_0	Rate constant for the uncatalyzed growth
K_a	Stern-Volmer quenching constant of the accessible fraction
k_c	Rate constant for the catalytic pathway
K_{SV}	Stern-Volmer quenching constant
k_q	Quencher rate coefficient
$[M_0]$	Initial concentration of monomer
OD	Optical density
S_0	Ground state
S_n	nth excited state

Chapter 1

Introduction

1.1 Molecular Sensors

The word *sensor* derives from the adjective *sensory* which has its origin in the Latin *sensorius*, related to the verb *sentire*, i.e. *to feel.* Thus, a sensor in something that feels something and gives a response to it. In the case of molecular sensors, a molecule or conjugation of molecules will feel the environment and due to its physical and chemical properties, they will give a certain response, a signal that will be transduced in a way that we can measure that response. The measurement of different levels of response upon different conditions of the environment of the molecular system leads us to the sensor. Molecular sensors are considered to be chemical sensors that detect molecules of interest [1]. Chemical sensors can be categorized according to the phase of the target analyte (gas, solid and liquid) or the transduction mechanism (optical, electrochemical, gravimetric [2]. Optical sensors are those in which the recognition of the analyte molecule is made through a signal transduction caused by an alteration of the optical properties of the sensing molecule leading to a signal that can be followed by photochemical methods like fluorescence or absorption depending on which property is affected. One molecule of interest for sensor development that regards many research is hydrogen peroxide. There has been research on optical sensing of a huge variety of analytes: from dissolved gases (e.g. hydrogen, oxygen, ammonia), ions, organic species, humidity, hydrazine or hydrogen peroxide [3]. The last is the analyte of interest for this research.

1.2 Hydrogen Peroxide Detection

Hydrogen peroxide is a compound that is common in living beings. However, above certain levels it is known to be cytotoxic. Hydrogen peroxide is generated in vivo by the dismutation of the radical superoxide (O_2^-) by enzymatic and non-enzymatic ways as well as being directly produced by oxidase enzymes [4]. It is also present in food and beverages, from which is so also absorbed into the human body [5]. H_2O_2 is also a product of the oxidation of glucose by the enzyme glucose oxidase being remarkably used for sensing of the former, mainly by electrochemical methods [6]. Thus, the assessment of the hydrogen peroxide concentration is very important in areas diverse as food industry or biomedical sciences, both direct or indirect by the detection of compounds in which reaction is involved. For this last case, as referred before, the detection of glucose is one of the most prominent applications due to its involvement in diseases like diabetes or the importance of monitoring its consumption by living cells in terms of its metabolic activity. With all these common applications, the sensing of hydrogen peroxide became a very widespread field of research for the most sensitive, cheap and practical sensors. Recent developments in detection of hydrogen peroxide regard both electrochemical and optical sensors. Electrochemical sensors of hydrogen peroxide have been recently developed with the use of materials like metal hexacyanoferrates, heme proteins, carbon nanostructures and metals as electrocatalysts [7]. Optical detection of H_2O_2 have been carried out recently using for instance systems of gold nanoparticles, quantum dots, carbon nanostructures, lanthanide-based nanoparticles or polymer-nanoparticles with embedded enzymes [8]. The detection principles in these systems are

luminescence and fluorescence quenching, fluorescence increasing, absorbance change or colorimetric detection by the oxidation of tetramethylbenzidine.

1.3 TMB oxidation system

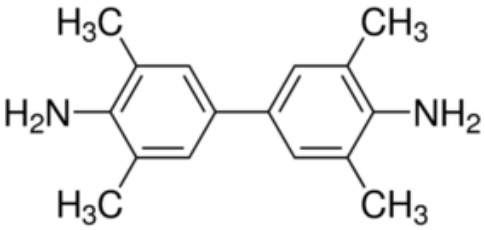

Figure 1 - Molecular structure of 3,3',5,5'-Tetramethylbenzidine

Tetramethylbenzidine is a derivative of benzidine, a molecule used in the past century as blood detector. However, since benzidine was found to be carcinogenic in opposition to TMB which was synthetized and founded to be non-carcinogenic, benzidine was replaced by TMB [9]. Benzidine and its derivatives are oxidative substrates for the Horseradish peroxidase reaction of reduction of hydrogen peroxide and the study of this reaction was well characterized by Josephy et al. [10] describing the formation from the colourless substrate of a blue coloured intermediate charger transfer complex with absorption peaks at 370 and 652 nm that would evolve to a final yellow coloured diimine product.

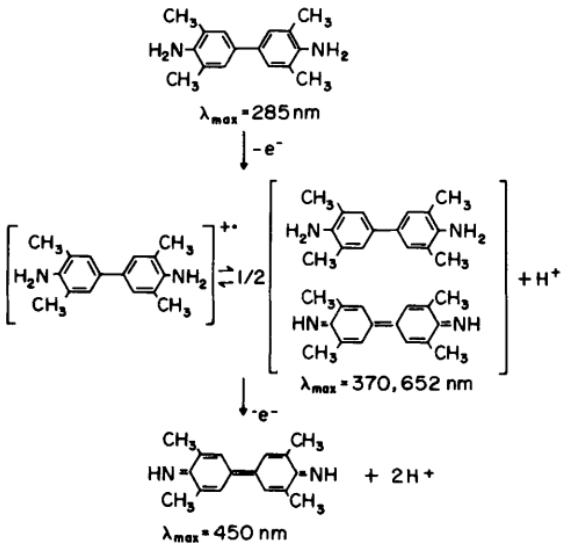

Figure 2 - Oxidation reaction of TMB elucidating the intermediate components and absorptions peaks [10]

The blue intermediate in certain conditions can be stable and due to its characteristic blue colour is has been studied for the colorimetric and optical detections and sensing of various compounds. Recently, several studies with the use of composites of carbon materials, metal nanoparticles and porphyrinoids as catalysts for the reaction in replacement of the enzyme HRP have been done [11]–[13] leading to a promising value of this reaction that was then chosen to be included in this work.

The development of the sensor based on the referred reaction was then viewed as possible to be carried out in a composite system with a carbon nanostructure, metal nanoparticles and porphyrinoids.

1.4 Carbon Nanostructures

When talking about carbon and its allotropes those that are referred in the first place are ones that are found in nature, which are diamond and graphite, both being 3-D structures that comprise sp^3 hybridization in the case of diamond and sp^2 in the case of graphite with the presence of the sp^2 layers stacked to give rise to a 3-D structure. During the last century, other allotropic forms were synthetized in laboratory and studied, with the ones that regarded more laboratorial interest being fullerenes, nanotubes and graphene [14]. They broadly consist in a monolayer of sp2 hybridized carbon, with fullerenes being the enrolment of that layer in a spherical structure resembling a football. In the case of carbon nanotubes, the enrolment is cylindrical with the possibility of using half of a fullerene to close one of the edges of the tube. These tubes can be single-walled and multi-walled featuring different electronic and mechanical properties depending on diameter and number of concentric tubes for the last.

Before the experimental studies in which a single layer of graphene was obtained there have been research in graphene related materials like graphite oxide and reduced graphene oxide for more than a century and half [15]. During the 20th century various researchers achieved graphite monolayers with Bohem and co-workers [16] proposing in the term “graphene” to designate single layers of graphite-like carbon. However, it was in 2004 that Geim and Novoselov produced graphene by mechanical exfoliation [17]. Since that, the interest in graphene and its properties highly grew due to their unique characteristics that can lead to applications on a wide range of areas of technology and research such as biomedical sciences [18], materials science [19] and electronics [20]. Some of the most important properties of graphene include high transparency, high mechanical strength and high conduction [21].

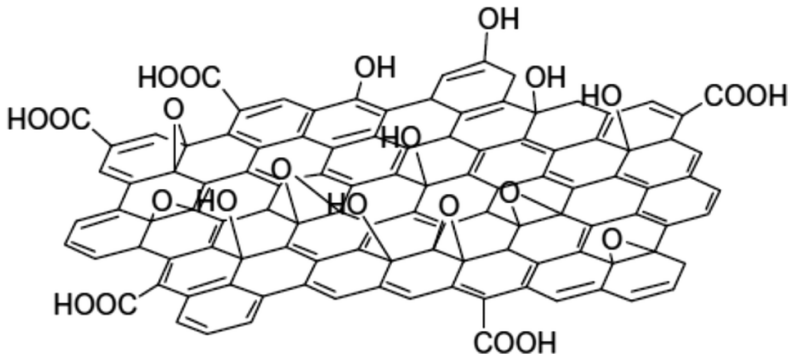

Figure 3 – Structure of graphene oxide showing its functional groups

The synthesis of graphene can be achieved by several methods, like chemical vapor deposition (CVD), reduction of graphene oxide (GO) or liquid exfoliation of graphite [22]. GO as a derivative of graphene that contains various oxygen groups (Figure 3) is also interesting to study by the fact of maintaining most of the properties of graphene [21] with the addition of being more water soluble which is relevant for the biocompatibility of its applications in biological sensing.

The option for graphene oxide and its possible biological sensing application was made considering the high surface area of the material and the easiness to decorate its surface with more components to achieve a synergetic effect. One of those materials are metal nanoparticles.

1.5 Metal Nanoparticles

The deposition of metal nanoparticles in graphene oxide and graphene was studied mainly for the cases of metals like Ag, Au, Pd and Pt. Methods for deposition of metal nanoparticles in layers of graphene and graphene oxide include sonication, microwave irradiation or photocatalytic deposition [23]. The main feature of the interaction between metal nanoparticles and the graphene layer is the fact that both have excellent electrons transfer properties. The synergy between the properties of graphene or graphene oxide and metal nanoparticles is what leads to the achievement of a better sensing platform than the use of just one of them. It is important to note that the optical properties of metal nanoparticles are dependent upon their size, interaction with other particles and medium condition [24]. This is very important to build a system which presents sensitivity to certain external factors to act as a sensor.

For the case of this work the main type of nanoparticles that is going to be used are gold nanoparticles. The main feature of gold nanoparticles that can be used to follow the integration in sensing platforms is its characteristic band in the absorption spectra that results from its Surface Plasmon Resonance (SPR), a phenomenon that is very sensitive to changes in the surroundings of the surface [25] and that is more detailed below. Since this changes come from the presence of a molecule or an environmental condition that we want to detect this is very promising for the application. It was also verified that the formation of composites of graphene layers with metal nanoparticles leads to a clearer signal than the case of solely the nanoparticles [26].

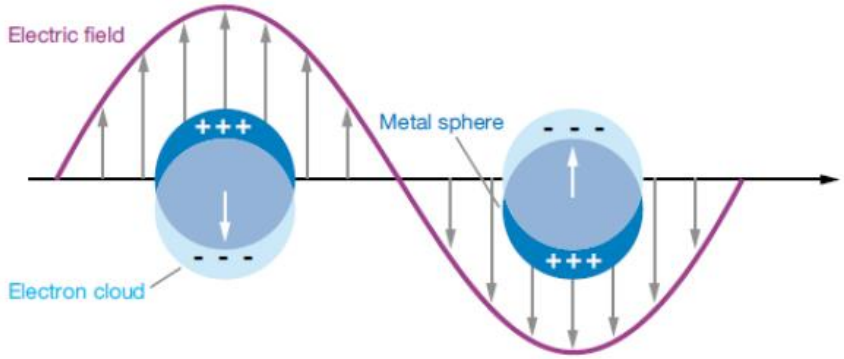

Figure 4 - Schematic of plasmon oscillation on a spherical nanoparticle showing the displacement of the conduction electron charge cloud relative to the nuclei [27]

When the wavelength of light is much larger than the nanoparticle size it can set up standing resonance conditions, as represented in Figure 4. Light in resonance with the surface plasmon oscillation causes the free-electrons in the metal to oscillate. As the wave front of the light passes, the electron density in the particle is polarized to one surface and oscillates in resonance with the light's frequency causing a standing oscillation. The resonance condition is determined from absorption and scattering spectroscopy and is found to depend on the shape, size, and dielectric

constants of both the metal and the surrounding material. This is referred to as the **surface plasmon resonance (SPR)**, since it is located at the surface. The oscillation frequency is usually in the visible region for gold and silver nanoparticles. Nanoparticles with geometries other than the spherical also offer the possibility of tuning the optical properties over a broad spectral range. Silver and gold nanoparticles having the shape of rods, triangles, cubes and stars have been produced [28] using distinct strategies for synthetic control such as seeding processes [29].

Nanoparticles have been studied and used in different applications, from biotechnology and targeted drug delivery to magnetic separation and photochemistry. One of the applications that has also gain interest in the last years is the use of metallic nanoparticles as a fluorescence enhancers (metal enhance fluorescence, MEF) [30]. Metal NPs can act as nanoantennas to collect and localize energy input and they can establish interactions with fluorophores placed in their close proximity, ultimately leading to an increase in fluorescence quantum yield and a simultaneous reduction of the emission lifetime of the fluorophore. The metal effect depends not only on the chemical nature of the metal but also on the particle shape and size, and on the particle-fluorophore inter-distance [31], [32]. Critical uses in medicine, for example to locally and selectively heat and kill cancerous tumours, are already being developed [33].

1.6 Photochemistry

Since the goal of the work is optical sensing the electronic transitions in the system of study will play a major role in its behavior. The atomic electronic transitions are generally described by the Pierre-Jablonski diagram (Figure 5) which represents the ground singlet state S_0 and the first and second excited states as singlet and triplet states. Singlet and triplet refer to the spin multiplicity of the electronic state. Singlet designates the state when the spins are paired and thus the total spin is zero. In the case of triplet, the electrons are unpaired so that the addition of the spin angular momentum of the electrons is 1, which implies the existence of three spatial orientations, i.e. the multiplicity of the state is 3 [34].

The transition between singlet and triplet state, denominated *intersystem crossing*, is spin-forbidden since the electrons need to change their spin but can occur in a very weak way due to spin–orbit coupling. The transition from an excited singlet state to an excited triplet state can be followed by the occurrence of radiative emission called *phosphorescence* which features a much longer lifetime than the emission from the singlet state, i.e. *fluorescence*. In the diagram the sub-levels in each electronic state represent vibrational states. An electron upon excitation can arrive at the ground vibrational state of an excited electronic level or at an upper level, from where it will go down to the ground state due to the process of vibrational relaxation.

So, after the incidence of light there is a process of absorption that leads to an excited state. From there can occur a radiative process like fluorescence or non-radiative processes like intersystem crossing and internal conversion (transition from one electronic state to another).

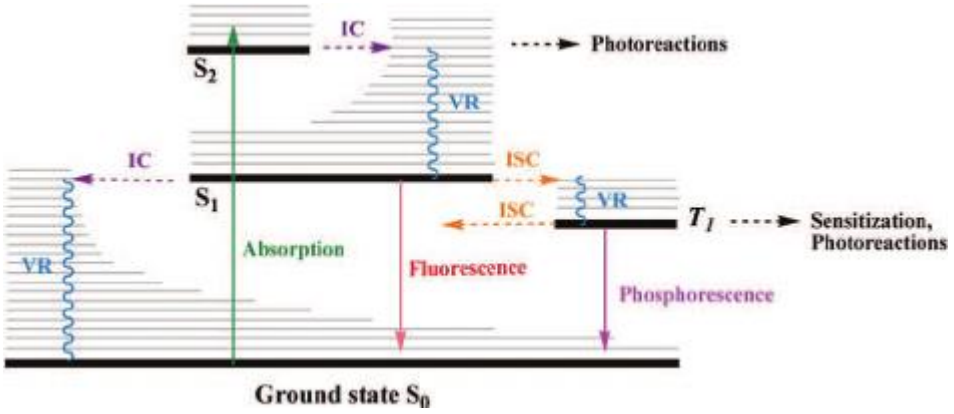

Figure 5 – Pierre-Jablonski Diagram [35]

The exploration of this photochemical features in the sensing targeted study would be achieved through the use of two different types of photoactive molecules: porphyrins and phthalocyanines.

1.7 Porphyrins

Porphyrins are macrocycles (i.e. cyclic molecules) constituted by four pyrrole linked by four methinic bridges (Figure 6) , which are present in living organism in their reduced, oxidized and metalated forms playing an important role in several vital functions like oxygen transport and storage, photosynthesis, electron transport, drug detoxification or hydrogen peroxide biochemistry [36]. This importance comes from their special properties of absorption, emission, charge transfer and complex formation due to their characteristic aromatic ring. Relating with the case of study, the HRP enzyme, that was referred as the natural catalyst of the reaction that would lead to the detection of hydrogen peroxide, have as co-factor a heme group, which structure is a porphyrin.

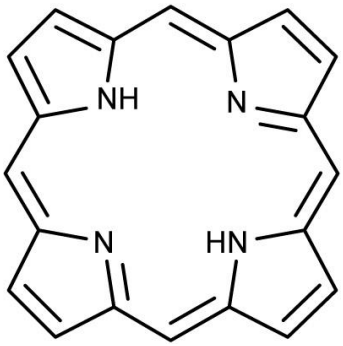

Figure 6 – General Structure of a free base porphyrin

Regarding their electronic absorption properties, it is shown in Figure 7 a UV-Vis spectra of a general free base porphyrin in which we can observe the two types of bands that are characteristic of this molecule: a very intense band in the 380-500 nm range – Soret or B-band –, and a series of four less intense bands in the 500-750 nm range – Q bands. The first corresponds to electronic transition $S_0 \rightarrow S_2$ while the second corresponds to $S_0 \rightarrow S_1$ transitions. The relative intensity of the 4 Q bands will depend on the positions of the substituents in the aromatic ring. The wavelength shift of the bands and the absorbance - that can be followed by UV-Vis absorption - fluorescence or another spectroscopic property dependent on parameters like pH, temperature, solvent or

presence of another allows to obtain information about equilibrium, kinetics or aggregation of porphyrins [37].

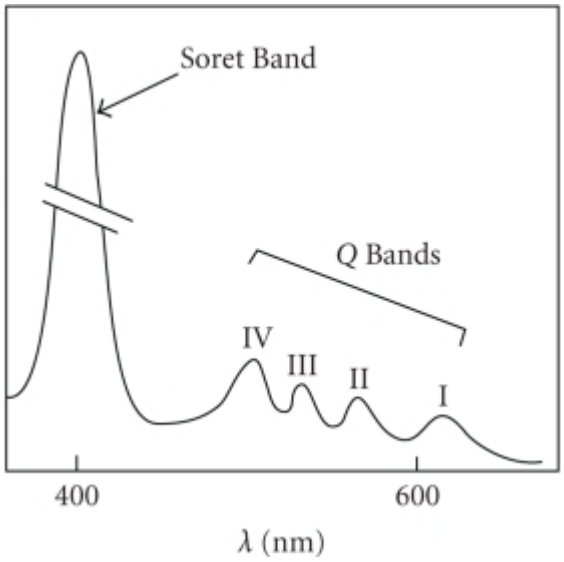

Figure 7 - General UV-Vis spectrum of a porphyrin [38]

As seen in the porphyrin macrocycle structure there are four nitrogen atoms, two of them linked to a hydrogen. The others can be protonated at low pH as well as the former can be deprotonated at high pH, depending on the pH of the solution we can have an equilibrium of two species. The presence of a different species leads to changes in the spectra, with a usual red-shift and modification on the Q bands [37], which will become two instead of four due to an increase in the molecule symmetry caused by the protonation at low pH, the same situation with metalated porphyrins [39].

Another relevant feature of porphyrins is the formation of dimers or higher order aggregates, which is dependent on a combination of factors like pH, solvent composition and ionic strength, being a very important process in the study of these molecules [40]. The aggregates will have different spectroscopic behavior that can be followed by UV-Vis absorption and fluorescence. This process caused by the strong π-π interactions between surrounding molecules may lead to two types of highly ordered molecular arrangements: H-type, with a vertical stacking of the molecules and J-type, with a side-by-side aggregation (see figure 8). According to theory, the last one reveals a red-shift of the Soret band relatively to that of the monomeric species, whereas the first one presents a blue-shift of the Soret band [41]. J-aggregates present a nearly resonant fluorescence (very small Stokes shift) narrow band, whereas H-aggregates exhibit low or no fluorescence.[42]

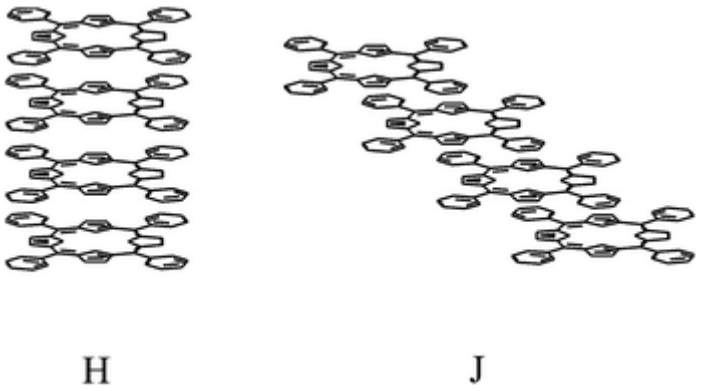

Figure 8 - Two types of aggregation for porphyrins [43]

The porphyrin under stud in this work is *meso-tetrakis*(p-sulfonatophenyl) porphyrin, better known by its abbreviation TSPP, which presents the structure depicted in Figure 9.

TSPP is an anionic porphyrin due to the presence of sulfonatophenyl groups in the *meso* positions of the main aromatic ring. This porphyrin forms both J and H aggregates, with the special feature of forming pure J aggregates. The formation of such well aligned aggregates is less common than that of H aggregates and it is promoted in acidic environments. In this case the zwitterionic nature of the molecule due to the presence of negative charged groups on the outside and the protonation of the pyrrole groups on the inside of the molecule [39] favours the electrostatic interactions between the peripheral group of one molecule and the core of the neighbour molecule, as depicted in Figure 8. The acid-base equilibrium is shown in figure 9.

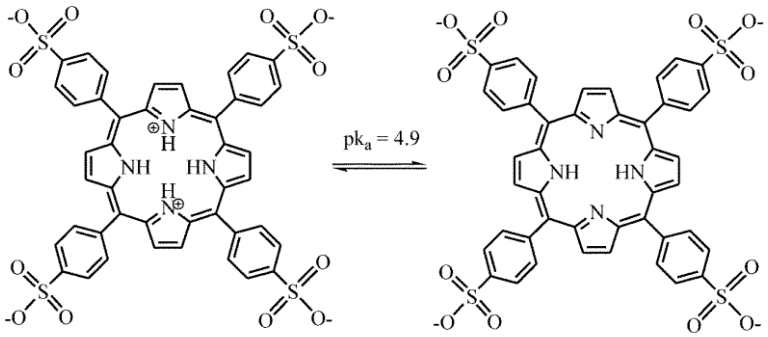

Figure 9 - Molecular structure of TSPP and its acid-base equilibrium in aqueous solution [44]

For the purpose and considering that the main goal is the interaction of this molecule with graphene and graphene oxide decorated with nanoparticles the behavior of TSPP in the presence of carbon nanostructures and another possible supporting molecule is crucial to the work. Characterization of this porphyrin in a system with carbon nanotubes and a supporting cationic polyelectrolyte [45] revealed the formation of stable J-type and H-type aggregates under certain conditions, which depended among other on the nature of the polyelectrolyte, its concentration and the solution pH.

1.8 Phthalocyanines

Phthalocyanines have an analogous structure to porphyrins compounds (Figure 6) since it is also a tetrapyrrole macrocycle with the pyrrole subunits being linked by nitrogen atoms instead of methine bridges and having a benzene cycle coupled to the pyrroles increasing the conjugation of the macrocycle [46]. Unlike porphyrins they do not exist in nature. They form complexes with metals (e.g. aluminium, zinc, copper) that are used for dying and organic electronics besides being available in free form and with a variety of substituents in its *meso* and beta positions. These complexes, unlike the previous case of the porphyrins, the Q band presents higher absorption intensity than the Soret band (Figure 11). Therefore, they present higher absorbance in the red part of the visible spectra than porphyrins.

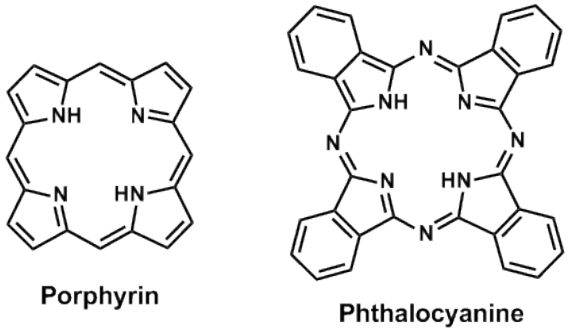

Figure 10 –Molecular structure of a porphyrin and a phthalocyanine

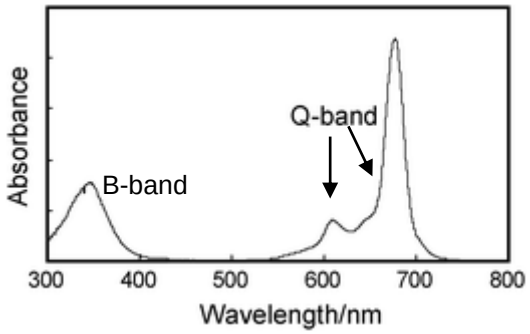

Figure 11 –Example of phthalocyanine spectra revealing the Soret/B band and the two Q bands [47]

The phthalocyanine used in this work is Aluminium phthalocyanine tetrasulfonate which is complexed with the metal aluminium and presents as TSPP four sulfonate groups that give the molecule a tetra negative charge which will increase its solubility and will be determinant for the interaction with the charged polymers used.

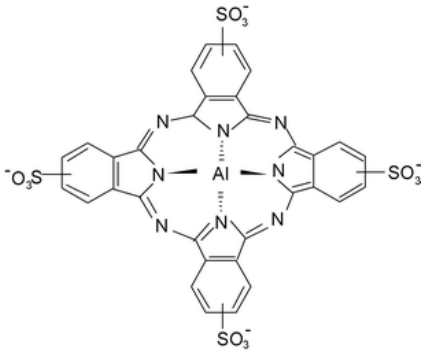

Figure 12 – Molecular structure of Aluminium phthalocyanine tetrasulfonate (AlPcS4)

Regarding the described importance of detection of hydrogen peroxide and in conjugation with the promising applications of optical sensors with graphene oxide – metal nanoparticles the study regarding the achievement of that kind of sensor was performed. The porphyrinoids were included as electron transfer tools and a signal transduction with the TMB oxidation was defined.

Chapter 2

Experimental Section

2.1 Materials

Bidistilled water; Citric Acid (Sigma-Aldrich); Sodium Phosphate dibasic heptahydrate (Sigma-Aldrich); Sodium Acetate anhydrous(M&B Laboratory Chemicals); Potassium Permanganate (Analak); Sodium Tetrachloroaurate(II) (Aldrich); N,N-Dymethylformamide (Sigma-Aldrich); Acetic Acid glacial pure (Epenhuysen Chemie); Hydrochloric Acid 37% (Sigma-Aldrich); 3,3',5,5'-Tetramethylbenzidine (Sigma-Aldrich); Hydrogen Peroxide 30% (Sigma-Aldrich); Chitosan, 110 000-150 000 g/mol (Sigma-Aldrich); Polyethylenimine, 25 000 g/mol (Sigma-Aldrich), *meso-tetrakis* (p-sulfonatophenyl) porphyrin – TSPP (Fluka, ≥ 98% purity); Horseradish Peroxidase (BBI Enzymes; Graphite powder, synthetic, conducting grade, -325 mesh, 99,9995% (Alfa Aesar), Aluminum phthalocyanine tetrasulfonate (Porphyrin Products Inc.)

2.2 Synthesis

Graphene Oxide Synthesis

Graphene oxide was synthetized according to the modified Hummers method[48]. For this, 2 g of graphite powder were suspended in 46 ml of concentrated sulfuric acid and left for 12 h under agitation. The suspension was then cooled until 0 ºC and 6 mg of $KMnO_4$ were gradually added, after which it was subjected to sonication for 3 hours. After this last process 92 ml of distilled water were slowly added and it was left boiling for 30 minutes. In order to finish the reaction 10 ml of H_2O_2 (30%) were added. The purification process consisted in removing the supernatant and adding 50 ml of HCl 5% and then water with the division of the product in several Falcon tubes -with maximum volume of 10 ml in each one – that were centrifuged 20 times (until the final pH was that of distilled water) with supernatant being removed after each centrifugation and distilled water added to fill the 10 ml volume, Only the last centrifugation was performed with the addition of ethanol. Afterwards, the obtained product was displaced in Petri dishes and dried in order to obtain the desired graphene oxide sheets.

Gold Nanoparticles Synthesis

Gold nanoparticles were obtained through the Turkevich method[49]. A solution of 46 ml of distilled water with 7 mg of gold salt was boiled and a solution of 13 mg of sodium citrate in 4 ml of water, at the same temperature, was added under agitation. The solution after changing the colour from transparent to red was brought to room temperature and stored in the dark.

2.3 Characterization Techniques

Absorption Spectroscopy

The absorption spectroscopy measurements were performed in a PerkinElmer Lambda 35 UV/Vis spectrophotometer with a fluorescence quartz cell - normal and reduced volume- with an optical path length of 1 cm, at room temperature. The spectroscopy of absorption in UV/Vis is one of the most common and basic spectroscopic techniques and widely used for its proportional relation with concentration it is based on the Lambert-Beer Law which is given by $A = \log I/I_0 = \varepsilon l c$, with A being the absorption which is calculated by the apparatus form the ratio between transmitted and the incident light, I and I_0, ε is the molecular extinction coefficient, l the length of the cell which the light crosses and c is the concentration of the species. The absorption signal besides the concentration is also dependent on molecular aggregation or exciton couplings which are relevant for the purposes of the analysis of this work as of the following of the aggregation and complexation of the porphyrinoids. The absorption spectrum itself consists on the plotting of the measured absorption values for the swept interval of wavelengths of incident light.

Raman Spectroscopy

Raman spectra were recorded between 700 and 1900 cm^{-1}, using a LabRAM HR Evolution (Jobin Yvon), working with a 532 nm laser line and a 600 gr/mm grating. Raman spectroscopy is a technique based on inelastic scattering of monochromatic light, usually from a laser source. Photons of the laser light are absorbed by the sample and then reemitted. Frequency of the reemitted photons is shifted up or down in comparison with original monochromatic frequency, which is called the Raman effect. This shift provides information about vibrational, rotational and other low transitions in molecules. It can be performed using solid, liquid or gaseous samples. In our case, we used solid samples. Raman spectroscopy presents a high selectivity, making it useful to identify and differentiate molecules and chemical species of great similarity [50].

Fluorescence Spectroscopy – steady-state

The steady-state fluorescence emission spectra were measured in a Fluorolog Tau-3 spectrofluorometer with the same quartz cell as for the absorption. The values of fluorescence intensity were corrected in the software of acquisition by considering the value of correction of the light intensity variation of the source at each wavelength as well as for the detector efficiency at each wavelength. The emission spectrum graphically represents fluorescence intensity variation in a wavelength interval, thus representing the emitted light in the given interval after its excitation at a given wavelength. Fluorescence spectra give information about how the species transition from the relaxed electronic excited state to the ground state. In comparison to UV-VIS, fluorescence spectroscopy has higher detection limit and sensitivity.

Fluorescence Decay

The equipment used to measure fluorescence decays was a HORIBA Jobin Yvon IBH FluoroLog-3 spectrofluorometer adapted time-correlated single photon counting (TCSPC) equipped with a Hamamatsu R928 photomultiplier tube. The samples analyzed in this equipment were excited with nanosecond pulses of 445 and 594 nm generated by NanoLED pulsed diodes (Horiba). Emission decays were analyzed using the software DAS6 v6.4 in which were fitted with reconvolution of the time-dependent profile of the light source (prompt). The best fit was assessed based on the parameter and the distribution of the weighted residuals.

Time-correlated single photon counting (TCSPC) is a common technique for the evaluation of fluorescence decays in the range of nanoseconds and even picoseconds. For the purpose, TCSPC was used for fluorescence lifetime measurements in solution by excitation of the sample by a pulsed laser, with the following generated photons being collected one by one along a period through a high number of excitation and emission cycles. The pulses have high repetition rates in order that the average of photons that reach the detector is less than one in each cycle. With this periodic excitation, it is possible from the single photons events collected all over the cycles to rebuilt the single cycle decay profile.

Fluorescence Lifetime Imaging Microscopy – FLIM

FLIM was performed with the confocal microscope MicroTime 200 (MT200) from PicoQuant which uses the time-correlated single-photon counting (TCSPC) technique. The source of excitation was a pulsed picosecond laser diode with a wavelength of 635 nm. For the measurements, a drop of the sample solution was disposed on a round cover glass and left drying to the next day allowing the deposition of the material. The sample was put in the microscope sample holder perpendicularly to the excitation light focused by a water immersion objective (60x, N.A. 1.2). The fluorescence emitted passes through an emission bandpass filter (centred at 695 nm with a 55 nm bandwidth) and a 30 mm pinhole which rejects out-of-focus light. Fluorescence is then detected with single-photon counting avalanche diodes (SPADs). Several areas of the deposed material were chosen for software capture in order to analyze the different lifetimes present in the different regions of the composites and construct the figure.

Transmission Electron Microscopy – TEM

TEM images were obtained with a Hitachi 8100, 200 kV, LaB6 filament analytical transmission electron microscope with ThermoNoran model SystemSix energy dispersive X-ray spectrometer (EDS) with light elements detector and digital image acquisition. The instrument includes a thermionic (LaB6) electron gun which emits electrons into the vacuum and accelerates them between the cathode and anode through a selected potential difference up to 200 kV. It was used as a facility.

2.4 Sensing Experiments

The experiments were performed in buffer solutions to control the pH of the medium. The buffer solutions used were first citrate-phosphate pH 3 and after acetate buffer pH 4.

The sensing experiments were made in two phases: the first with use of the HRP enzyme, the second with the use of the systems of study. Both involved merely the usage of absorption spectroscopy for the evaluation of the main peak at 652 nm originated by the oxidation of the sensing molecule TMB. All samples were made in Eppendorf's and the order of addition of the components was always the following: buffer solution – hydrogen peroxide – TMB – catalyst (HRP or the composite).

The irradiation was performed with the Xenon lamp from the spectrofluorometer without use of the monochromator to have access to all wavelengths. It was also made use of a Schott 399 cut-off filter. This setup however only allowed a beam focus on the quartz cell not allowing the illumination of all the sample.

Chapter 3

Results and Discussion

3.1 Characterization of synthesized material

The first step of the work was the morphological and spectroscopic characterization of the synthesized material: gold nanoparticles and graphene oxide.

3.1.1 Gold Nanoparticles

The gold nanoparticles synthetized as described before by the Turkevich method were subject of observation through Transmission Electron Microscopy to evaluate the shape and size. As seen in the image obtained the nanoparticles reveal the expected spherical shape with a reasonable homogeneity in terms of size. Through software analysis of the TEM images it was determined an average size of 17.5 ± 0.25 nm. An absorption spectrum of the synthetized solution was also performed (Figure 14) revealing its plasmonic band c.a. 525 nm.

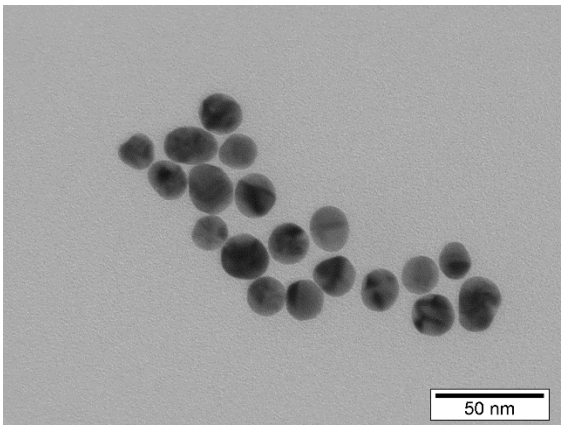

Figure 13 – TEM image of the synthetized gold nanoparticles

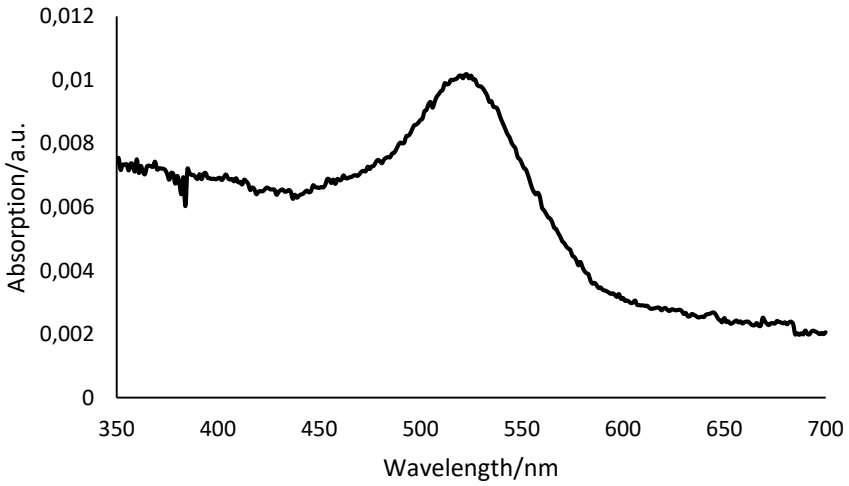

Figure 14 – Absorption spectrum of gold nanoparticles solution

Taking into account these results, an estimate of the extinction coefficient could be obtained (ε^{525}=8x10^{8} M^{-1}cm^{-1}) and was used to assess the concentration of AuNP in solution [51], [52].

3.1.2 Graphene Oxide

Proceeding the same way with the graphene oxide obtained by the described modified Hummers method it was possible to obtain the TEM image below. It is revealed in a half micrometre scale a darker region that corresponds to the presence of the carbon material lattice where the observed wrinkled structure confirms the presence of few-layer graphene oxide. The RAMAN spectrum of the material was also obtained (Fig. 15-A). The fact of being graphene oxide is revealed by the presence of its two main characteristic bands: D band (c.a. 1350 cm^{-1}) and G band (c.a. 1600 cm^{-1}) [53]. The latter is associated to the sp^2 bonded carbon in a hexagonal lattice whereas the former is related with sp^3 carbon atoms of defects and disorders introduced by the oxidation process. The intensity ratio of the two bands is indicative of extensive amount of defects as pretended. The absorption spectrum of graphene oxide is depicted in Figure 15-B revealing the main band (c.a. 230 nm) correspondent to electronic transitions in the carbon-carbon double bonds and a shoulder (c.a. 300 nm) from the carbon-oxygen bonds.

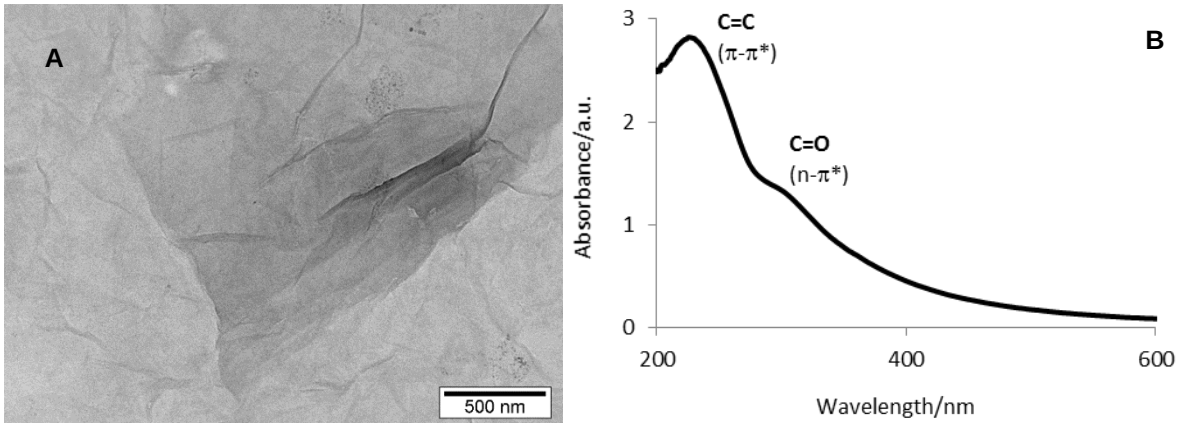

Figure 15 – TEM image of synthetized graphene oxide sheet (A) and UV-Vis absorption spectrum of graphene oxide dispersed in distilled water (B)

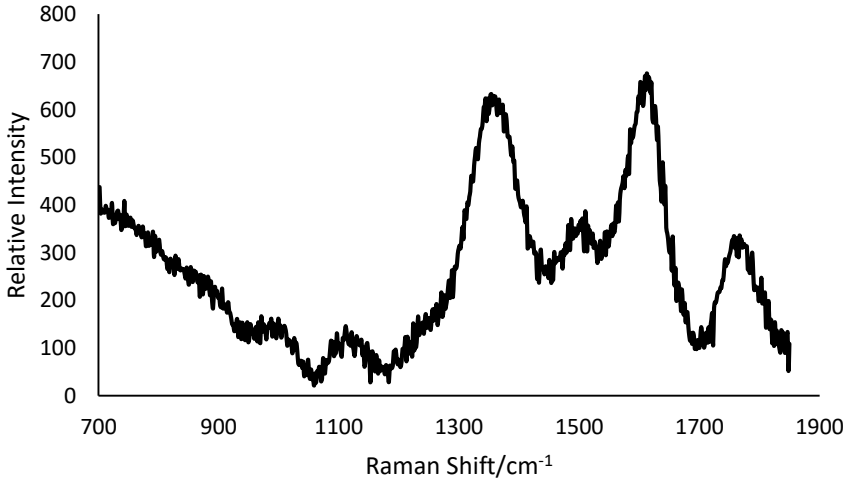

Figure 16 – RAMAN spectrum of the synthetized graphene oxide

3.1.3 Composites

A TEM image of the composite of the graphene oxide and the gold nanoparticles was also obtained and showed below. In the hundreds of nanometres scale it reveals the spherical gold nanoparticles reasonably well dispersed through the grey areas corresponding to the carbon material.

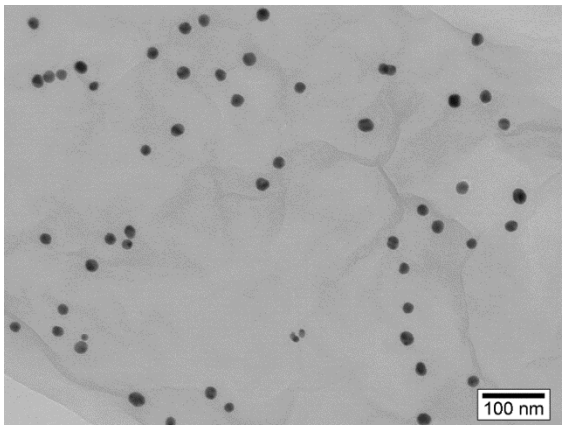

Figure 17 – TEM image of the composite of graphene oxide with gold nanoparticles

3.2 Spectrophotometry

In order to evaluate the possible interactions of chosen porphyrinoids with nanomaterials, absorption and fluorescence analysis were performed. The effect of polyelectrolytes on such interactions was also sought, in particular, its possible effect on the aggregation of TSPP at distinct pHs, was explored. Three groups of systems were studied: porphyrin-based systems with polyelectrolyte, porphyrin-based systems without polyelectrolyte and phthalocyanine-based systems with polyelectrolyte. For each system absorption and fluorescence spectra were measured and, also, for most the systems transient state fluorescence analysis was performed for the determination of the fluorescence lifetimes of the given system.

3.2.1 Porphyrin with Polyelectrolyte Systems

The main systems analyzed started with TSPP and involved the presence of one of two polyelectrolytes: the polysaccharide Chitosan or the polycation polyethylenimine (PEI). The spectral analysis of the systems of the porphyrin with each of the electrolytes was carried out at pH 3.5 and 6.5, at which the di-anionic and tetra-anionic form of TSPP prevailed, respectively. A concentration of 2 μM of TSPP was used for all the recorded spectra.

Chitosan

For the systems with the porphyrin only in the presence of chitosan the following results were obtained.

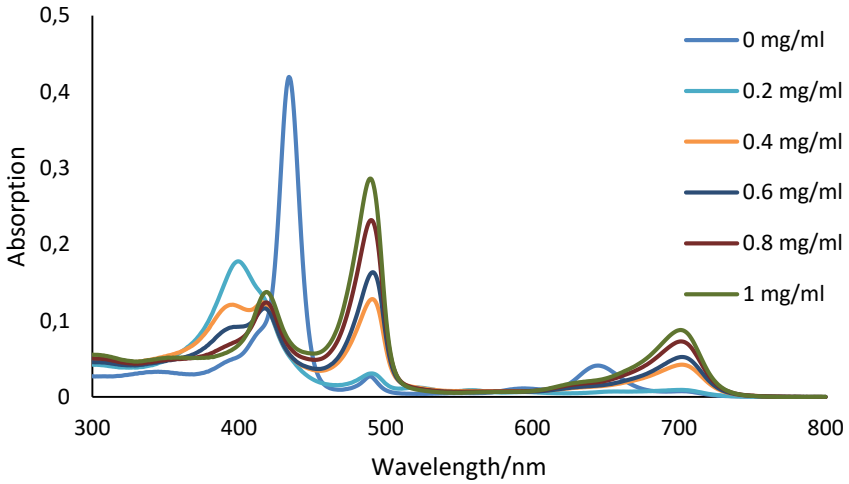

Figure 18 – Absorption spectra of TSPP in aqueous solution (pH 3.5) in the presence of increasing concentrations of Chitosan

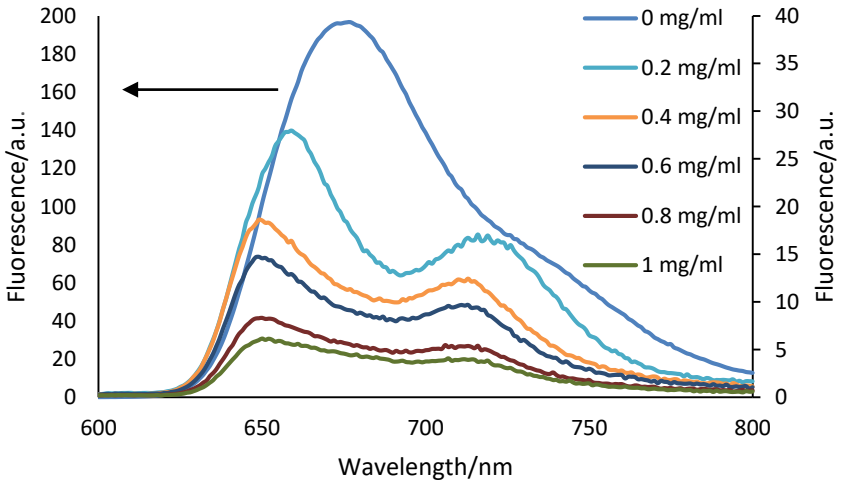

Figure 19 – Fluorescence spectra of TSPP in aqueous solution (pH 3.5) in the presence of increasing concentrations of Chitosan (λ_{exc} = 423 nm)

In both absorption and fluorescence spectra, it is clear that the increasing concentration of Chitosan leads to the formation of J-aggregates revealed by the increasing intensity of the 494 nm band in absorption and by the splitting of the fluorescence spectra in two bands with a progressive decrease in intensity due to the less fluorescence of the formed aggregates. However, it is verified by the presence of a small band that for the null concentration of Chitosan a small amount of aggregate is already present. At the lower concentrations of added chitosan the Soret band peak shifts to the blue (~400 nm) which concomitantly decreases upon addition of chitosan followed by the increase of the 494 nm band. The blue-shifted Soret band has been assigned to the formation of an H-aggregate (probably a dimer). This small aggregate is the first arrangement stabilized by the presence of small

amounts of chitosan which upon further addition of the polysaccharide, grows and changes to a head-to-tail arrangement.

The obtained lifetime for the monomer (absence of chitosan) was 3.84 ns which is in agreement with available data for similar conditions[39]. The following lifetimes as shown in Table A1-1 reveal the need for a three exponential fit that leads to three time components: a short one in the sub-nanosecond range corresponding to the aggregate, a middle one that varies between 3.7 and 3.9 ns, and a long component that keeps at 11 ns which is a value that is shown in literature attributed to a formed complex [41].From the pre-exponentials it is revealed that the aggregate usually contributes with the larger population, apart from the two higher concentrations of chitosan in which the monomer has a similar or higher contribution.

A circular dichroism spectrum (see Figure A2-1 in Annex) was also recorded for this system in the absence of chitosan and at concentrations at which J-aggregates prevail. In the absence of the polymer there is no CD signal which is expected since the TSPP is not chiral. However, upon addition of chitosan, a clear CD signal appears indicating that the polymer induces the chirality of the system.

Proceeding with the same system but now at pH 6.5:

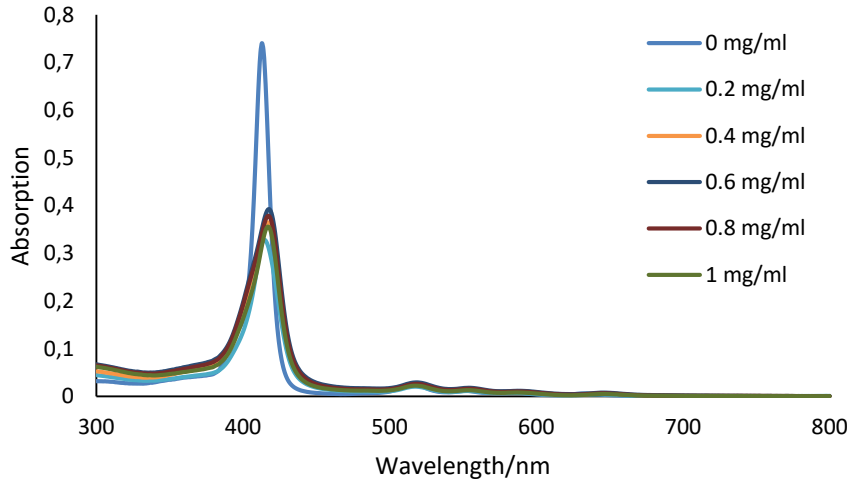

Figure 20 - Absorption spectra of TSPP in aqueous solution (pH 6.5) in the presence of increasing concentrations of Chitosan

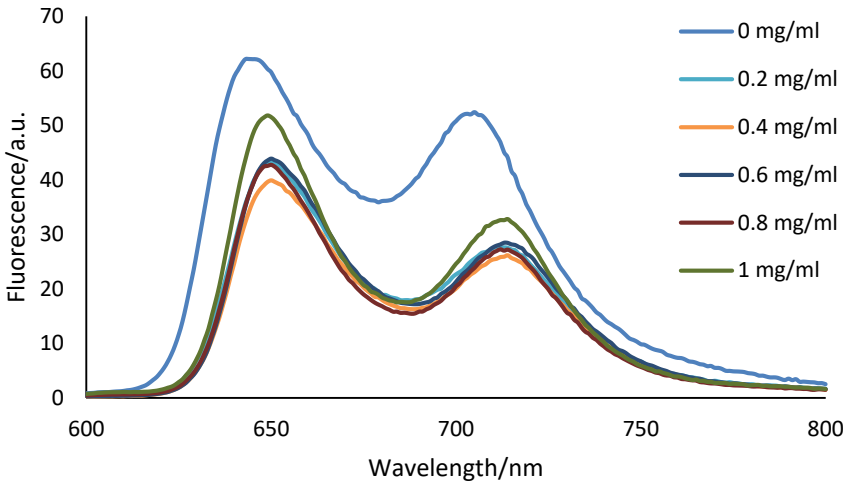

Figure 21 - Fluorescence spectra of TSPP in aqueous solution (pH 6.5) in the presence of increasing concentrations of Chitosan (λ_{exc} = 423 nm)

At pH=6.5, we are in the presence of the neutral form of TSPP, as it is clear by the presence of the peak of its Soret band blue-shifted relatively to the acid form (~413 nm). With the progressive addition of chitosan, it is noticeable a red-shift of the spectra immediately for the lower concentration. It is also clear a reduction of the intensity of absorption and fluorescence upon the addition of chitosan. In the case of the fluorescence spectra it reveals a decrease in the fluorescence intensity for the two lower concentrations of chitosan that is inverted with an increase for the further concentrations. Regarding the lifetimes (Table A1-2), the one for the monomer is 9,9 ns which is again in conformity with the value available in the literature[39]. In the presence of chitosan, the lifetime of the monomer becomes around 5-6 ns and a new long component of almost 12 ns appears. As described before this new component may be attributed to a complex, with the novelty that now the contribution of the complex is predominant, with an increase with the concentration. This justifies the occurred red-shift and indicates that the tetraanionic TSPP is more prone to complexation with chitosan than the acid one.

Chitosan and GO

The next component added to the study system was graphene oxide. The concentration of chitosan was fixed at 0,4 mg/ml and the concentration of GO was progressively increased.

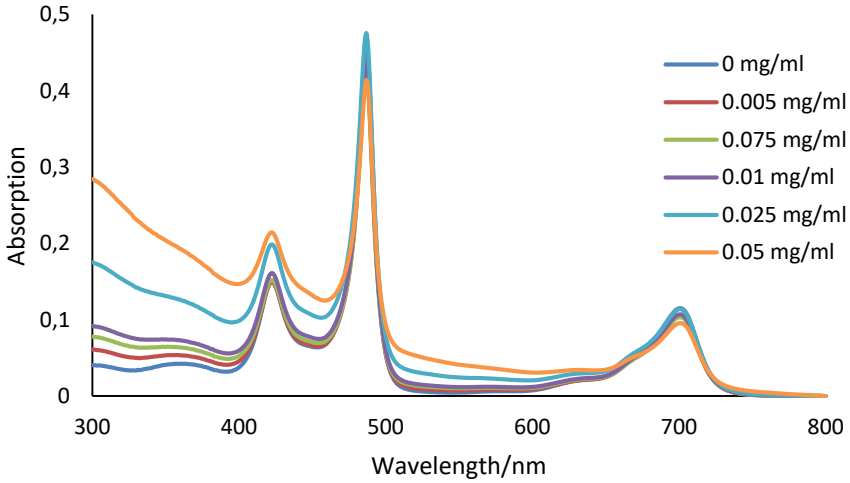

Figure 22 - Absorption spectra of TSPP in aqueous solution (pH 3.5) in the presence of Chitosan and increasing concentrations of GO

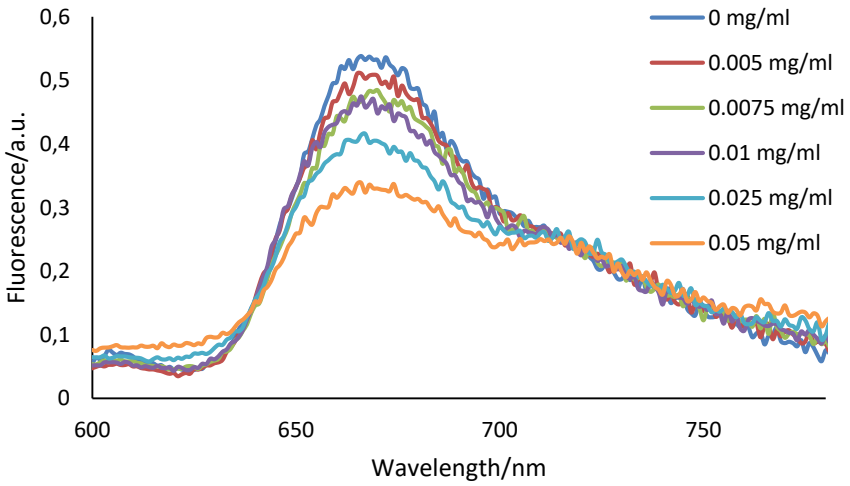

Figure 23 - Fluorescence spectra of TSPP in aqueous solution (pH 3.5) in the presence of Chitosan and increasing concentrations of GO (λ_{exc} = 423 nm)

This analysis started with only the presence of chitosan revealing the predominant presence of J-aggregate as previous seen for those conditions. With the addition of GO the significant aspects regards the fluorescence spectra in which it can be seen that the fluorescence of the band of the aggregate (c.a. 718 nm) remains stable, occurring only the decrease of the fluorescence intensity of the band of the monomer. The lifetimes (Table A1-3) show the presence of two components in the range expected for the monomer. However, by determining the medium lifetimes from the two components and the f fractions it is verified a medium lifetime of 3,7 ns for the first sample which fits with the same system in the previous analysis with only chitosan at 0,4 mg/ml. Upon the addition of

chitosan, the medium lifetime globally tends to decrease which fits with the information gathered from the fluorescence spectra. Plotting the ratios of the medium lifetimes and fluorescence areas with the sample without GO we can evaluate the contribution of static and dynamic processes in the quenching of fluorescence:

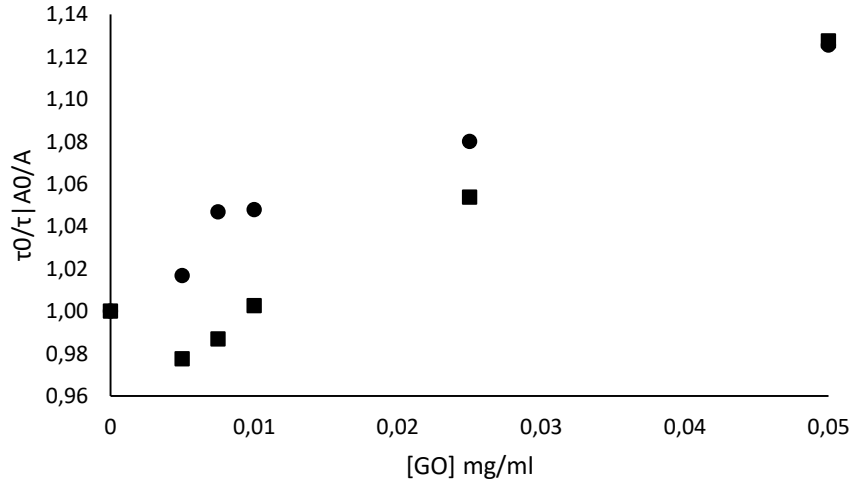

Figure 24 – τ_0/τ (square dots) and A_0/A (circular dots) ratios for increasing concentrations of GO

It is clear that there is a contribution of static processes relevant since there is a clear difference between the dynamic component (lifetimes) and static plus dynamic component (fluorescence areas). However, the data is not clear enough in the lower concentration range to quantify.

For the case of tetraanionic TSPP it wasn't achieved more significant information with the expected presence of quenching of fluorescence with increasing concentrations of GO.

Chitosan and AuNP

Following the study, now instead of graphene oxide, gold nanoparticles were added. The concentration of chitosan was again fixed at 0,4 mg/ml and the volume of nanoparticle solution was progressively increased.

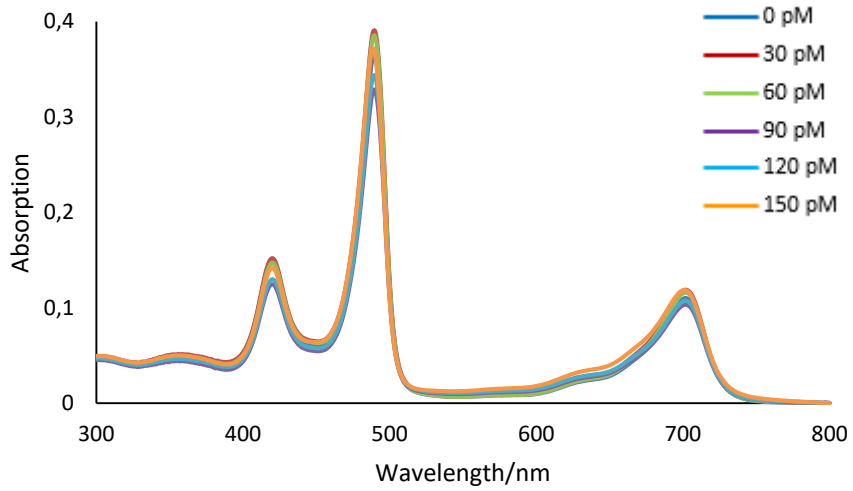

Figure 25 - Absorption spectra of TSPP in aqueous solution (pH 3.5) in the presence of Chitosan and increasing concentrations of AuNP

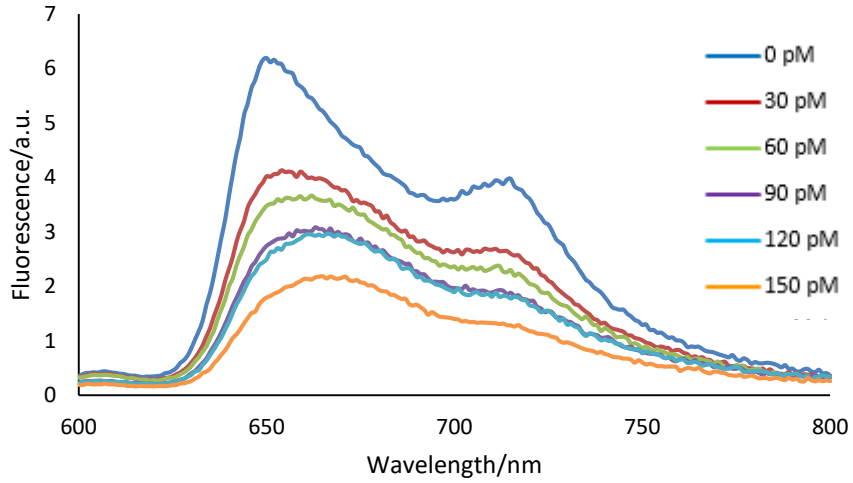

Figure 26 - Fluorescence spectra of TSPP in aqueous solution (pH 3.5) in the presence of Chitosan and increasing concentrations of AuNP (λ_{exc} = 432 nm)

In this case the absorption spectra don't show a noticeable variation with the increasing gold nanoparticle volume added. The typical surface plasmon resonance band of these NPs (~525 nm) is submerged by the absorption of TSPP. However, the fluorescence spectra show a clear quenching of the fluorescence. Taking a look at the obtained lifetimes (Table A1-4) it is seen as well as in the first system with only chitosan the presence of three distinct lifetimes that were there attributed to the J-

aggregate, the monomer and the complex, this by increasing order of lifetime. Analysing the variation of each component with the increasing volume there is no clear variation that could explain the decrease in fluorescence that is seen in the spectra. Since the monomer is the most fluorescent element it could be expected a decrease in its contribution but that is not verified. Nevertheless, by calculating the medium lifetimes as done in the previous system, a variation of the medium lifetime between 5 and 4.1 ns occurs. This may indicate that there is really a contribution from dynamic processes and not only from static one as could be pointed if there was no decrease in the lifetimes.

For the tetraanionic TSPP there was no significant variation in the absorption spectra only a small decrease in fluorescence upon the addition of gold nanoparticles was detected, Figure 27 and 28. Fluorescence lifetimes (Table A1-5) showed no significant variation, with the presence of the same two components obtained for the binary system chitosan - tetraanionic TSPP, assigned to the monomer and to the complex.

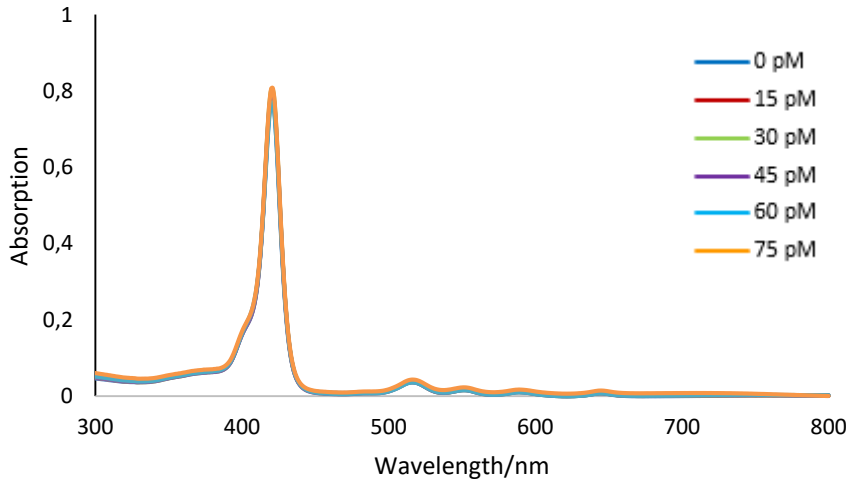

Figure 27 - Absorption spectra of TSPP in aqueous solution (pH 6.5) in the presence of Chitosan and increasing concentrations of AuNP

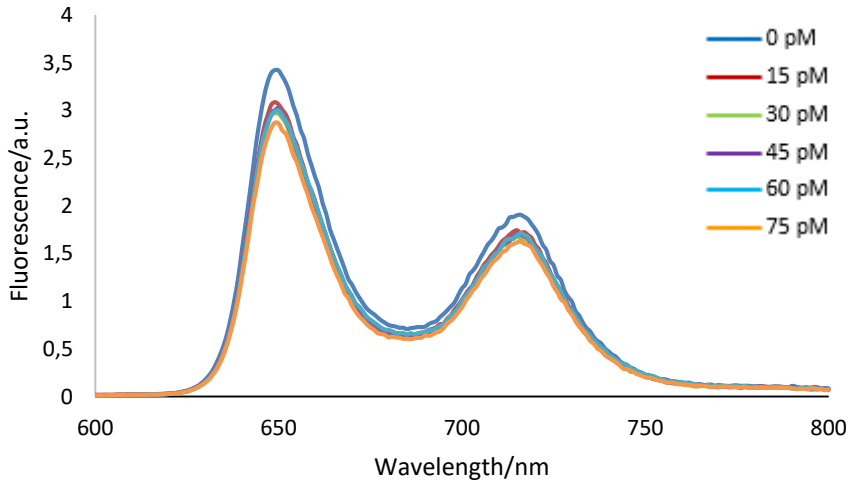

Figure 28 - Fluorescence spectra of TSPP in aqueous solution (pH 6.5) in the presence of Chitosan and increasing concentrations of AuNP (λ_{exc} = 423 nm)

Chitosan, GO and AuNP

Finally, the system with the four components was analyzed. In addition to the fixed concentration of 0.4 mg/ml of chitosan already used, the concentration of GO was fixed in 0.05 mg/ml and the volume of gold nanoparticles was varied from zero to 200 microliters.

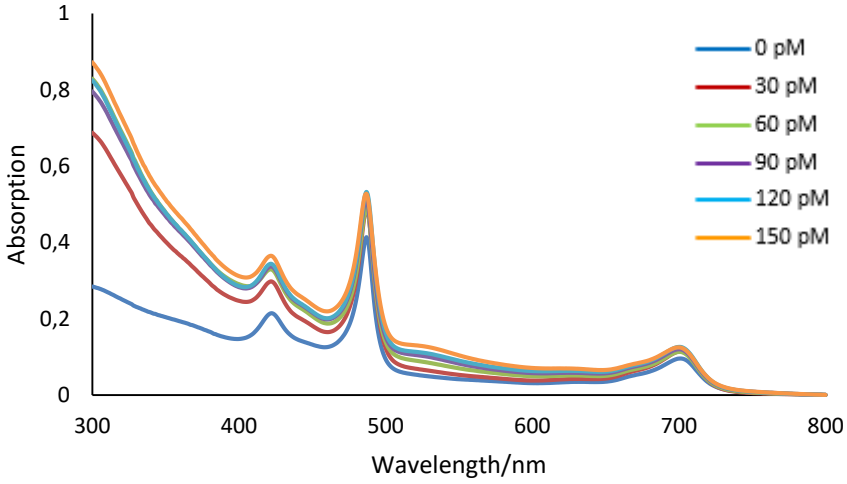

Figure 29 - Absorption spectra of TSPP in aqueous solution (pH 3.5) in the presence of Chitosan, GO and increasing concentrations of AuNP

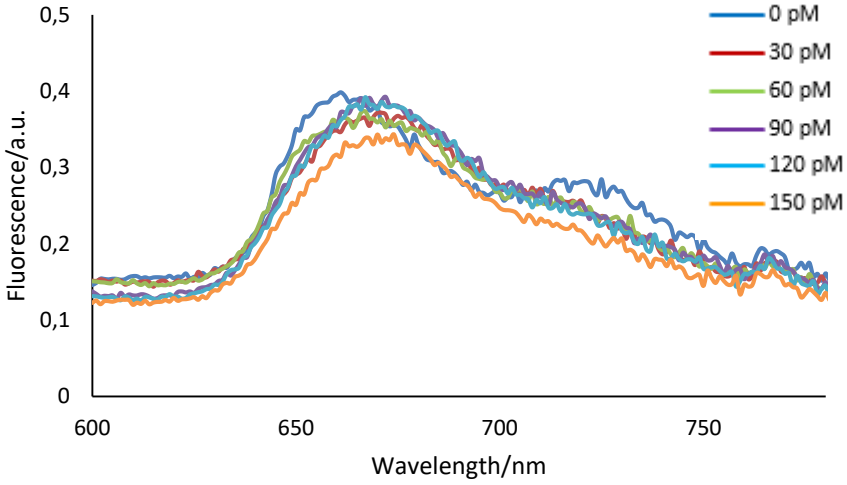

Figure 30 - Fluorescence spectra of TSPP in aqueous solution (pH 3.5) in the presence of Chitosan, GO and increasing concentrations of AuNP (λ_{exc} = 423 nm)

The absorption spectra peaks do not show a significant change upon the addition of the nanoparticles. Besides, the intensity of the aggregate peak becomes higher without no further significant variance. Analysing the fluorescence, there is a reduction that it isn't significant, with the most noticeable decrease being in the intensity of the band of the aggregate upon the addition of the smallest concentration of AuNP. From the transient-state information (Table A1-6) the most noticeable is the disappearance of the long lifetime after the smallest concentration of AuNP, indicating a

possible destruction of the complex. Regarding the lifetimes of the aggregate and the monomer, the higher population proportion of the lifetime of the aggregate as well as a reduced lifetime may indicate a higher contribution form this component that leads to the decrease in fluorescence occurred. No MEF effect from the introduction of AuNPs was discernible for this system.

PEI

Along with the use of chitosan, experiments with polytheylenimine were also made, using the same procedure as previously, with the same concentration of TSPP of 2 µM and the equivalent systems.

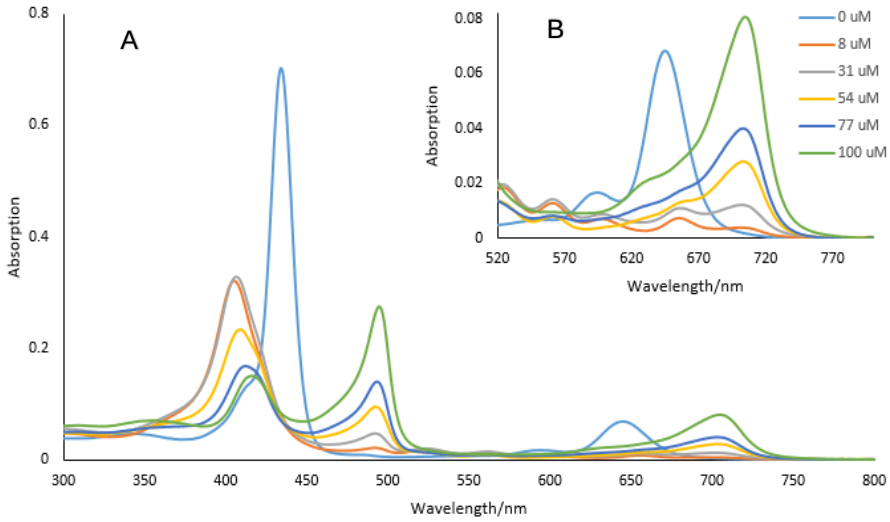

Figure 31 - A - Absorption spectra of TSPP in aqueous solution (pH 3.3) in the presence of increasing concentrations of PEI; B – inset of the Q bands of the forming aggregate

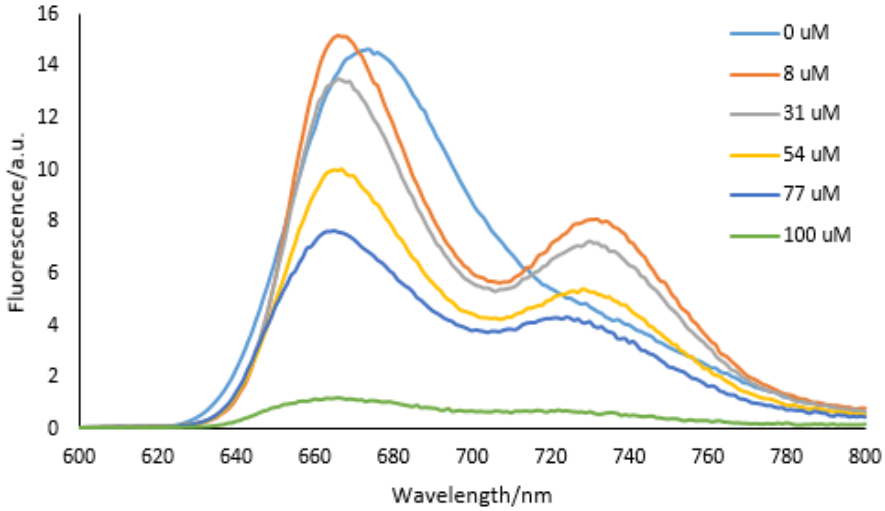

Figure 32 - Fluorescence spectra of TSPP in aqueous solution (pH 3.3) in the presence of increasing concentrations of PEI (λ_{exc} = 430 nm)

The behavior of the system with the addition of PEI is similar to the previous case with chitosan. Upon the addition of the polycation the formation of H-aggregates followed by that of J-aggregates is promoted. In the fluorescence spectra as previously seen, there is also a clear quenching of the fluorescence with increasing concentrations of the polyelectrolyte. The obtained lifetime (Table A1-7) for the monomer in the absence of the polyelectrolyte is 3.9 ns, which is again in agreement with what was determined before in the chitosan system. Moreover, upon addition, there is an increase of the complexity of the decay, with a long lifetime of 11 ns corresponding to the complex as well as a short lifetime around 0.2 ns that as before it is ascribed to the J-aggregate. A lifetime that varies between 8 and 2 ns with the concentration of PEI may be attributed to the formed H-aggregate, taking into account previous studies [41]. These aggregates are non-fluorescent or have a very low yield of fluorescence [54].

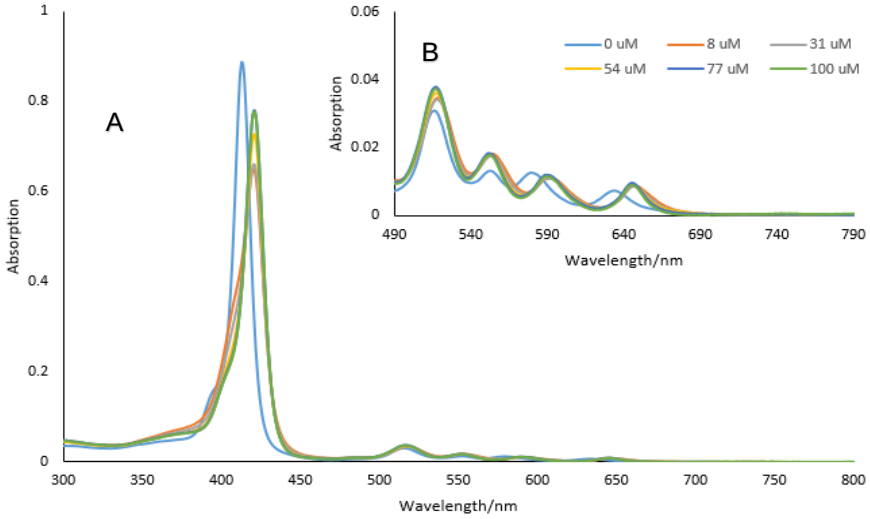

Figure 33 - A - Absorption spectra of TSPP in aqueous solution (pH 6.4) in the presence of increasing concentrations of PEI; B – inset of the Q bands

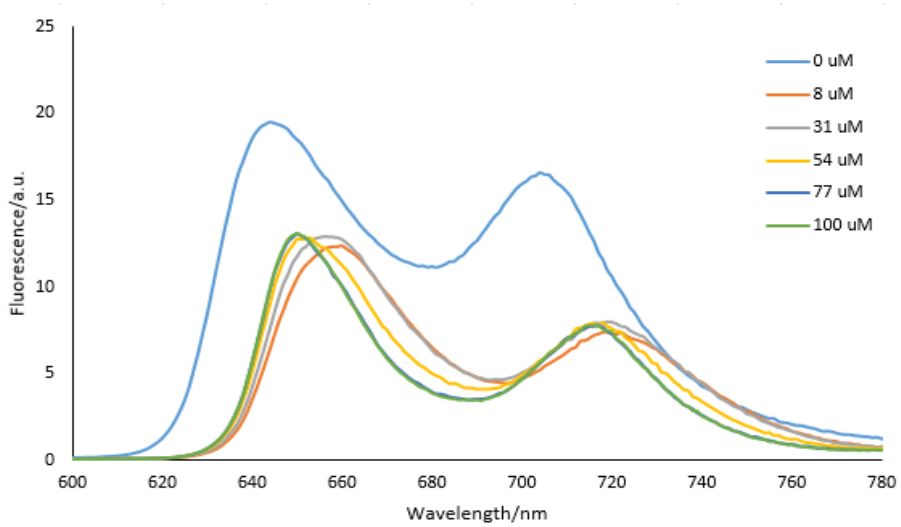

Figure 34 - Fluorescence spectra of TSPP in aqueous solution (pH 6.4) in the presence of increasing concentrations of PEI (λ_{exc} = 397 nm)

The observation of the absorption spectra reveals a red-shift upon the addition of PEI that was already noticed in the presence of chitosan and attributed to a molecular complex caused by strong interactions between the porphyrin and the polymer. The fluorescence spectra reflect this by revealing the red-shift and also a quenching of fluorescence caused by the formation of the less fluorescent complex. With the increase of PEI concentration, there is no further significant change in the fluorescence intensity of TSPP. The analysis of the lifetimes (Table A1-8) shows, as expected, a lifetime of 10 ns for the monomer and a shorter lifetime that has already been attributed to the presence of H-aggregates. However, the lifetime data is inconclusive regarding the complex formation, not revealing the expected lifetime around 11 ns. This may be due to the fact that the excitation conditions of the stationary and transient analysis of fluorescence were different, with the fluorescence spectra being obtained by excitation at 397 nm and the fluorescence decay being obtained with a laser excitation at 445 nm. Nevertheless, by calculating the average lifetime from the two obtained it shows a reduction of from 7.8 to 5.8 ns.

PEI and GO

The first component added to the system of the porphyrin with PEI was GO. From now on a fixed PEI concentration of 100 µM was used for all studied systems. In the present one, the graphene oxide concentration was varied between 0 and 0.05 mg/ml.

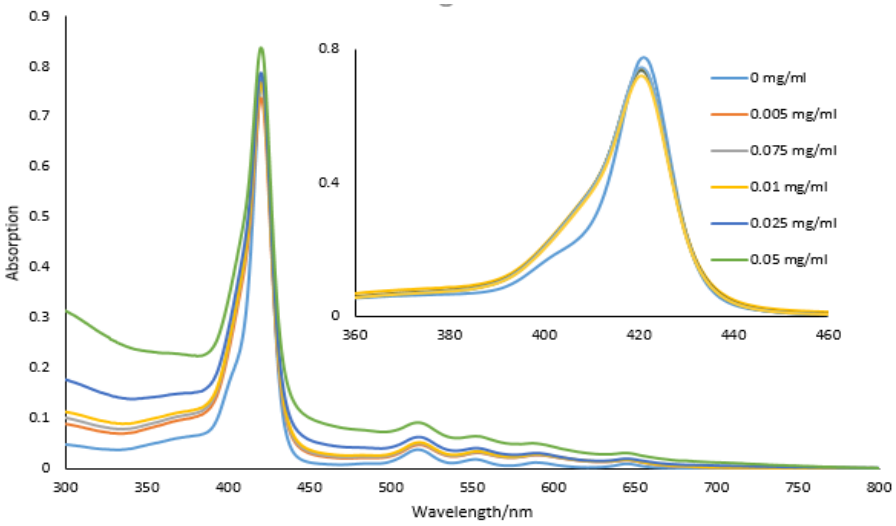

Figure 35 - Absorption spectra of TSPP in aqueous solution (pH 6.5) in the presence of PEI and increasing concentrations of GO

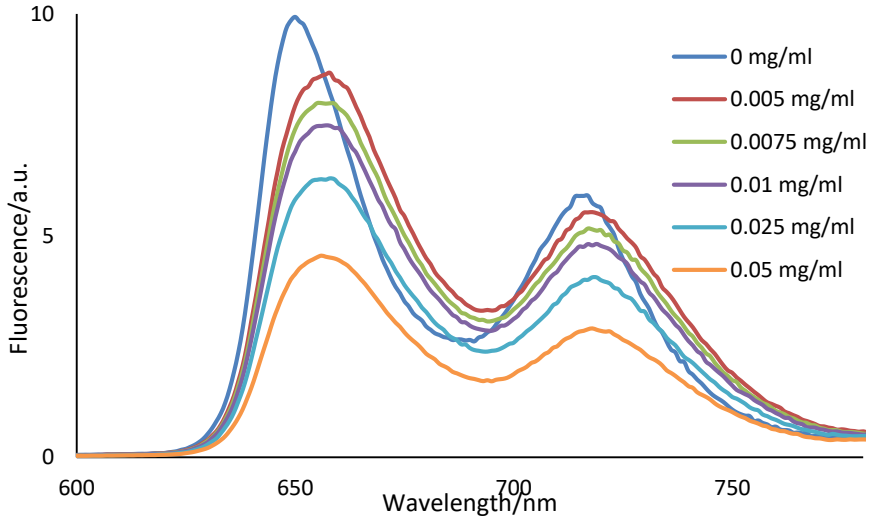

Figure 36 - Fluorescence spectra of TSPP in aqueous solution (pH 6.5) in the presence of PEI and increasing concentrations of GO (λ_{exc} = 397 nm)

The absorption spectra show the contribution from GO absorption as well as TSPP. In the inset the signal was “cleaned” from the contribution of the former and it is possible to see that in the Soret band region there was an enlargement due to the presence of GO. These features point to the stabilization of H-aggregates by GO. Regarding fluorescence spectra, it is revealed a red-shift with the presence of GO as well as a concomitant decrease of the intensity. This quenching effect is well understood in terms of the aggregation effect imposed by GO. However, the efficiency of the

quenching is quite high which probably indicates that other effect from GO interaction with TSPP is introducing an additional deactivation channel for the porphyrin. This hypothesis is backed up by the lifetimes (Table A1-9), since it is noticed the presence of lifetimes around 8 and 2 ns that are characteristic of H-aggregates. There is also an overall decrease in the lifetimes in accordance to the already referred quenching.

PEI and AuNP

The same procedure was performed for the system with presence of gold nanoparticles instead of GO. In this case the concentrations of AuNP added were between 0 and 160 µL.

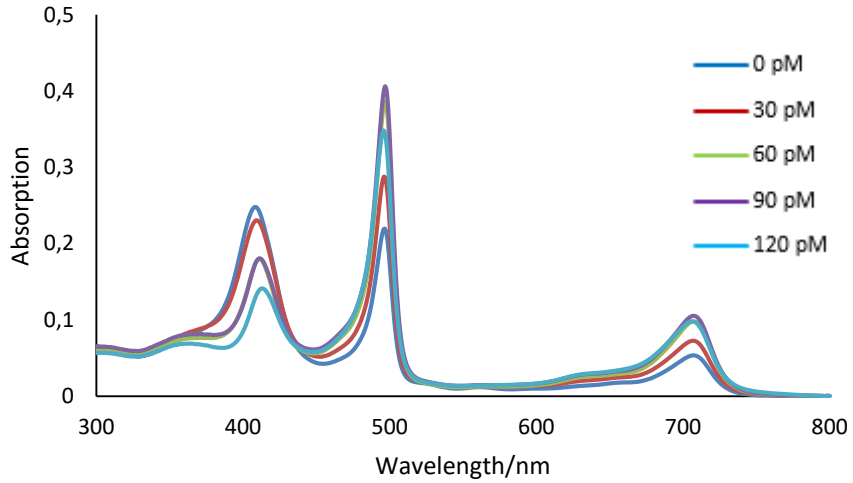

Figure 37 - Absorption spectra of TSPP in aqueous solution (pH 3.5) in the presence of PEI and increasing concentrations of AuNP

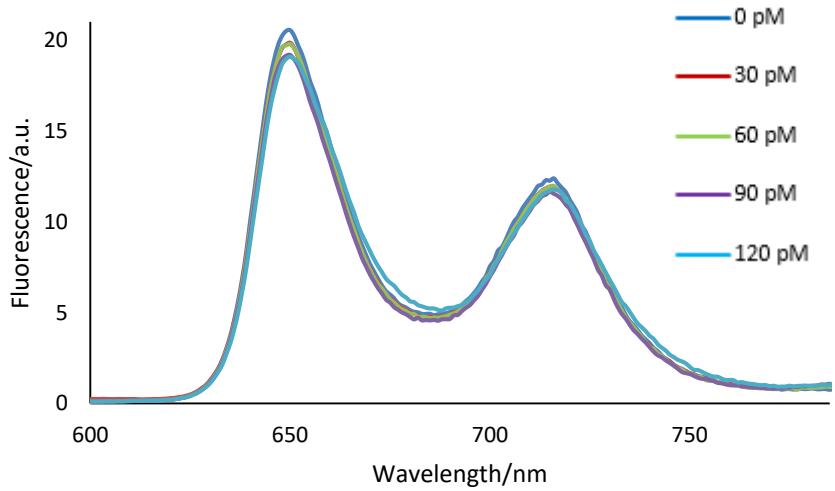

Figure 38 - Fluorescence spectra of TSPP in aqueous solution (pH 3.5) in the presence of PEI and increasing concentrations of AuNP (λ_{exc} = 418 nm)

The absorption spectra for the acid TSPP show that the spectrum with absence of the nanoparticles is as expected the same as obtained before in the study with only PEI, with the presence of aggregates. With the increasing concentration of AuNP there is a tendency more formation J-aggregates. However, this has no repercussions in the fluorescence of the system since there is only noticeable a small decrease in its intensity. The lifetime analysis (Table A1-10) shows no more significant information with the same lifetimes as showed in the system with only PEI, namely the short one coming from the J-aggregate; the long one attributed to the complex of interaction between TSPP and PEI and the lifetime around 2 ns, assigned to the H-aggregate. Again, no MEF effect from the introduction of AuNPs was discernible for this system.

Now, regarding the tetraanionic form.

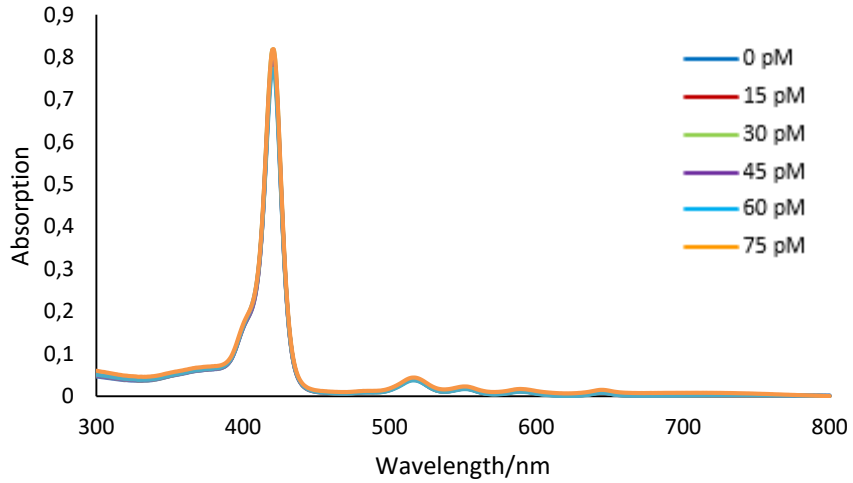

Figure 39 - Absorption spectra of TSPP in aqueous solution (pH 6.5) in the presence of PEI and increasing concentrations of AuNP

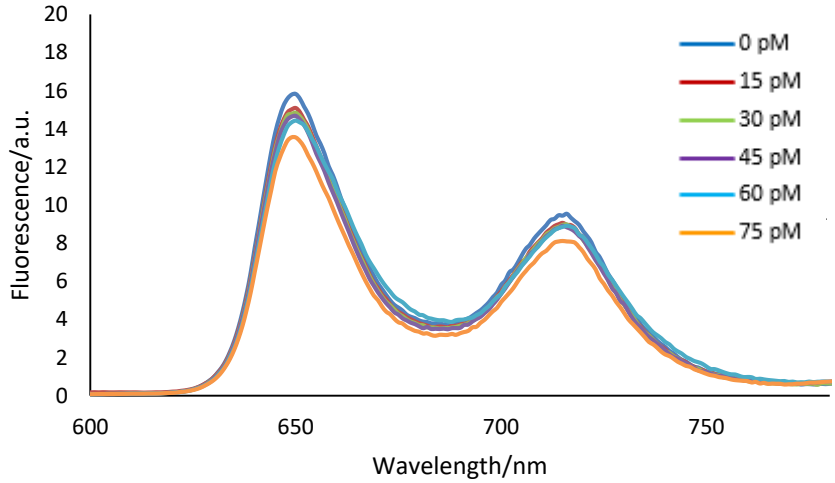

Figure 40 - Fluorescence spectra of TSPP in aqueous solution (pH 6.5) in the presence of PEI and increasing concentrations of AuNP (λ_{exc} = 397 nm)

For the case of pH 6.5 the spectra are almost identical to the system at the same pH with only PEI. The increasing volumes of nanoparticle solution don't affect the absorption spectra that remains practically the same along the experiment and there is only a small intensity decrease in the fluorescence spectra. The lifetimes obtained (Table A1-11) are also in agreement with what was seen before and there is no significant variation with the increasing concentrations of AuNP. This shows that by opposition to what happened with GO, the gold nanoparticles don't seem to have any effect in the TSPP-PEI spectral behavior.

PEI, GO and AuNP

Finally, the experiment was made with all the components, with a fixed concentration of 0.05 mg/ml of graphene oxide and increasing the volume of nanoparticles solution from 0 to 200 µL. Results are shown for the two analyzed pH's as usual.

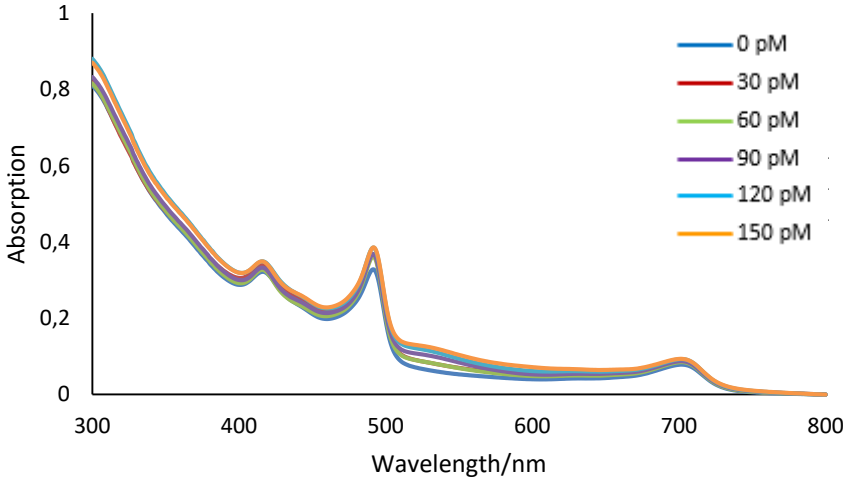

Figure 41 - Absorption spectra of TSPP in aqueous solution (pH 3.5) in the presence of PEI, GO and increasing concentrations of AuNP

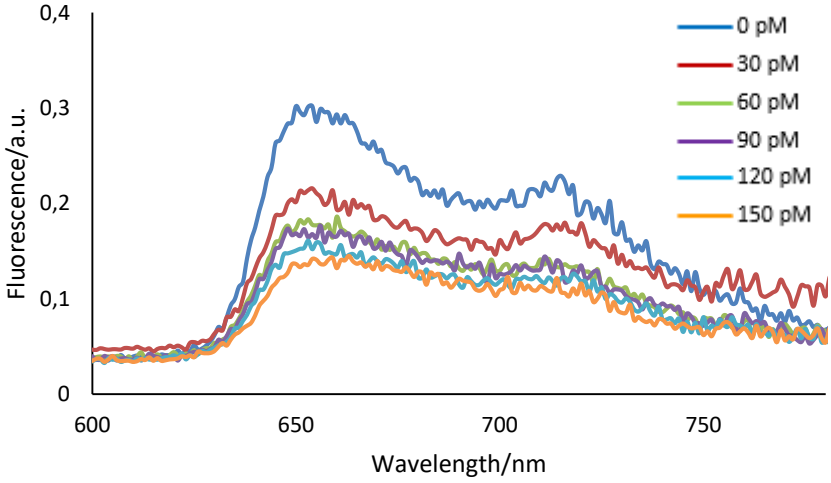

Figure 42 - Fluorescence spectra of TSPP in aqueous solution (pH 3.5) in the presence of PEI, GO and increasing concentrations of AuNP (λ_{exc} = 418 nm)

As shown before there is the presence of a J-aggregate promoted by the polyelectrolyte. In this case with the fixed concentration of GO, the increasing concentrations of AuNP lead to a small increase of the aggregate revealed by the increasing intensity of its absorption band. This may justify the quenching in the fluorescence since this aggregate is less fluorescent. Since we are again the presence of a complex mixture of monomer and aggregates the lifetime analysis (Table A1-12) is not trivial. However, there is a clear predominance of shorter lifetimes originated from the aggregates, with the presence of a reminiscence of a long lifetime that may be from the already seen complex. In the absorption spectra is also clear the plasmonic band of the gold nanoparticles (c.a. 525-530 nm) that as expected increases with the volume.

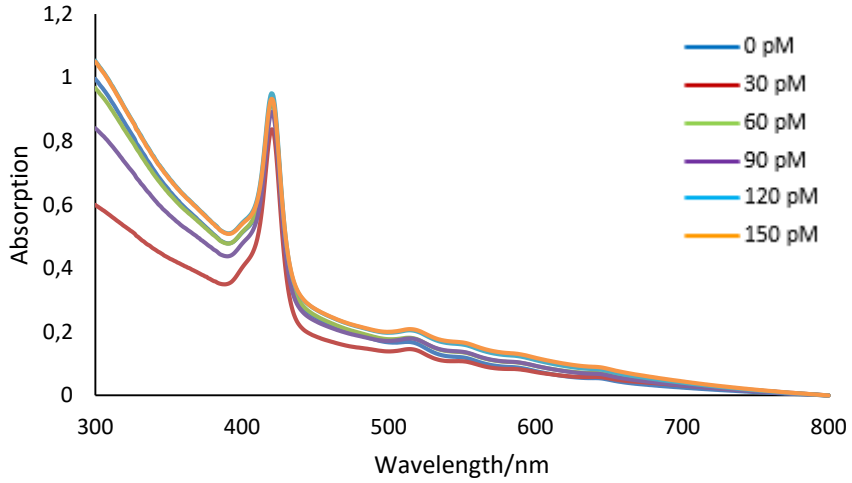

Figure 43 - Absorption spectra of TSPP in aqueous solution (pH 6.5) in the presence of PEI, GO and increasing concentrations of AuNP

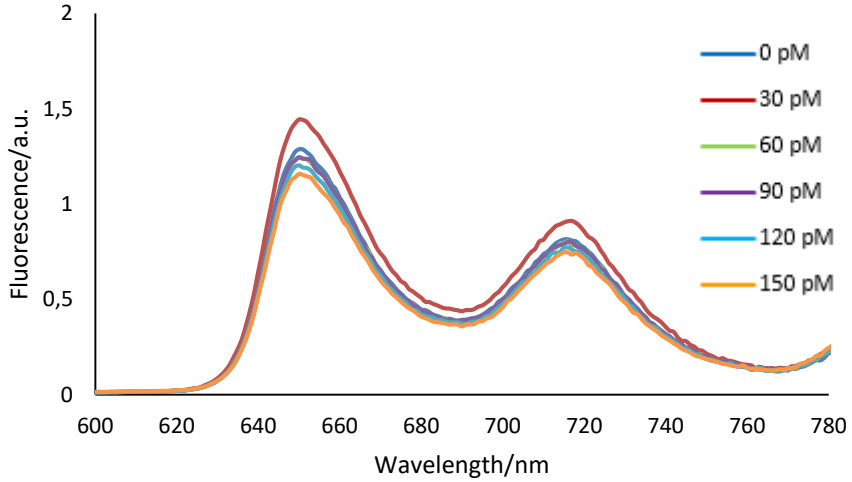

Figure 44 - Fluorescence spectra of TSPP in aqueous solution (pH 6.5) in the presence of PEI, GO and increasing concentrations of AuNP (λ_{exc} = 397 nm)

The absorption spectra one more time don't reveal any particular alteration beyond the effects of the increasing dispersion of the system due to an increasing concentration of nanoparticles and the presence of dispersed graphene oxide. The fluorescence spectra pulling apart the lowest volume seem to indicate small quenching of fluorescence. This is in agreement with the lifetimes (Table A1-13) that show no variation. The obtained lifetimes are the same as in the same system without AuNP and increasing GO, with the particular case of the appearance of a short lifetime that may have its origin the scattering increase of the system.

3.2.2 Polymer Interaction Kinetics

Since it was verified an aggregation process of TSPP both in the presence of chitosan and PEI, a kinetic study of the aggregation was performed with both polymeric systems. To evaluate the sensitivity of the system to the order of addition of the components, two measures were performed for each system, with the addition of TSPP to the polymeric system and vice-versa. The spectra for the kinetics of aggregation of TSPP promoted by PEI with both addition methods are shown below.

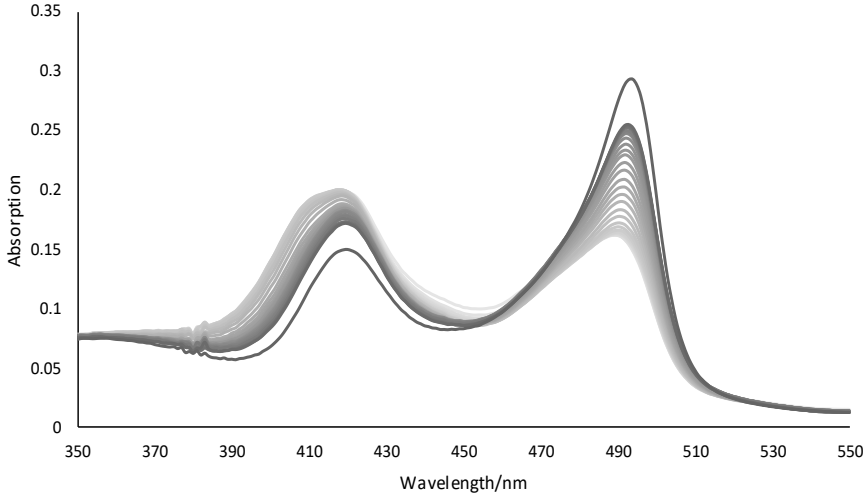

Figure 45 – Spectral representation of the kinetics of aggregation of TSPP in the presence of PEI (from light to dark grey; PEI added first than TSPP)

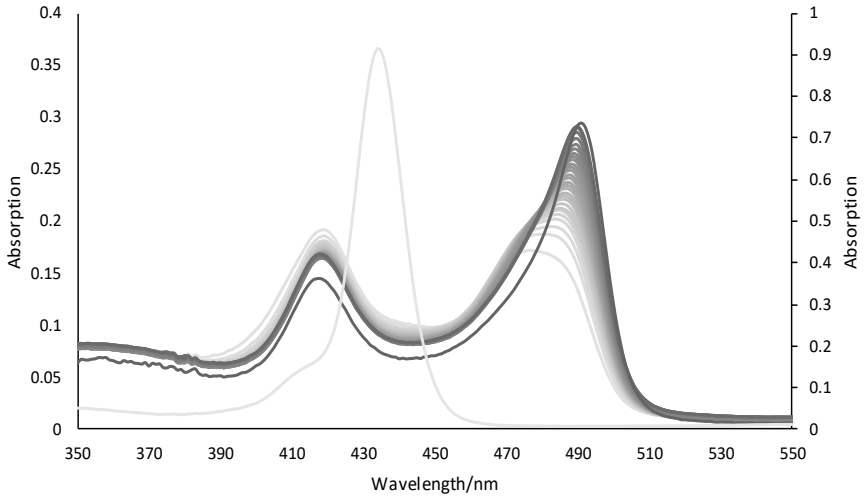

Figure 46 - Spectral representation of the kinetics of aggregation of TSPP in the presence of PEI (from light to dark grey; TSPP added first than PEI)

With the obtained spectral data, kinetic curves were built plotting the absorption of TSPP at the wavelength of the formed J-aggregate along time, for both addition methods.

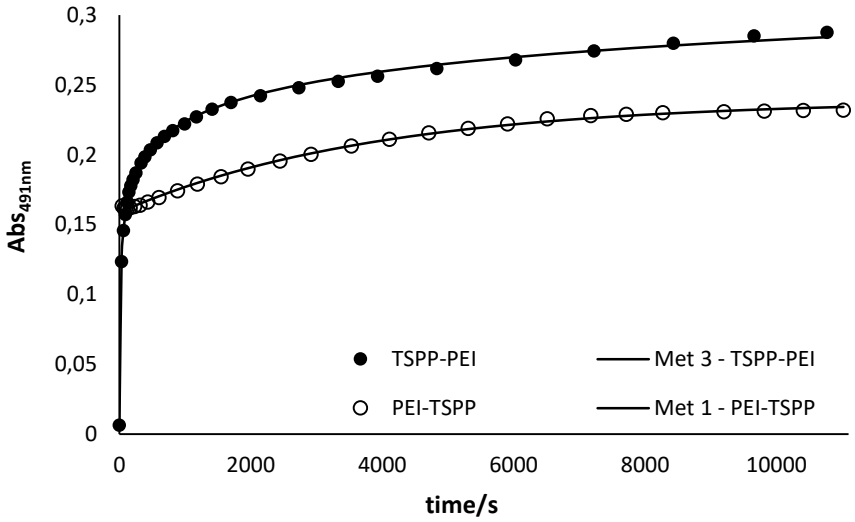

Figure 47 – Kinetic curves of PEI system for the two addition methods (PEI added to TSPP- full dots; TSPP added to PEI – hollow dots)

The kinetic curves were adjusted through the use of kinetic models, described in the graph as Method 1 (eq.1) and Method 3 (eq.2), both obtained from the literature[55][56],

$$\mathrm{OD} = \mathrm{E_m}[\mathrm{M_0}]\mathrm{e}^{-\mathrm{kt}} + \mathrm{E_j}[\mathrm{M_0}]\left(1 - \mathrm{e}^{-\mathrm{kt}}\right) + \mathrm{E_j}[\mathrm{J}] \quad (1)$$

where E_m and E_j are the extinction coefficients for the monomer and aggregate respectively, at the aggregate peak, k is the rate constant of the aggregation and [M_0] and [J] are the initial concentration of monomer and the formed concentration of aggregate, respectively. As for the other model, an induction time involving the formation of a critical nucleus (the rate-determining step) has to be accounted for,

$$OD = OD_\infty + (OD_0 - OD_\infty)\{(1 + (m-1)(k_0 t + (n+1)^{-1}(k_c t)^{n+1})\}^{\frac{-1}{m+1}} \quad (2)$$

where OD∞ is the absorption of the aggregate in the final, and the others are kinetic parameters: k_o is the rate constant for the uncatalyzed growth, k_c is the rate constant for the catalytic pathway; *n* is a parameter that describes the growth of the chromophore assembly as a power function of time and *m*, which is a parameter related to the size of the critical nucleus.

The fitted parameters for the models used (Method 1 for PEI-TSPP and Method 3 for TSPP-PEI) are displayed next:

Table 1 – Kinetic parameters obtained for method 1, where TSPP was added to a PEI solution

E_m (M^{-1} cm^{-1})	**E_j (M^{-1} cm^{-1})**	**k (s^{-1})**
3E-09	4E+04	3E-04

Table 2 – Kinetic parameters obtained for method 3, where PEI was added to a TSPP solution

m	**k_o (s^{-1})**	**n**	**k_c (s^{-1})**
27	1E-05	0.02	5E-02

*The value of m is extremely high, which together with the low value obtained for n (<<1) indicates the existence of covariance between the two values. Therefore, we cannot take any information from such values and the remain kinetic parameters have to be viewed as indicative of its order of magnitude.

An analogous procedure was performed for the system with chitosan.

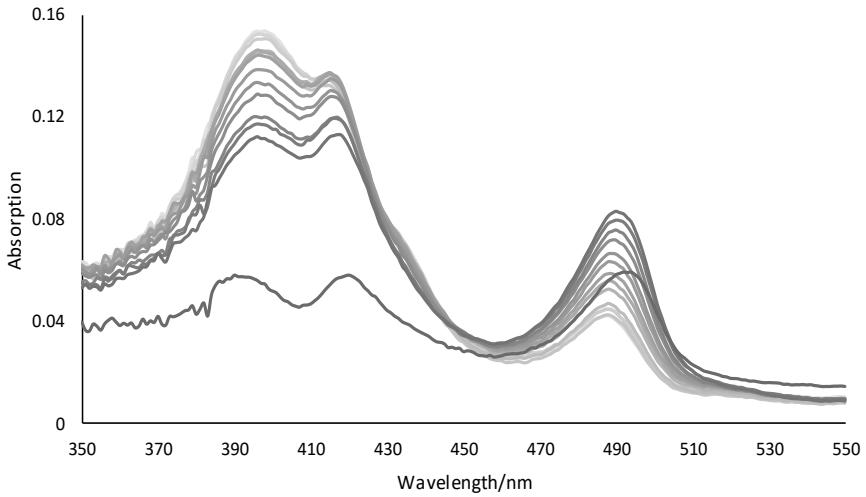

Figure 48 - Spectral representation of the kinetics of aggregation of TSPP in the presence of Chitosan (from light to dark grey; Chitosan added first than TSPP)

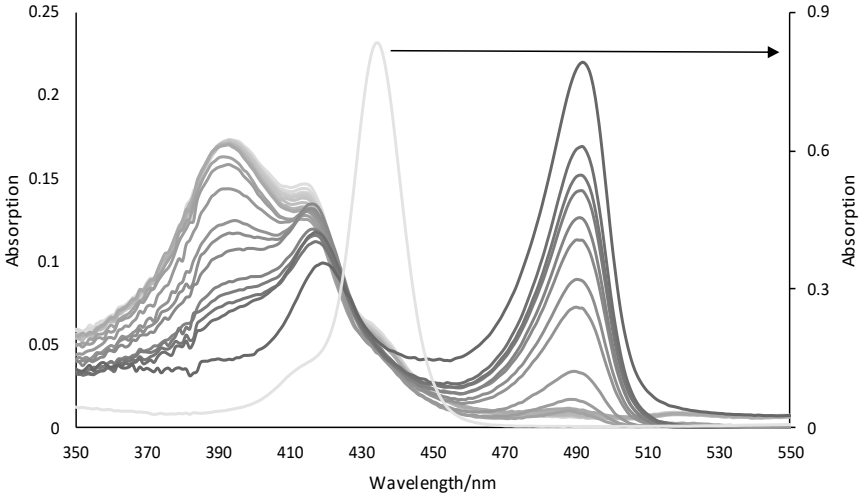

Figure 49 - Spectral representation of the kinetics of aggregation of TSPP in the presence of Chitosan (from light to dark grey; TSPP added first than Chitosan)

Here the kinetic curves were represented with the usage of two axes due to the very different time of analysis and in order to make the graphs clearer for analysis.

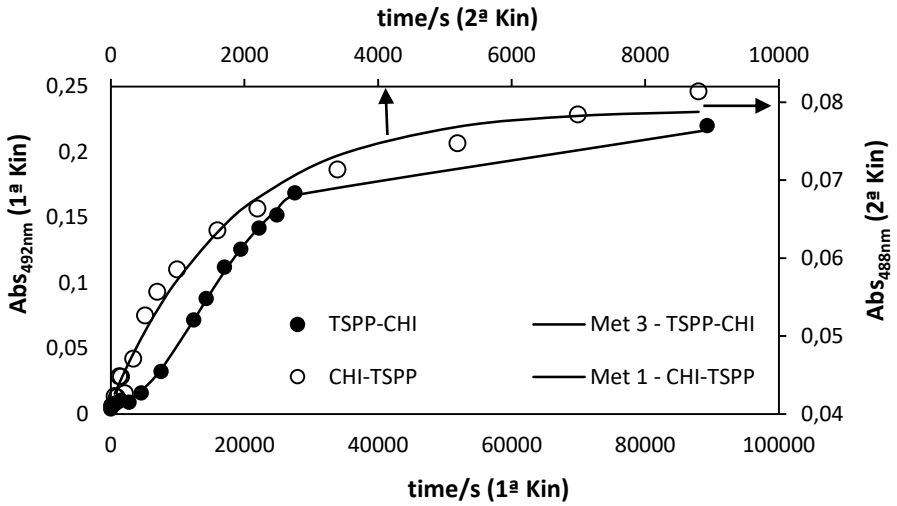

Figure 50 – Kinetic curves of Chitosan system for the two addition methods (Chi added to TSPP- full dots; TSPP added to Chi – hollow dots)

Table 3 - Kinetic parameters obtained for method 1, where TSPP was added to a Chitosan solution

E_m (M^{-1} cm^{-1})	E_j (M^{-1} cm^{-1})	k (s^{-1})
2071	4E+04	5E-04

Table 4 - Kinetic parameters obtained for method 3, where Chitosan was added to a TSPP solution

m	k_o (s^{-1})	n	k_c (s^{-1})
2	1E-05	2	8E-05

After the analysis of each system it was verifiable that for both the same kinetic model was applicable for the same addition method which demonstrates a resemblance in the kinetics of the aggregation in the presence of both polymeric systems. The necessity of the usage of two different models for adjusting the data is clear when observing the kinetic curves, with more visibility in the last due to the different evolution of it. When the polymer is added to the TSPP solution there is a lag time until the absorption of the aggregate starts ascending quickly, in opposition to the inverse addition in which this is immediate. This is in accordance with available kinetic studies with TSPP[56] and it originates from the fact that when TSPP is pipetted to the bulk solution it is highly concentrated and immediately enters in the contact with aggregating medium, whereas for the inverse addition the porphyrin is already diluted in solution. Nonetheless, the values obtained for PEI added first display a certain covariance and its physical meaning is not easily explainable. For the system in which the template is added second, chitosan leads to a faster aggregation kinetics.

3.2.3 Porphyrin without Polymer Systems

The previous studies with the polymeric systems – Chitosan and PEI – were made in order to verify if they eased the interactions between the porphyrin and the other components of the system – AuNP and GO. However, since it was verified that the polymers used promoted the aggregation of TSPP, an analysis without their presence was made to verify how the systems would behave. This experiment was made at acidic pH since it is the medium in which the aggregates occurred.

The first system analyzed involved the variation of the concentration of GO in the presence only of TSPP, which remained with a concentration of 2 µM.

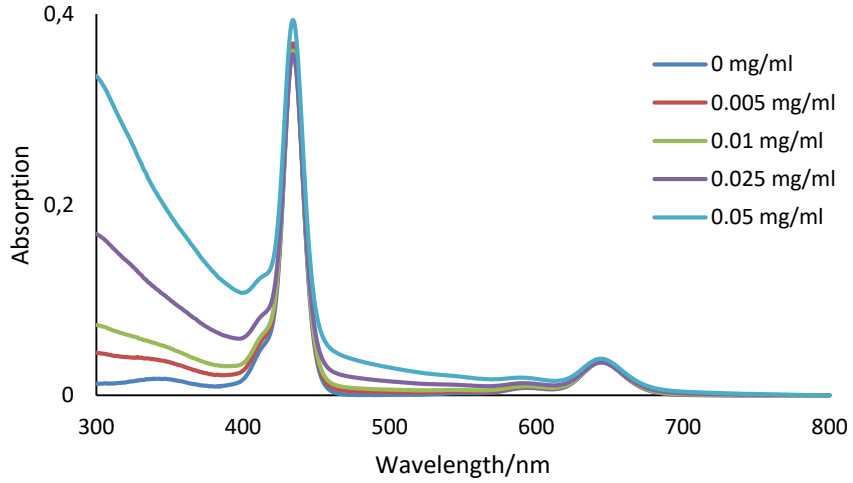

Figure 51 - Absorption spectra of TSPP in aqueous solution (pH 3.3) in the presence of increasing concentrations of GO

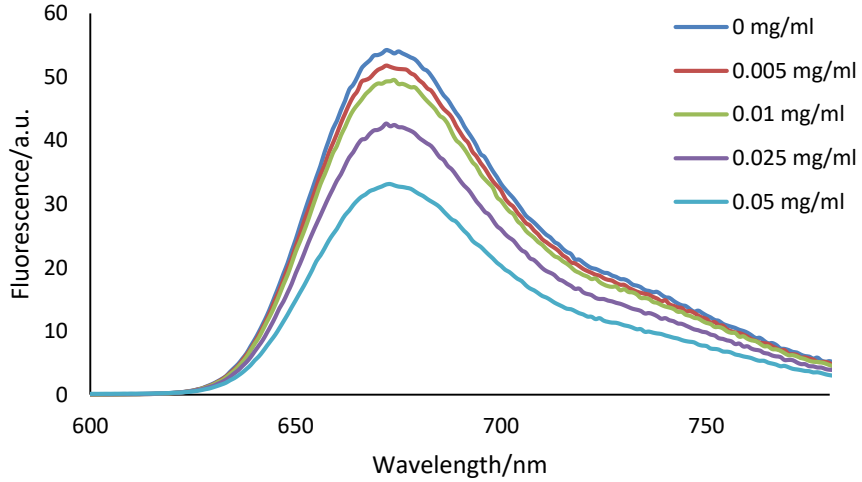

Figure 52 - Fluorescence spectra of TSPP in aqueous solution (pH 3.3) in the presence of increasing concentrations of GO (λ_{exc} = 445 nm)

The absorption spectra show nothing more than the effects of the increasing dispersion of the system due to the addition of graphene oxide. However, the fluorescence spectra reveal a very clear

quenching of the fluorescence of the porphyrin which becomes more significant with GO increasing concentration. With the data from these spectra and calculating the areas of fluorescence by the rectangle method it was possible to plot the ratio between the area without the quencher (GO) and the area of each concentration as a function of the concentration, in order to obtain a Stern-Volmer plot. Making the fit with the Stern-Volmer equation assuming the existence of both dynamic and static quenching (Eq. 3), it was possible to draw a fitting line and obtain the parameters.

$$\frac{I_0}{I} = 1 + (K_a + K_{SV})[Q] + K_a K_{SV}[Q]^2 \quad (3)$$

$$K_{SV} = k_q \tau_0$$

With K_{SV} being the Stern-Volmer quenching constant, K_a the constant of complexation GO-TSPP in the fundamental, k_q the quencher rate coefficient and τ_0 the lifetime of the solution without quencher.

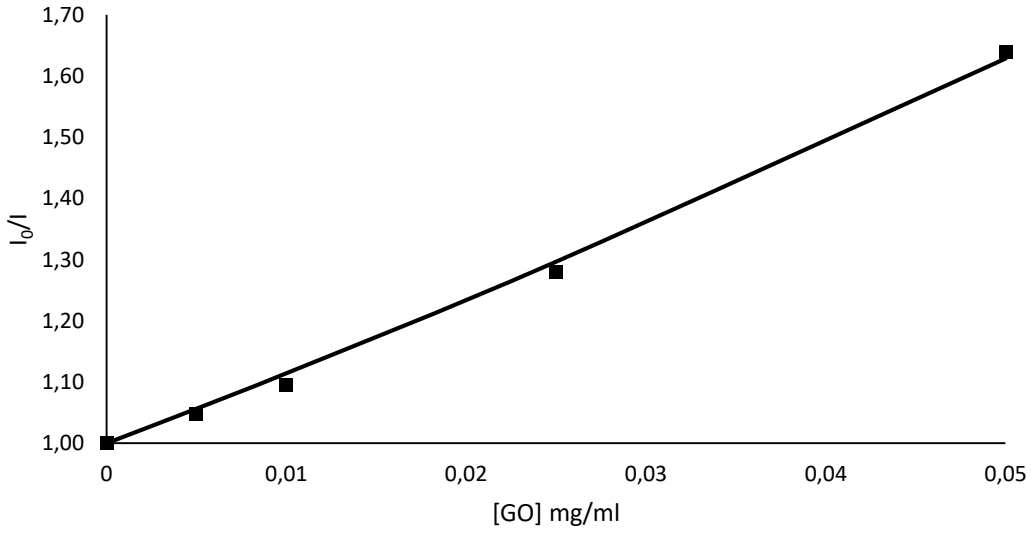

Figure 53 – Stern-Volmer plot for the quenching of fluorescence of TSPP with increasing concentrations of GO

Table 5 –Fitted Stern-Volmer equation parameters for the quenching of fluorescence of TSPP with increasing concentrations of GO

K_{sv} (ml mg^{-1})	3.9
K_a (ml mg^{-1})	7.3
k_q (ml mg^{-1} s^{-1})	1.0E+09

The other system analyzed was the one with all the components. Again, the concentration of GO was fixed to 0.05 mg/ml and in this case the volume of nanoparticles was varied from 0 to 70 µL.

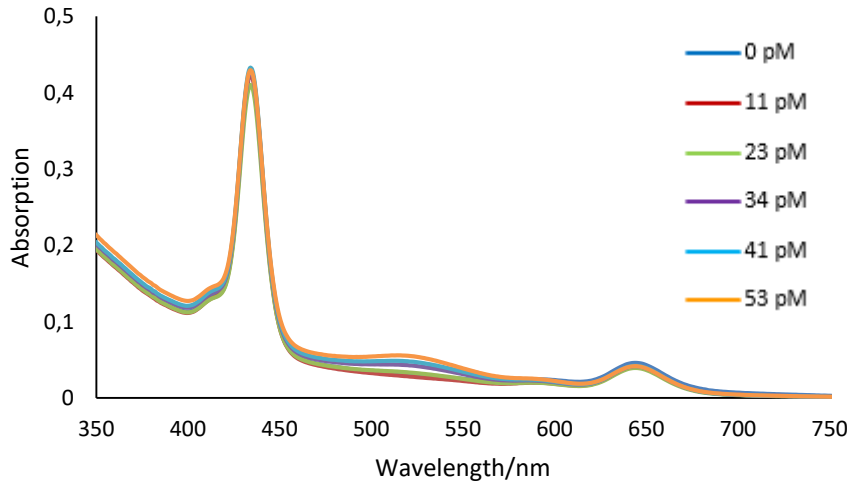

Figure 54 - Absorption spectra of TSPP in aqueous solution (pH 3.3) in the presence of GO and increasing concentrations of AuNP

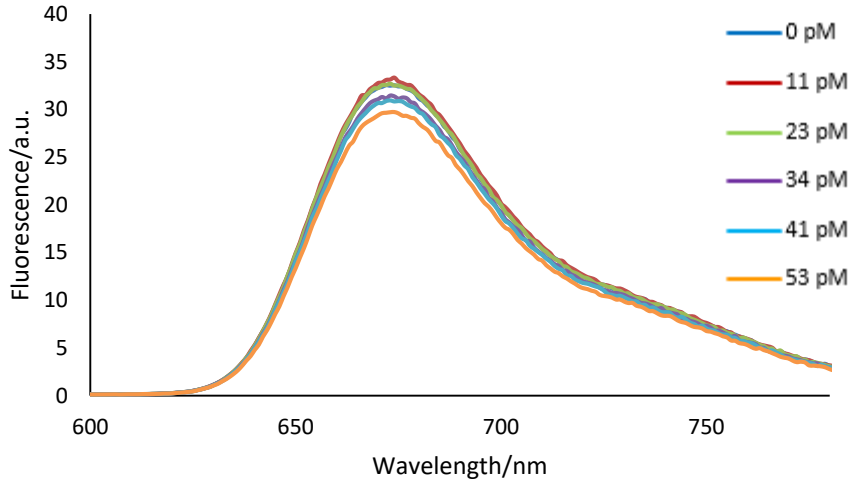

Figure 55 - Fluorescence spectra of TSPP in aqueous solution (pH 3.3) in the presence of GO and increasing concentrations of AuNP (λ_{exc} = 445 nm)

In this system, it is clear in the absorption spectra the plasmonic band of the nanoparticles with no further effect. There is a small quenching observed in the fluorescence spectra. This is in accordance with systems studied in the presence of the polymers where the same effect was verified.

3.2.4 Phthalocyanine Systems

Besides the used porphyrin the system was also tested with another class of photoactive molecules, namely a phthalocyanine. The used one was aluminum phthalocyanine tetrasulfonate (AlPcS4) which in comparison to TSPP had the advantage of having only one form for all the range of pHs and the same peripheral groups Tests were made as for the porphyrin with the two polymers and with the different conjugations of components already used.

Chitosan

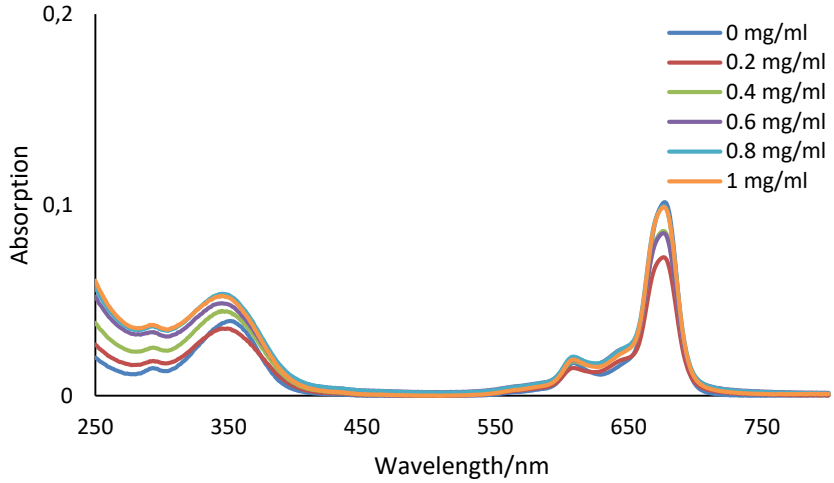

Figure 56 - Absorption spectra of AlPcS4 in aqueous solution in the presence of increasing concentrations of Chitosan

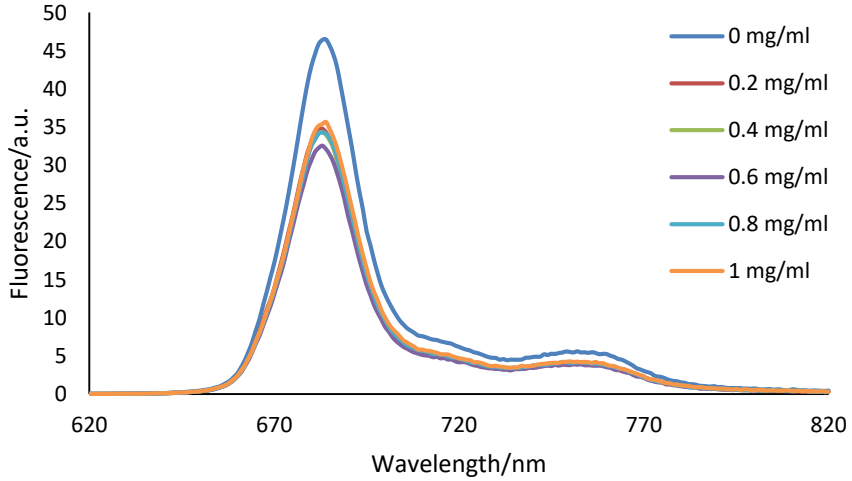

Figure 57 - Fluorescence spectra of AlPcS4 in aqueous solution in the presence of increasing concentrations of Chitosan (λ_{exc} = 600 nm)

For the system of the phtalocynanine with only chitosan the only effect that may be seen is a quenching with the addition of chitosan. Moreover, the lifetime analysis provided a single lifetime that remains stable around 5.2 ns, which is the characteristic lifetime of the phthalocyanine [57], [58].

Chitosan + GO

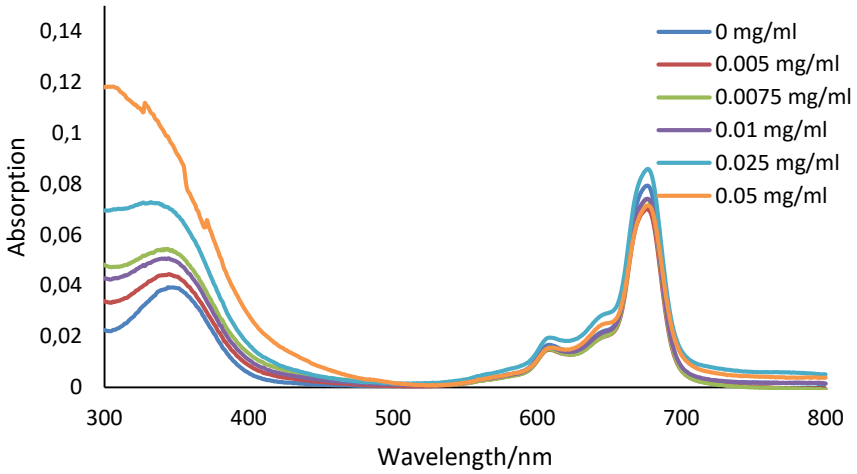

Figure 58 - Absorption spectra of AlPcS4 in aqueous solution in the presence of Chitosan and increasing concentrations of GO

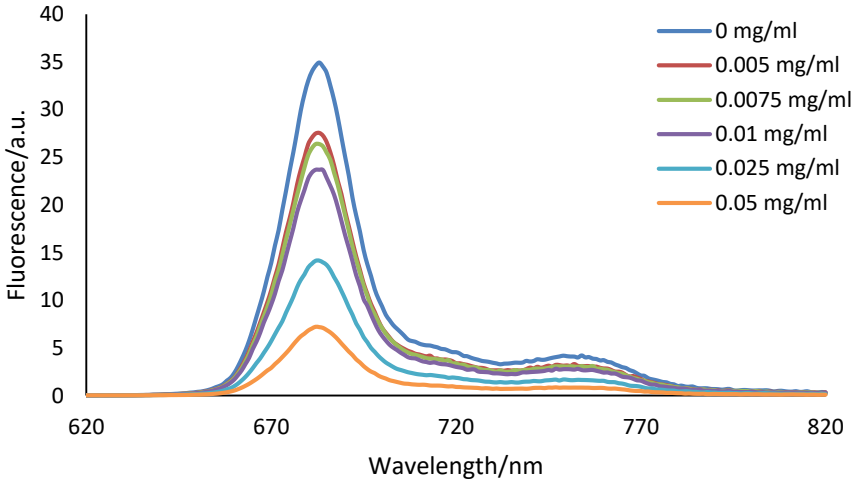

Figure 59 - Fluorescence spectra of AlPcS4 in aqueous solution in the presence of Chitosan and increasing concentrations of GO (λ_{exc} = 600 nm)

In this case, the addition of graphene oxide to the system led to a significant quenching in the fluorescence of the phthalocyanine. However, besides being affected by the high light scattering and absorption of GO, the lifetime (Table A1-14) remains as in the previous system around 5.2 with the increasing concentration of the quencher not having any effect. Only for the highest concentration of GO a shorter lifetime of 0.2 ns (this is shorter than the resolution of the equipment) has some weight in the decay. Nevertheless, the observed quenching of the fluorescence made it possible to build a Stern-Volmer plot to which a fitting was made as in the previous case (TSPP/GO at pH 3.5) in order to obtain the Stern-Volmer equation parameters.

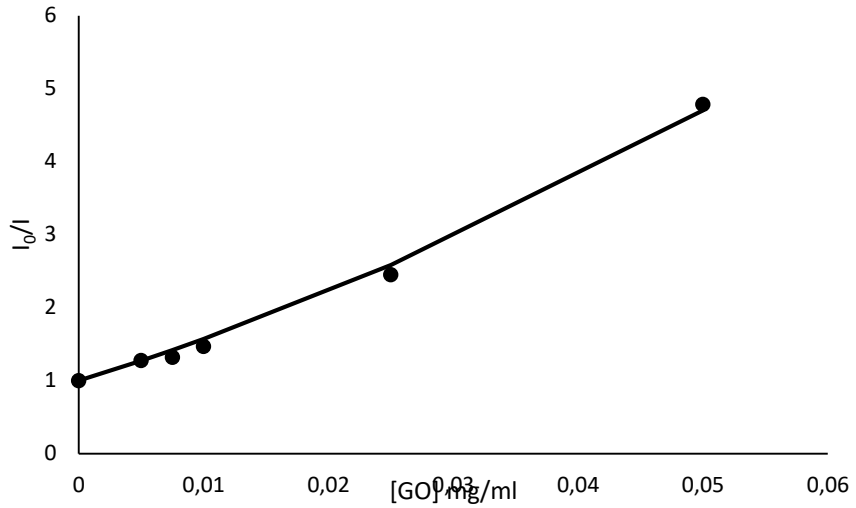

Figure 60 – Stern-Volmer plot for the quenching of fluorescence of AlPcS4 by increasing concentrations of GO in the presence of chitosan

Table 6 – Fitted Stern-Volmer equation parameters for the quenching of fluorescence of AlPcS4 by increasing concentrations of GO in the presence of chitosan

K_{sv} (ml mg^{-1})	10
K_a (ml mg^{-1})	43
k_q (ml mg^{-1} s^{-1})	2.0E+09

Chitosan + AuNP

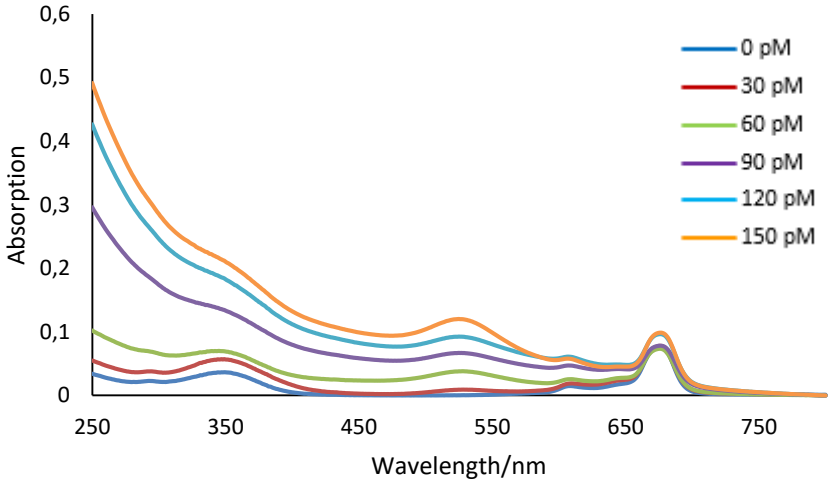

Figure 61 - Absorption spectra of AlPcS4 in aqueous solution in the presence of Chitosan and increasing concentrations of AuNP

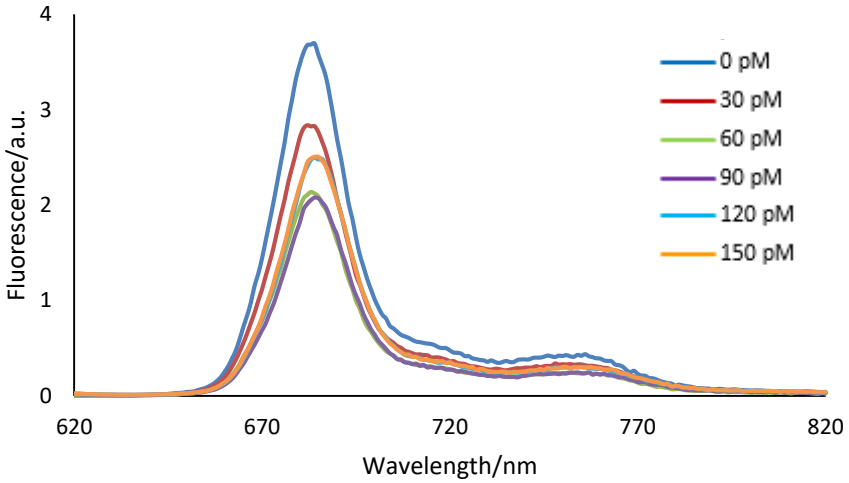

Figure 62 - Fluorescence spectra of AlPcS4 in aqueous solution in the presence of Chitosan and increasing concentrations of AuNP (λ_{exc} = 600 nm)

In the absorption spectra besides a small increase in the intensity of the main Q band at the highest volumes, there is no more significant modification, which is also difficult to identify due to the high dispersion of the system caused by the colloidal dispersion of the gold, with its plasmonic band c.a. 530 nm being very clear increasing its intensity with the growing volumes. The fluorescence spectra of the phthalocyanine reveals a decrease of its intensity that is inverted in the two highest volumes, in which there is an increase in the fluorescence intensity. This is in accordance with the fluorescence lifetimes (Table A1-14), since they reveal the presence of a smaller lifetime around 2.5 ns for the highest concentrations. The occurrence of a smaller lifetime with an increase in the fluorescence intensity in the presence of metallic nanoparticles is part of the phenomena of Metal-Enhanced Fluorescence (MEF). Thus, we may be in the presence of this effect, being significant for the highest volumes tested.

Chitosan + GO + AuNP

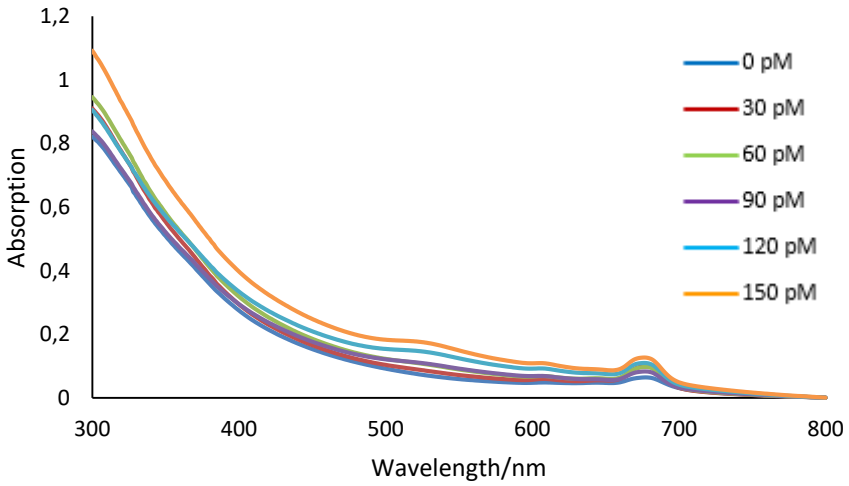

Figure 63 - Absorption spectra of AlPcS4 in aqueous solution in the presence of Chitosan, GO and increasing concentrations of AuNP

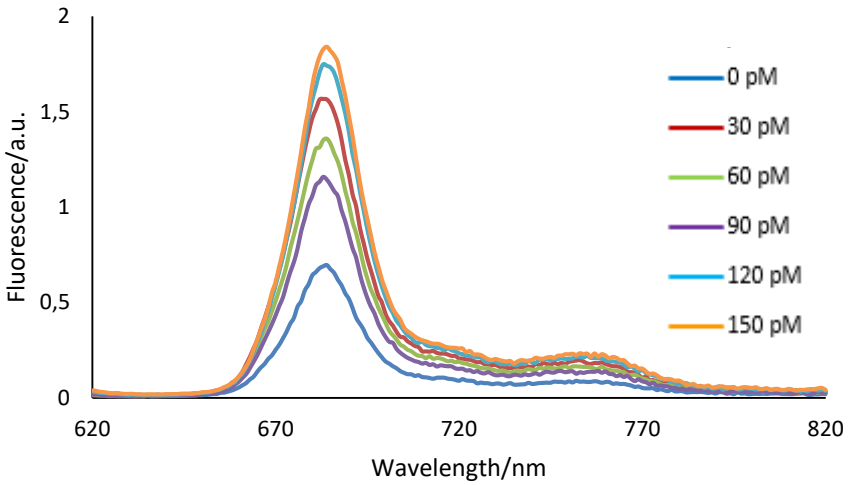

Figure 64 - Fluorescence spectra of AlPcS4 in aqueous solution in the presence of Chitosan, GO and increasing concentrations of AuNP (λ_{exc} = 600 nm)

For the system with all the components we see again as in the system with the nanoparticles what was there attributed to a possible MEF effect, since for the higher concentrations of nanoparticles we have an increasing of the fluorescence intensity. The lifetimes (Table A1-16) are also similar with that system with the presence of a shorter component and two components around 4 and 2 ns. However, in comparison with the referred system, there is now an increasing of the fluorescence above the intensity of the sample without nanoparticles. This may be due to the fact of the graphene oxide which is now present being a promoter of this effect.

PEI

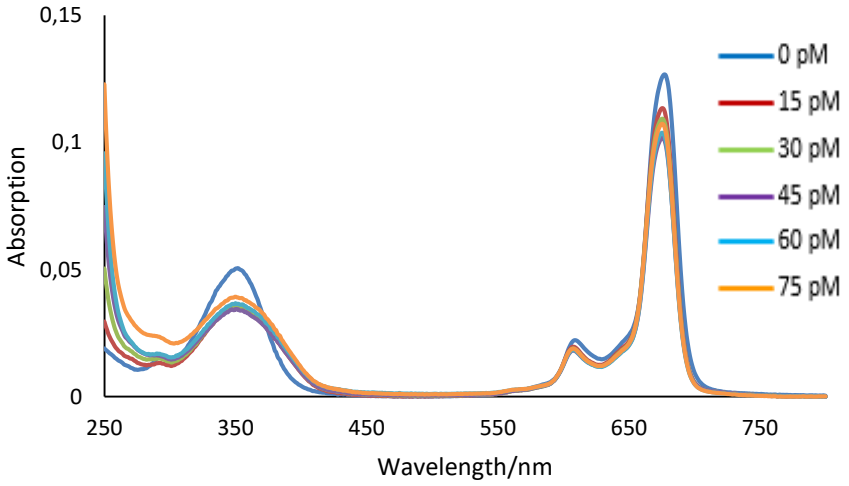

Figure 65 - Absorption spectra of AlPcS4 in aqueous solution in the presence increasing concentrations of PEI

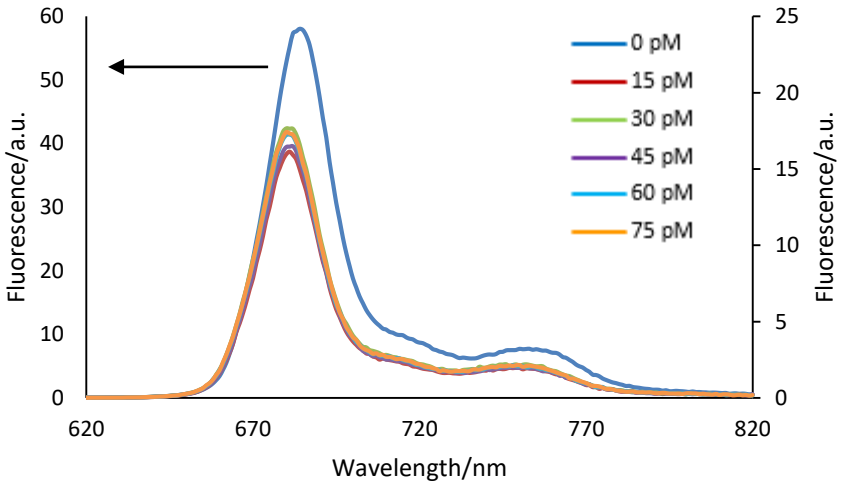

Figure 66 - Fluorescence spectra of AlPcS4 in aqueous solution in the presence of increasing concentrations of PEI (λ_{exc} = 600 nm)

With the addition of PEI, the spectra show a clear effect of the interaction between the phthalocyanine and the polyelectrolyte. In the absorption spectra, this is revealed by the enlargement of the Soret band (c.a. 354 nm) and a decrease in the intensity of the main Q band. The replication of this in the fluorescence spectra is a high quenching of fluorescence as well as a blue-shift of the spectra. This may be due to the formation of aggregates that as seen before lead to a complex fluorescence decay. This is also seen in this situation with the presence of the phthalocyanine monomer lifetime without the presence of PEI being lead, with the addition of the polyelectrolyte, to the presence of three lifetimes (Table A1-16): two in the same order of magnitude of the monomer but lower and another one 1-fold below, around 0.2 ns.

PEI + GO

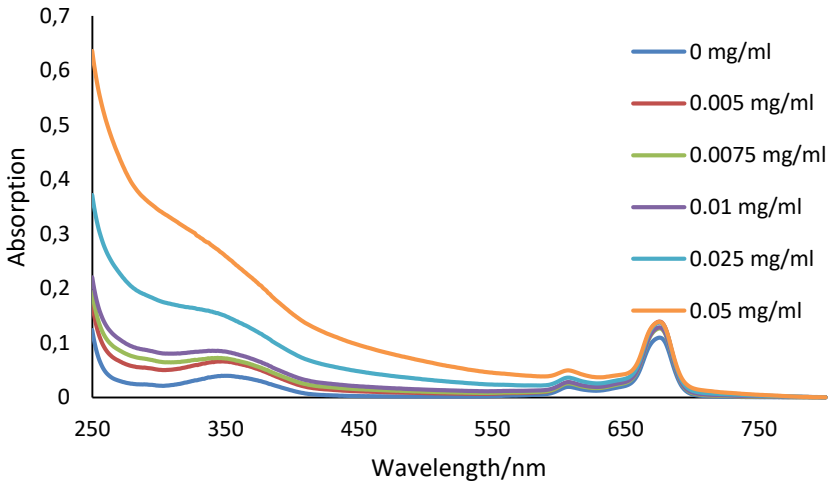

Figure 67 - Absorption spectra of AlPcS4 in aqueous solution in the presence of PEI and increasing concentrations of GO

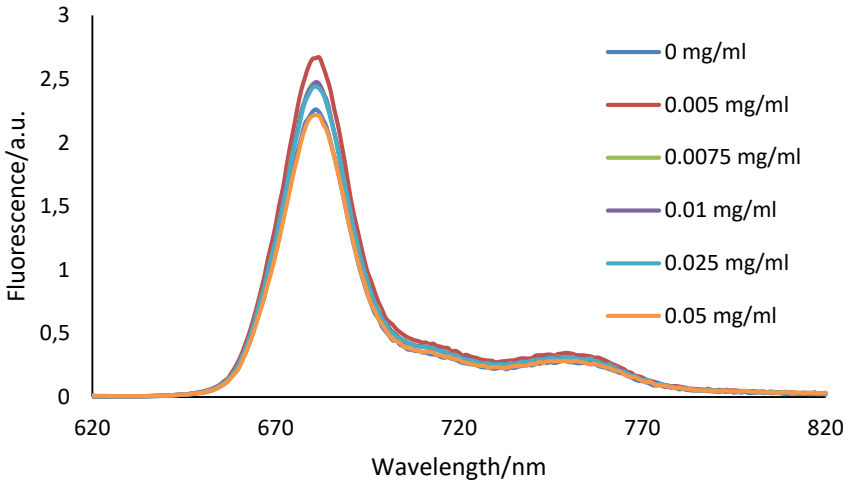

Figure 68 - Fluorescence spectra of AlPcS4 in aqueous solution in the presence of PEI and of increasing concentrations of GO (λ_{exc} = 600 nm)

Both the absorption and fluorescence spectra don't reveal any particular effect of the addition and increasing concentration of graphene oxide. The system seems to behave like the last one without GO, which is also reflected in the lifetimes with them being the same as before.

PEI + AuNP

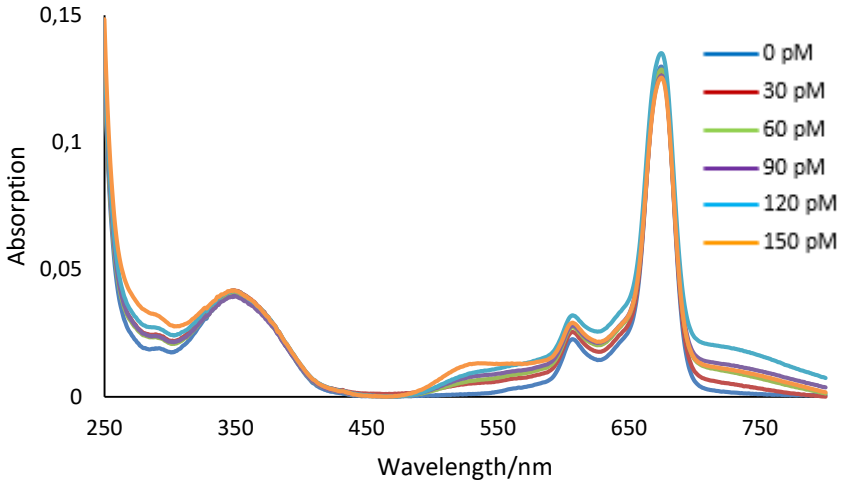

Figure 69 - Absorption spectra of AlPcS4 in aqueous solution in the presence of PEI and increasing concentrations of AuNP

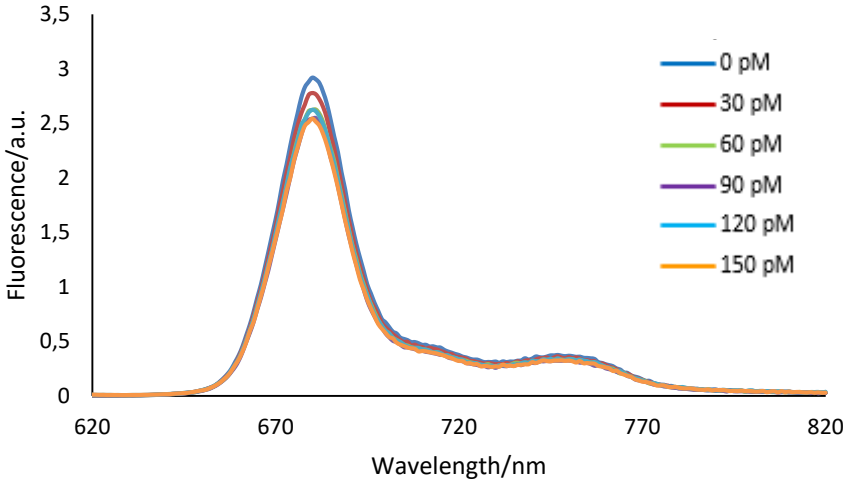

Figure 70 - Fluorescence spectra of AlPcS4 in aqueous solution in the presence of PEI and increasing concentrations of AuNP (λ_{exc} = 600 nm)

In the system with the nanoparticles instead of GO there is also no visible significant effect. Only a small decrease in the fluorescence intensity is observable. The lifetimes remain almost constant and equal to the system before.

PEI + GO + AuNP

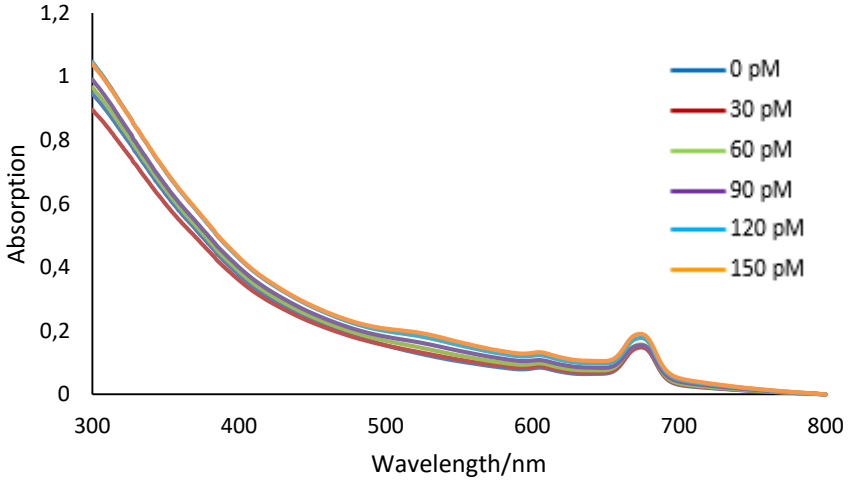

Figure 71 - Absorption spectra of AlPcS4 in aqueous solution in the presence of PEI, GO and increasing concentrations of AuNP

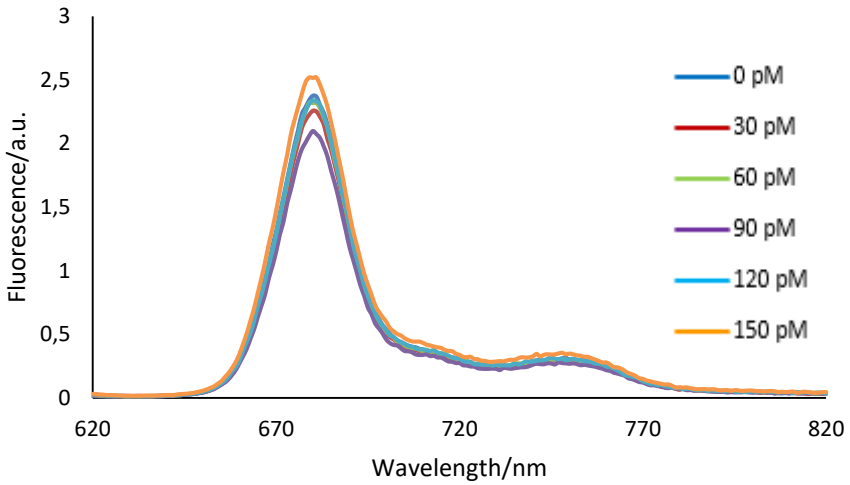

Figure 72 - Fluorescence spectra of AlPcS4 in aqueous solution in the presence of PEI, GO and increasing concentrations of AuNP (λ_{exc} = 600 nm)

For the system with all the components we see the same effect that in the equivalent with chitosan. Nevertheless, in the presence of PEI the increasing in the fluorescence intensity is lower for this system and it wasn't verified in the correspondent system with only nanoparticles as it was seen in the presence of chitosan. This may indicate that MEF effect is more prone to occur in this system with chitosan rather than polyethylenimine. The lifetimes (Table A1-16) are similar to the ones of the equivalent system with chitosan.

3.3 FLIM Characterization

Proceeding with the characterization of the systems under study, several data was obtained through fluorescence microscopy, namely fluorescence lifetime imaging microscopy (FLIM) for both the porphyrin and the phthalocyanine in the absence and presence of the components of the systems. The data and images obtained are described below. It is important to note that all the fluorescence being shown comes from the porphyrinoids, since the intensity of the excitation laser is not enough for providing the fluorescence of the graphene oxide.

The first system here analyzed is the one of the porphyrin with chitosan and GO. As seen in Fig. 60-A in the lifetime distribution upon the addition of each component to the system the average lifetime decreases. The FLIM images on the right show this by the appearance of darker regions upon the addition of the polymer (C) and the existence of blue spots distributed around the shown graphene sheets (D) that correspond to short lifetimes. The inset D' shows a formed J-aggregate. This is in accordance with previous fluorescence analysis in which it was verified that the addition of chitosan to the porphyrin at pH 3.5 induced the formation of J-aggregate, with a short lifetime as well as the fact that the presence of graphene oxide in the system quenched the fluorescence leading to a shorter average lifetime.

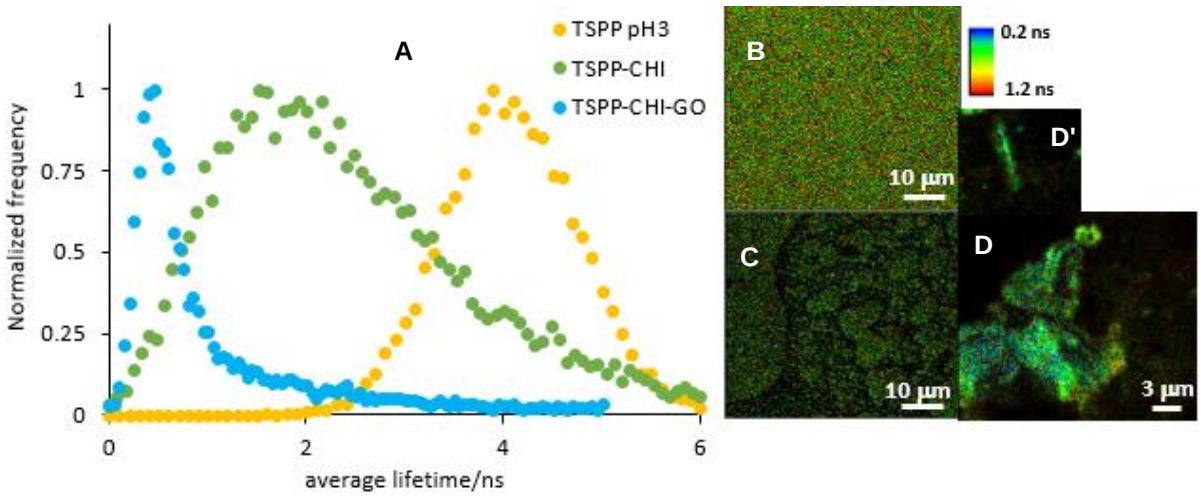

Figure 73 - Average fluorescence lifetime distribution (A) FLIM images (B, C, D) obtained from decay analysis of about 20 point measurements of cast drop solutions at pH=3 of TSPP (B), TSPP-CHI (C) and TSPP-CHI-GO (D) (with inset D' of image D)

For the equivalent system with PEI, the results are similar with the novelty being the fact that upon the addition of the polyelectrolyte there is no great reduction of the average lifetime, only the enlargement of the distribution. This fact is coherent with the fact that in the lifetimes analysis it was identified the molecular complex caused by the strong interactions between the porphyrin and PEI that produces a long lifetime at the same time as the referred J-aggregate produces a short lifetime, with the distribution being enlarged. For the presence of GO the effect is similar to the last analysis. The imaging shows the loss of uniformity with the presence of PEI (Fig. 61-C) and pictures, in the presence of GO, two of its sheets: one with a lighter blue color revealing high presence of quenched TSPP in it, and a greener sheet where the effect is not so clear.

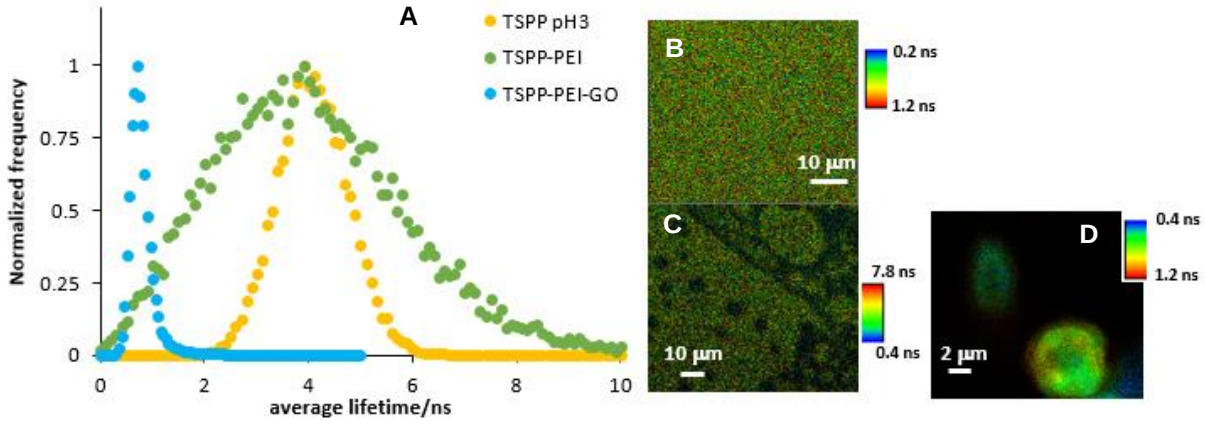

Figure 74 - Average fluorescence lifetime distribution (A) FLIM images (B, C, D) obtained from decay analysis of about 20 point measurements of cast drop solutions at pH=3 of TSPP (B), TSPP-PEI (C) and TSPP-PEI-GO (D)

As a final point about the FLIM analysis with the porphyrin a comparison between the full component system at the two-studied pH's is presented in Figure 74. The two graphene sheets displayed in the figure below reveal that the one of the acidic pH presents a high density of blue spots corresponding to short lifetimes, while in the case of pH 7, the blue areas are visible but the distribution of lifetimes in the graphene oxide sheet is more heterogenous. This may indicate that the distribution of the polyelectrolyte and the gold nanoparticles in the carbon material sheet is better achieved in the acidic medium revealing a better quenching of the porphyrin molecules in the sheet. This is something only noticed here in the deposited system since in the solution analysis no relevant differences between these two systems were gathered.

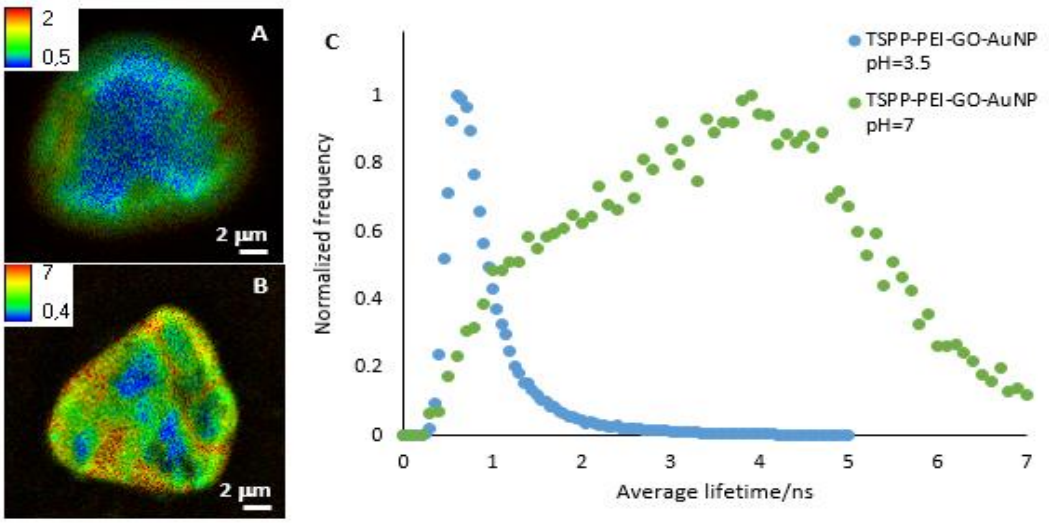

Figure 75 - FLIM images (A, B) and average fluorescence lifetime distribution (C), obtained from decay analysis of about 20 point measurements of cast drop solutions of TSPP-PEI-GO-AuNP at pH 3.5 (A) and pH 7 (B).

For the case of the phthalocyanine, it is shown in two following figures, the images and histograms for two situations: AlPcS4 with chitosan and with PEI, and the effect of the addition of GO. It is visible that only in the presence of the polymer there is a homogeneity in the lifetime distribution revealed both from the pictures and from the sharp curves of the histograms. With the addition of graphene oxide, it becomes visible in the FLIM images the occurrence of the blue short lifetime regions that would be the graphene sheets. The histograms indicate that the introduction of GO leads to a decrease in the lifetime that is more significant in the case of the phthalocyanine with chitosan. This however due to the fact that the interaction of PEI with the signaling molecule had already reduced the lifetimes, which can be seen by the comparison of this systems with the FLIM data of the phthalocyanine alone [59].

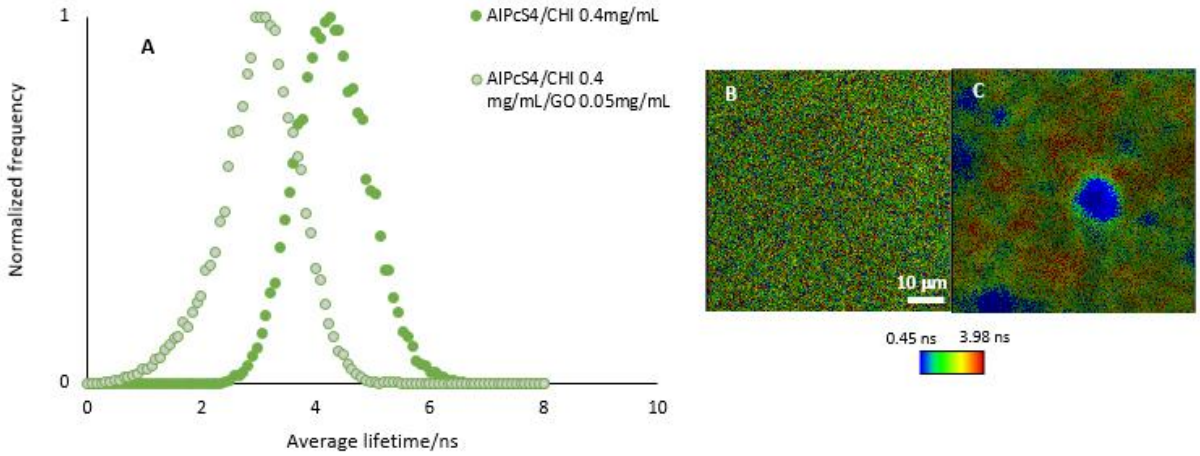

Figure 76 - Average fluorescence lifetime distribution (A) FLIM images (B and C) obtained from decay analysis of about 20 point measurements of cast drop solutions AlPcS4-Chi (B) and AlPcS4-Chi-GO (C)

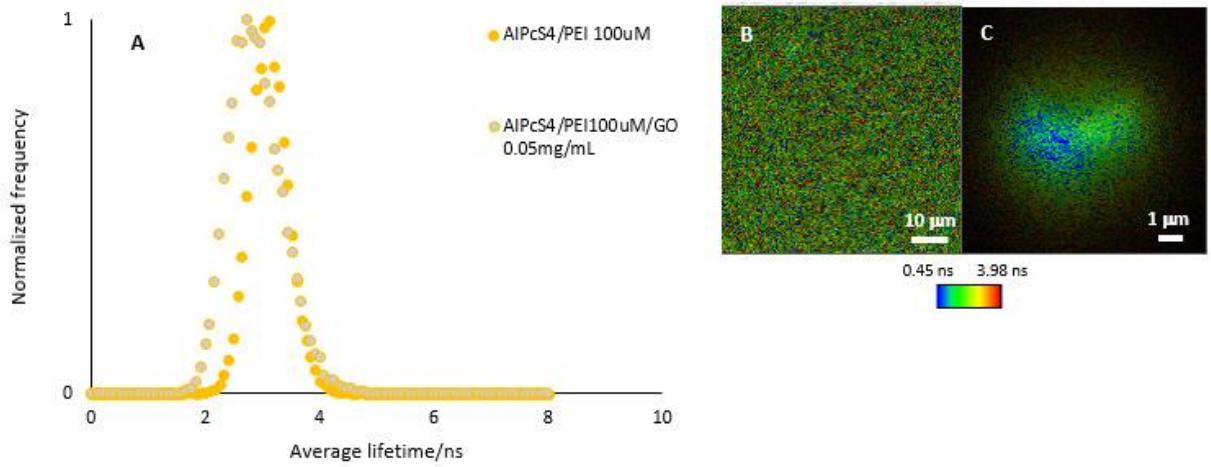

Figure 77 - Average fluorescence lifetime distribution (A) FLIM images (B and C) obtained from decay analysis of about 20 point measurements of cast drop solutions AlPcS4-PEI (B) and AlPcS4-PEI-GO (C)

The final approach is the comparison between the systems with all the components for each polymer. From the data below, the histogram clearly reveals more heterogeneity for the PEI system. This has correspondence in the FLIM image with the structure of the graphene sheet with the fluorescence signal being present only in its edges with these varying from areas of longer lifetimes to areas of higher density of short lifetimes. On the other hand, in the system with chitosan that present a sharper histogram presents the image of an almost circular graphene oxide sheet with well distributed lifetimes, being the shorter ones in its centre.

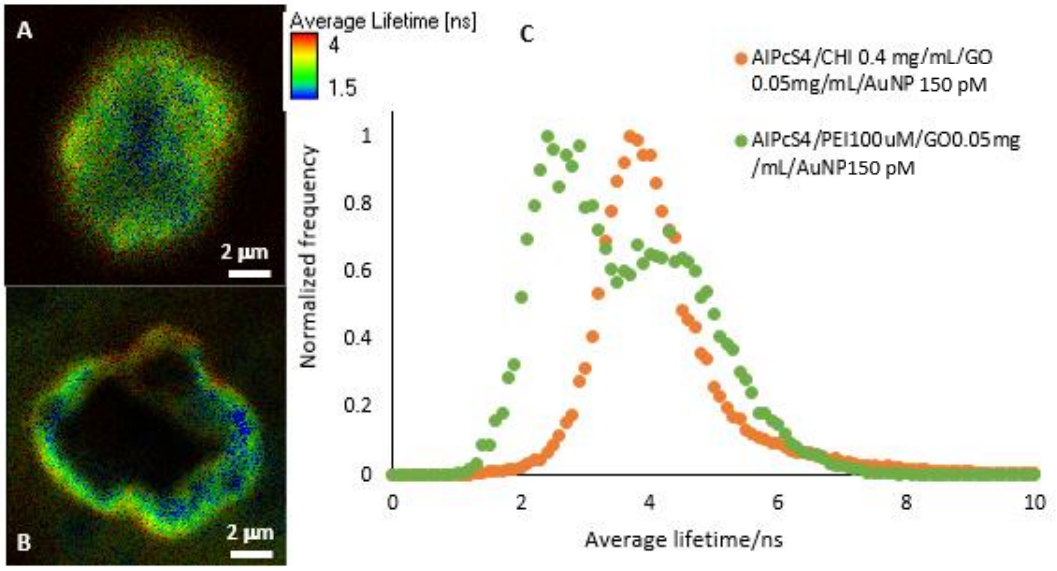

Figure 78 - FLIM images (A, B) and average fluorescence lifetime distribution (C), obtained from decay analysis of about 20 point measurements of cast drop solutions of aqueous AlPcS4/Polyelectrolyte/GO/AuNP (A-Chitosan and B-PEI).

After the study of the various systems and taking into consideration the reaction of oxidation of TMB that would be catalysed for the purpose of sensing the choice for catalyst was the system of TSPP without polymer at acidic pH. The option for the porphyrin instead of the phthalocyanine comes from the week interaction observed between the last and the other components of the system (i.e. GO and AuNP) in comparison to the verified with TSPP. The discard of the polymeric systems is based on the observed aggregation that reduced the fluorescence of the system while the option for an acid pH is determined by the optimum medium for the occurrence of the sensing reaction.

3.4 Sensing Analysis

In the sensing studies, the goal is to find out if the hybrid systems prepared and characterized above display peroxidase-like catalytic activity with improved sensitivity as compared to the natural system. Horseradish peroxidase (HRP) has been widely used to fabricate sensors for detection of the products of the glucose oxidase and hydrogen peroxide is the main product of glucose oxidase (GOx)-catalysed reaction [60]- HRP catalysis the reaction of 3,3',5,5'- tetramethylbenzidine (TMB) in the presence of H2O2. The former is a colourless compound that turns blue when oxidized (absorbing strongly at c.a. 652 nm) thus allowing to follow its variation over time in a very simple and relatively cheap way using UV-Vis absorption. Thus, before applying our systems several analyzes were made using the enzymatic system.

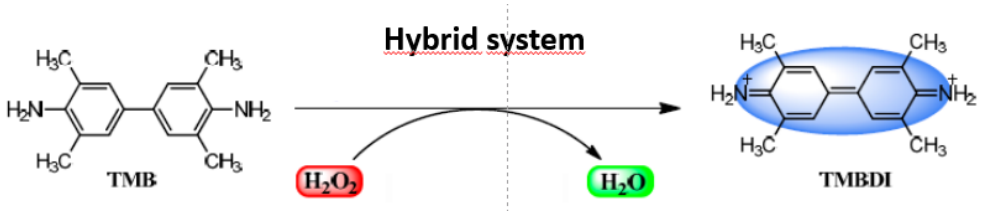

Figure 79 - Schematic representation of hybrid GO-AuNP catalyzed peroxidase mimic, oxidation of TMB into TMBDI in the presence of H2O2 and colorimetric chane used for detection.

3.4.1 TMB with HRP

The concentrations of HRP, TMB and H_2O_2 were optimized as described further below. With the optimized concentration of these components it was possible to evaluate the evolution of the spectra of the oxidized TMB through time as showed below. It is clear the formation of the two characteristic bands of the oxidized TMB (c.a. 372 nm and c.a. 652 nm) as well as a smaller band from the enzyme itself.

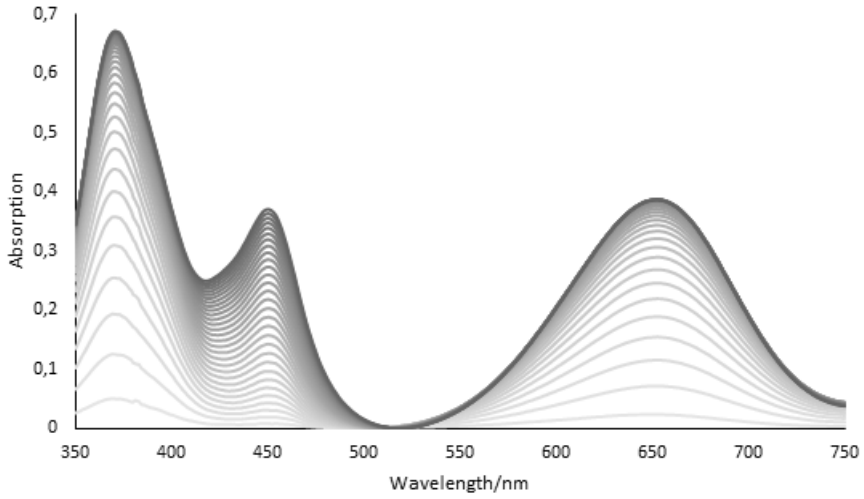

Figure 80 – Time evolution of absorption spectra for the oxidation of TMB (from light to dark grey)

Since in the first place the used solvent for TMB was dimethylformamide (DMF) and regarding the fact that this compound may have some effect on the environment of the system, mainly if the volume used was superior to 1% of the total, it was tested as solvent HCl 0,2 M, which had been used in early studied with this molecule[10]. A comparison between the oxidation process with TMB in each of the solvents was made. In Figure 81, it is possible to observe the two spectra obtained for the oxidized TMB achieved in the two solvent conditions. As noticeable, there is no significant difference between the use of the two solvents. Thus, since there are also no differences in terms of storage of the solution, it was decided to work with TMB in hydrogen chloride.

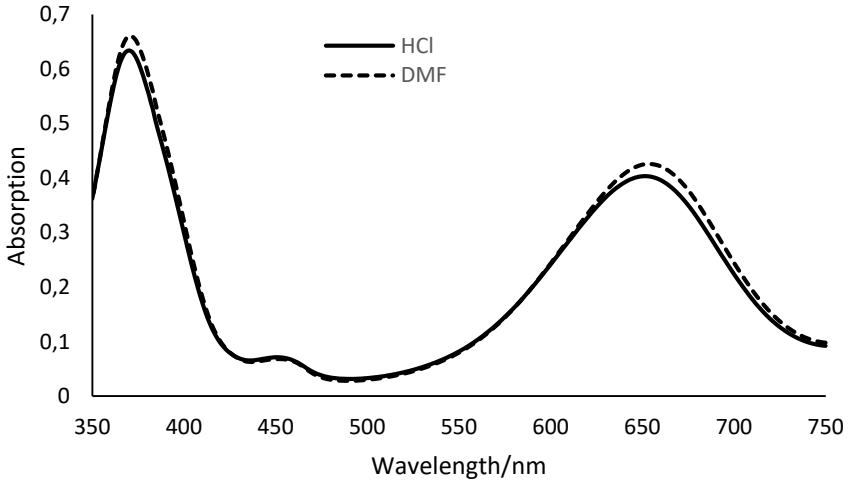

Figure 81 – Absorption spectra of oxidized TMB prepared in two different solvents

As described before there was a need for the optimization of the concentrations and proportions of the components of the reaction of reduction of hydrogen peroxide by HRP. This is due to the high sensibility of the reaction to these parameters. Several studies shown below describe the evolution in time of the main peak of the oxidized TMB in different conditions through an optimization process.

The first optimization shown in the graph below involved testing the proportion of hydrogen peroxide in relation to TMB with the enzyme concentration fixed at 250 ng/ml. Proportions of 3:2 and 1:2 of H_2O_2 to a fixed concentration of TMB of 10 µM were tested and as it is possible to see for the 3:2 proportion the reaction was very quick and the product was consumed immediately. For the 1:2 proportion the reaction occurred in almost 3 minutes and the product remained almost stable for the time period. Thus, a proportion of 1:2 of hydrogen peroxide to TMB was used in all the following experiments.

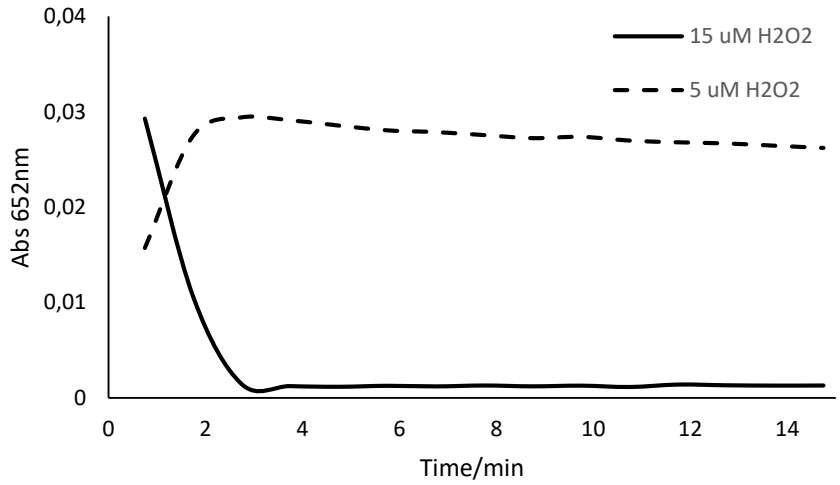

Figure 82 - Time-based evolution of the absorption peak at 652 nm in the case of two different concentrations of H_2O_2 with an enzyme concentration of 250 ng/ml and TMB concentration of 10 µM

Using the optimized proportion, the concentration of the enzyme was tested by comparing the obtained curve with the concentration of 250 ng/ml that had been used before with a lower concentration of 10 ng/ml. As seen in Fig. 63 the curves converge to the same point with the reaction with lower concentration of HRP being slower, which would be expected since the concentration of the catalyst has a paramount contribution to the velocity of the reaction.

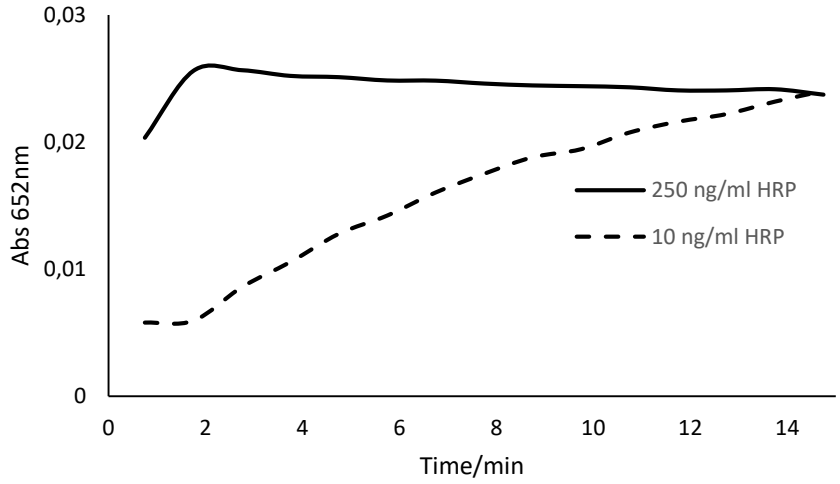

Figure 83 - Time-based evolution of the absorption peak at 652 nm in the case of two different concentrations of HRP with TMB and H_2O_2 concentrations of 10 and 5 µM respectively

The next experiment consisted in using the same proportion of hydrogen peroxide to TMB, test a higher concentration of the components, namely in this case 1-fold higher. This was due to try to achieve a higher signal, which as seen in the graph below was accomplished by the achievement of an absorption intensity 1-fold higher.

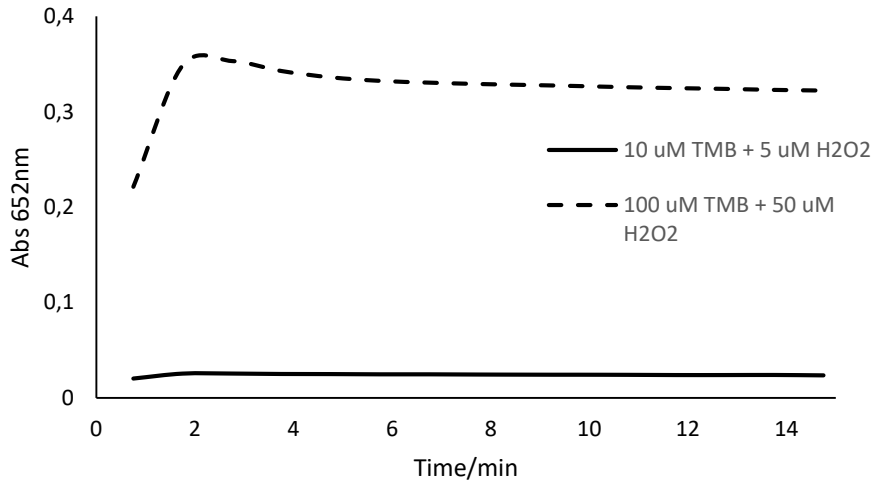

Figure 84 - Time-based evolution of the absorption peak at 652 nm in the case of two different orders of magnitude of same proportion of TMB and H_2O_2 with an enzyme concentration of 250 ng/ml

As done before, the concentration of enzyme was also analyzed in this new concentration of the components. The results were similar to the obtained in the other experience with the slower reaction that in this case, after 15 minutes, reaches an absorption value higher than the one of the higher concentration of HRP. This is obviously due to the fact that the reaction with higher concentration of enzyme had already consumed some of the product, but since the final value for the lower concentration is around the one in the peak of the lower one it means that after 15 minutes the reaction is almost complete.

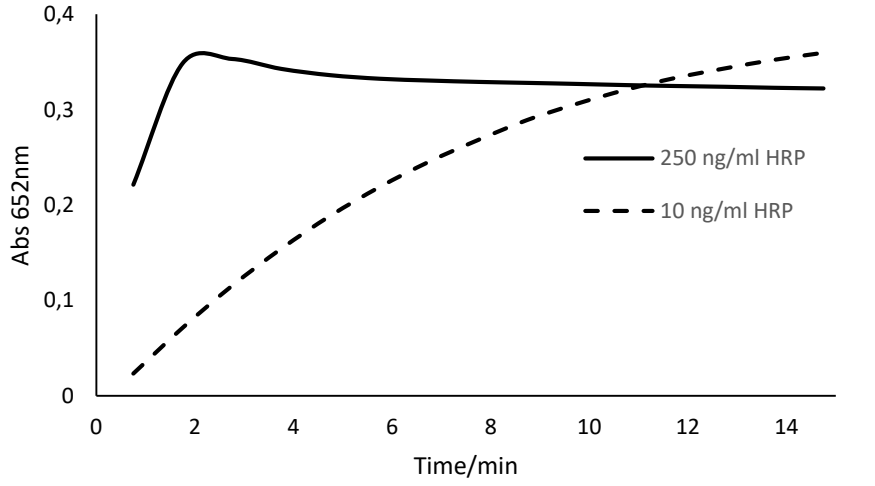

Figure 85 - Time-based evolution of the absorption peak at 652 nm in the case of two different concentrations of HRP with TMB and H_2O_2 concentrations of 100 and 50 µM respectively

3.4.2 TMB with composite

After the experiments with the enzyme HRP and with the proportions and concentration of TMB and H_2O_2 the following step was the test of the reaction with our studying systems, with the final goal being the sensitivity of the reaction of oxidation of TMB to a varying concentration of hydrogen peroxide so that the testes system could be used as a sensor for H_2O_2.

One of the first tests consisted in the evaluation of a simple system with only the porphyrin of study (TSPP) with a concentration of 1 µM, a fixed concentration of 100 µM of TMB. The concentration of hydrogen peroxide was varied between 5 and 100 µM and, as seen below, it is noticeable a tendency of increasing of the absorption at the main peak of the oxidized TMB with the concentration of H_2O_2 which shows the peroxidase-like catalytic ability of TSPP. Since this analysis was made in the micromolar range this reveals a good sensitivity that could lead to a promising sensing application.

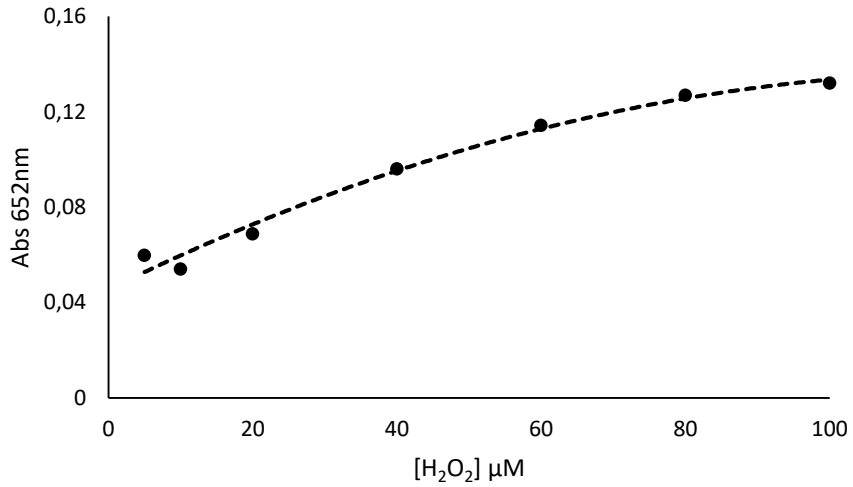

Figure 86 – Absorption peak at 652 nm value for oxidation of TMB in the presence of increasing concentrations of H_2O_2

Nevertheless, the main problem that was faced with the testing of the oxidation of TMB by hydrogen peroxide with our systems of study as catalyst was the time needed for the reaction to occur. In fact, the system was need to let react overnight in order to the reaction be complete. Thus, in order to try to speed the reaction, the reaction system was irradiated with the Xenon lamp [13]. The comparison between the irradiated sample and the one that reacted for 21 h is shown in Fig. 87. From there it is noticeable that the irradiation speeds the reaction, although not enough to achieve the same level as the non-irradiated. This question posed as a main issue in the development of our sensing system.

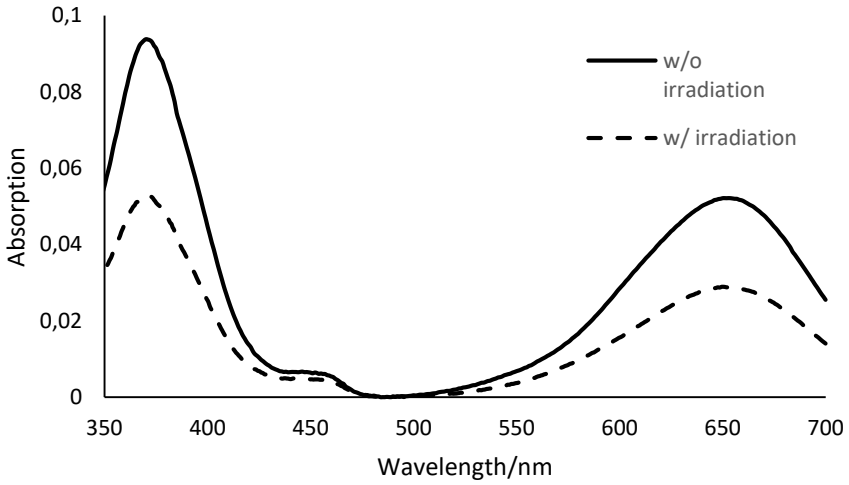

Figure 87 – Spectra of oxidized TMB in the presence of GO/AuNP composite after 21 hours without irradiation and immediately after irradiation with the Xenon lamp

Using the procedure of letting the reaction to happen overnight, the system was tested with all the components studied before We started by exploring the pH effect upon the system, pertinent taking into account the results of our studies above which involved two charged species (TSPP and GO) with pKa in the range of 4 to 6. Besides, the catalytic activity of HRP was also reported to be dependent on the solution pH [61].

A) pH effect

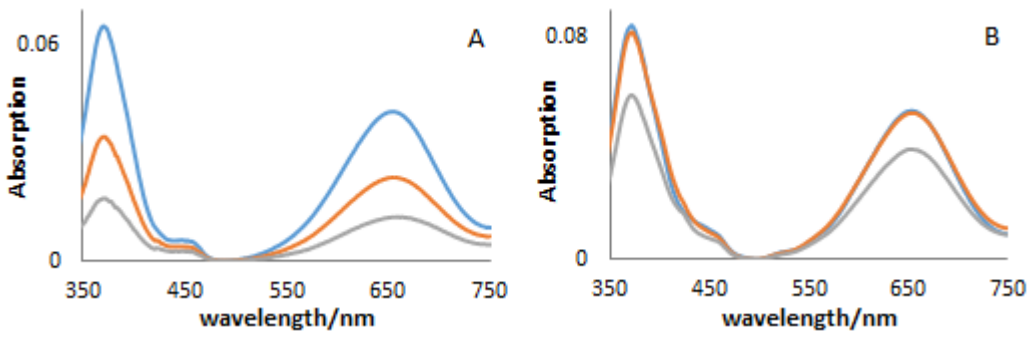

Figure 88 - Spectra of oxidized TMB in the presence of H_2O_2 using (A) GO and (B) TSPP as catalysts after 21 hours at different pHs (blue- pH 4.4; orange – pH 5; grey – pH 5.6).

The solution pH has a significant effect on the catalytic ability of both GO and TSPP. Another curious pH effect was detected when testing the catalytic ability of TSPP working at pH 3. Under such conditions the formation of J-aggregates was induced which was completed in the first 3 minutes of the reaction. Afterwards, an increase of the band corresponding to the oxidized TMB occurred. This can be understood by the role of the amino groups of TMB that stabilize the in-line aggregate through a hydrogen bond network which acts between the anionic sulfonate groups and the charged protonated nitrogen atoms of the porphyrin. This must be similar to the effect reported above for PEI and chitosan.

Taking into account these results, pH 4.4 was selected for the posterior tests. A preliminary study using just one of the components, TMB or H_2O_2, showed that in all cases the reactions only took place when both were present. Temperature is known to also influence the reaction [62], therefore it was kept constant for all experiments at 25 ºC.

B) No addition of porphyrin

First it is shown in Fig. 89 the system without the porphyrin, in which the oxidation is achieved in all cases. Nonetheless, the system composite of GO and the gold nanoparticles was the most efficient, which highlights the synergistic effect of the interaction between the two components.

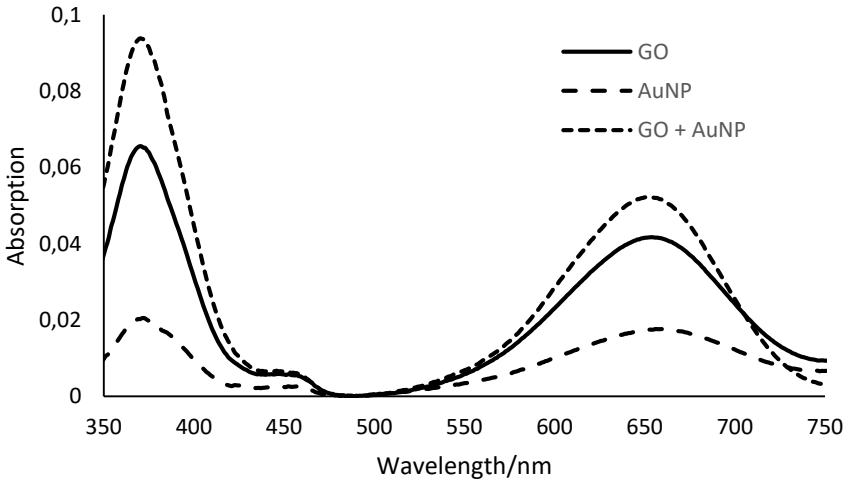

Figure 89 – Absorption spectra for the oxidation of TMB in the presence of H_2O_2 and graphene oxide and gold nanoparticles alone or in composite

C) Addition of porphyrin

Proceeding to the analysis with the porphyrin, Fig. 90 shows that the reaction occurred in the presence of the porphyrin, as shown already, and that the addition of gold nanoparticles led to an enhancement of the signal of the reaction, again pointing out the synergistic effect of the interaction between the two components. A strange result was the non-occurrence of significant reaction in the presence of graphene oxide that is not in accordance with all the remaining data. The interaction TSPP – GO seems to prevail and therefore, and none of the two components is available for the oxidation of TMB.

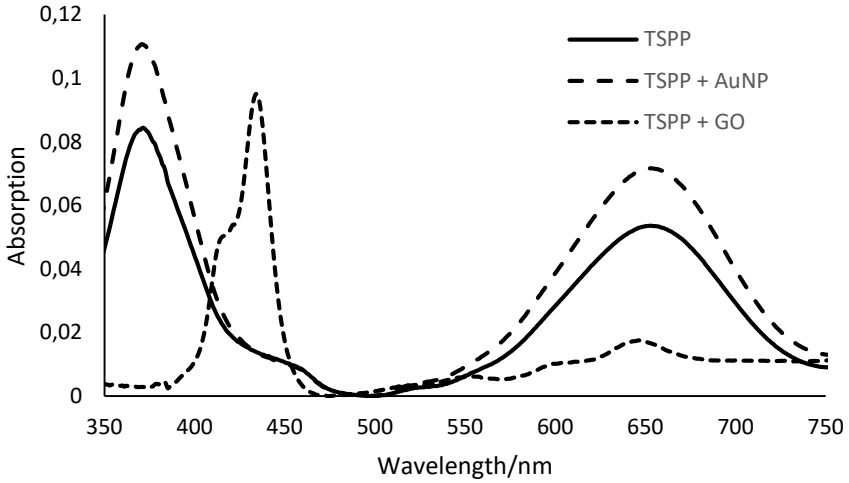

Figure 90 - Absorption spectra for the oxidation of TMB in the presence of H_2O_2 and TSPP without and with gold nanoparticles or graphene oxide

Chapter 4

Conclusions and Prospects

A study of systems with a photoactive molecule (porphyrin or phthalocyanine) associated or not with composites of gold nanoparticles and graphene oxide was made. This involved a characterization of the synthetized carbon material and nanoparticles. Transmission electron microscopy images showed the graphene oxide sheets and the spherical nanoparticles allowing to estimate the size of the latter. RAMAN spectra was performed for the carbon material confirming its nature as graphene oxide.

Furthermore, the spectroscopic analysis of the system revealed information about the interaction of the components of the systems. It was revealed that the presence of the studied polymers – chitosan and PEI – promoted the aggregation of TSPP in its acid form, leading to the formation of mainly J-aggregates, with H-aggregates being also noticed in the presence of PEI. Besides this, a formation of a strong interaction between the porphyrin and the polymers was traduced in the appearance of a molecular complex that was noticed by the red-shift in the spectra and the presence of a long lifetime in the fluorescence decay analysis. With the addition of graphene oxide there is a quenching of the fluorescence with its increasing concentration. For the case of the chitosan system an analysis was made verifying the occurrence of static and dynamic processes of fluorescence quenching. In the case of PEI system, it was noticed that the presence of GO reduced the effect of the polyelectrolyte. The addition of only gold nanoparticles produced little effect on the spectra with exception of the acid form of TSPP in the presence of chitosan. For the composite with the nanoparticles and the carbon material it was also shown nothing more than a small quenching of the fluorescence of the porphyrin with the increasing volume of nanoparticles, for all cases. The lifetime analysis here was compromised by the presence of a mixture of aggregates, monomer and even the referred complex.

The kinetics of TSPP aggregation process induced by polymers was analyzed using distinct aggregation kinetic models. Curiously, the aggregation kinetics of TSPP was not particularly affected by the nature of the template used (PEI vs. chitosan) but showed a remarkable dependence on the order of mixing components. A faster aggregation process occurred when the polymer was added in the first place due to the immediate interaction of the pipetted concentrated TSPP with the bulk of polymeric system, whereas for the opposite order of mixing a lag time was observed. Therefore, there was an additional process involving the formation of a “critical nucleus” which is the rate-determining step in the process, before the fast grow of the J- aggregate.

A similar analysis was performed in which TSPP interaction with the nanocomposites was tested in the absence of polymers. Under such conditions, it was revealed a clear quenching of TSPP fluorescence in the acid form with the addition of graphene oxide and its increasing concentration. It was possible to build a Stern-Volmer plot. The equivalent system with the addition of gold nanoparticles showed little of the latter.

The same procedure was made with the phthalocyanine, in this case in the presence of polymers. Only PEI seems to have a clear effect in the spectral properties of AlPcS4, where the blue-shift of the absorption spectra together with the appearance of a shorter lifetime, indicated the formation of non-specific aggregates. GO alone is known to have almost no effect on the spectral features of the phthalocyanine due to very effective electrostatic repulsions. However, in the presence

of chitosan an efficient quenching of the dye's fluorescence took place. On the other hand, it was known that this phthalocyanine interacted with AuNP (especially with Au nanorods). This seems also to be the case for the system with chitosan-AuNP but not with PEI-AuNP. For the former system, there is a quenching that is inverted for the highest concentrations of AuNP with an increasing in fluorescence that was attributed to a possible Metal Enhanced Fluorescence effect. This effect was even more pronounced for the systems with all the components (GO-AUNP-polymer), which in the case of chitosan led to fluorescence intensities higher than the sample without nanoparticles. For the system with PEI the effect could also be observed but with less significance. These results highlight the importance of GO in the support and distance control of the AuNPs and the dye. This was a clear case of a synergistic effect gained from the combination of both nanomaterials.

Finishing this part, the FLIM analysis allowed the visualization of the fluorescent areas in the drop cast of the solutions as well as the lifetime distributions. It was verified the reduction of lifetimes upon the addition of the polymers and more significantly, with the addition of GO to the system. In the latter case, it was possible to visualize graphene sheets with the dye covering its surface. It was revealed a more efficient reduction of lifetimes with the acid TSPP than with the tetraanionic TSPP, and the presence of a more uniform distribution with lower lifetime in the first case. For AlPcS4 it was also extractable the information of a more uniform distribution of lifetimes in the presence of chitosan than with the PEI counterpart, in which the dye is concentrated in the edges of the graphene sheets.

Since the objective of this study was the detection of hydrogen peroxide, the sensing experiments were the final and decisive step. Through the testing of the system with the analyte of study and our sensing molecule TMB in the presence of its natural catalyst HRP it was possible to reach the optimal conditions for the reaction in terms of reaction signal and velocity. They were achieved with concentrations of 100 µM of TMB and 50 µM of H_2O_2, achieved in the presence of 10 ng/ml of HRP.

Under these concentrations and proportion, the system was tested with the photoactive molecule TSPP and the composites. An experiment with increasing concentrations of hydrogen peroxide in between 5 and 100 µM in the presence of TSPP and TMB lead to a response of the system with an increase of the signal of the TMB oxidation that lead to a sensitivity of the system to the analyte. This is a good indicator to the possibility of the building of a sensor in that range of concentrations. However, the reaction of oxidation of TMB was verified under our conditions to be very slow with the experiments involving the reaction to occur overnight. It was tested the easing of the reaction upon the irradiation of the reaction solution that actually made the reaction occur quicker, despite not with the same intensity. Experiments with the other components were performed, revealing the occurrence of the reaction except for the TSPP/GO system. TSPP/AuNP and GO/AuNP revealed to be the most efficient systems.

With this study, it was possible to achieve great information about the behavior of the interaction of the system with the porphyrin and the phthalocyanine in the presence of graphene oxide and nanoparticles. The MEF effect is of paramount importance in the field of bioimaging and cancer therapy either by exploring its potential in photodynamic therapy (due to the presence of the porphyrinoid sensitizer) or the photothermal effect provided by the presence of AuNP. Another

important indication from this work was the reinforcement of the potential peroxidase-like activity of the hybrid, which indicate the possibility of the usage of the studied system to build a molecular sensor for hydrogen peroxide. This field is of great importance taking into account the possibility to be extended to measures of glucose levels with improved sensitivity. The combination of GO and AuNP provide several advantages as compared to others, which include: their extremely large surface area and the extended possibilities of further functionalization (e.g. with porphyrinoids; biomarkers, etc.); they are robust and stable system; easy to prepare and to purify; and their cost is lower than those with the natural peroxidases.

Nonetheless, further tests should be performed. Future developments to this work may involve the improvement of the reaction of oxidation of TMB that was used as sensing molecule. This shall be done to achieve a faster time-response. Furthermore, optimization of the composites may be done to increase their efficiency as catalysts. A catalysis study through kinetics of the reaction is an aspect that wasn't performed and would be a fundamental step in the process of the construction of the sensor. With the enhancement of the reaction the evaluation of its sensitivity to the concentration of the analyte would be the final step with the testing of various ranges of concentrations, and the analysis of the linearity of the response upon the usage of different conditions. All this in the quest to achieve a linear response to the concentration of H_2O_2 that could be fitted to a calibration curve and that would allow the detection of unknown concentrations of our analyte in the nanomolar range of concentrations.

References

[1] J. X. J. Zhang and K. Hoshino, “Introduction to Molecular Sensors,” in *Molecular Sensors and Nanodevices*, 2014, pp. 1–42.

[2] P. K. Sekhar, E. L. Brosha, R. Mukundan, and F. H. Garzon, “Chemical Sensors for Environmental Monitoring and Homeland Security,” *Electrochem. Soc. Interface*, vol. 19, no. 4, pp. 35–40, 2010.

[3] X. Wang and O. S. Wolfbeis, “Fiber-Optic Chemical Sensors and Biosensors (2008 - 2012),” *Anal. Chem.*, vol. 85, no. 2, pp. 487–508, 2013.

[4] B. Halliwell, M. V. Clement, and L. H. Long, “Hydrogen peroxide in the human body,” *FEBS Lett.*, vol. 486, pp. 10–13, 2000.

[5] L. H. Long and B. Halliwell, “Antioxidant and Prooxidant Abilities of Foods and Beverages,” in *Methods in Enzymology*, vol. 335, 2001, pp. 181–190.

[6] T. von Woedtke, U. Fischer, and P. Abel, “Glucose oxidase electrodes : effect of hydrogen peroxide on enzyme activity ?,” *Biosens. Bioelectron.*, vol. 9, pp. 65–71, 1994.

[7] W. Chen, S. Cai, Q.-D. Ren, W. Wen, and Y.-D. Zhao, “Recent advances in electrochemical sensing for hydrogen peroxide : a review,” *Analyst*, vol. 137, pp. 49–58, 2012.

[8] N. A. Burmistrova, O. A. Kolontaeva, and A. Duerkop, “New Nanomaterials and Luminescent Optical Sensors for Detection of Hydrogen Peroxide,” *Chemosensors*, vol. 3, pp. 253–273, 2015.

[9] V. R. Holland, B. C. Saunders, F. L. Rose, and A. L. Walpole, “A Safer Substitute For Benzidine Detection of Blood,” *Tetrahedron*, vol. 30, no. 18, pp. 3299–3302, 1974.

[10] P. D. Josephy, T. Eling, and R. P. Mason, “The Horseradish Peroxidase-catalyzed Oxidation of 3,5,3’,5’- Tetramethylbenzidine,” *J. Biol. Chem.*, vol. 257, no. 7, pp. 3669–3675, 1982.

[11] Y. Jv, B. Li, and R. Cao, “Positively-charged gold nanoparticles as peroxidiase mimic and their application in hydrogen peroxide and glucose detection w,” *Chem. Commun.*, vol. 46, pp. 8017–8019, 2010.

[12] Q. Liu, Y. Ding, Y. Yang, L. Zhang, L. Sun, P. Chen, and C. Gao, “Enhanced peroxidase-like activity of porphyrin functionalized ceria nanorods for sensitive and selective colorimetric detection of glucose,” *Mater. Sci. Eng. C*, vol. 59, pp. 445–453, 2016.

[13] G. Wang, X. Xu, X. Wu, G. Cao, Y. Dong, and Z. Li, “Visible-Light-Stimulated Enzymelike Activity of Graphene Oxide and Its Application for Facile Glucose Sensing,” *J. Phys. Chem. C*, vol. 118, pp. 28109–28117, 2014.

[14] E. H. L. Falcao and F. Wudl, “Carbon allotropes : beyond graphite and diamond,” *J. Chem. Technol. Biotechnol.*, vol. 82, pp. 524–531, 2007.

[15] D. R. Dreyer, R. S. Ruoff, and C. W. Bielawski, “From conception to realization: An historial account of graphene and some perspectives for its future,” *Angew. Chemie - Int. Ed.*, vol. 49, pp. 9336–9345, 2010.

[16] H.-P. Boehm, R. Setton, and E. Stumpp, “Nomenclature and Terminology of Graphite Intercalation Compounds,” *Pure Appl. Chem.*, vol. 66, no. 9, pp. 1893–1901, 1994.

[17] K. S. Novoselov, A. K. Geim, S. V Morozov, D. Jiang, Y. Zhang, S. V Dubonos, I. V Grigorieva, and A. A. Firsov, “Electric Field Effect in Atomically Thin Carbon Films,” *Science (80-.).*, vol. 306, pp. 666–669, 2004.

[18] C. Chung, Y.-K. Kim, D. Shin, S.-R. Ryoo, B. H. Hong, and D.-H. Min, “Biomedical Applications of Graphene and Graphene Oxide,” *Acc. Chem. Res.*, vol. 46, no. 10, pp. 2211–2224, 2013.

[19] V. Singh, D. Joung, L. Zhai, S. Das, S. I. Khondaker, and S. Seal, “Graphene based materials: Past, present and future,” *Prog. Mater. Sci.*, vol. 56, pp. 1178–1271, 2011.

[20] F. Bonaccorso, Z. Sun, T. Hasan, and A. C. Ferrari, “Graphene photonics and optoelectronics,” *Nat. Photonics*, vol. 4, pp. 611–622, 2010.

[21] P. T. Yin, T.-H. Kim, J.-W. Choi, and K.-B. Lee, “Prospects for graphene–nanoparticle-based hybrid sensors,” *Phys. Chem. Chem. Phys.*, vol. 15, no. 31, p. 12785, 2013.

[22] N. Zhang, M. Yang, S. Liu, Y. Sun, and Y. Xu, “Waltzing with the Versatile Platform of Graphene to Synthesize Composite Photocatalysts,” *Chem. Rev.*, vol. 115, p. 10307−10377, 2015.

[23] I. V. Lightcap and P. V. Kamat, “Graphitic Design: Prospects of Graphene-Based Nanocomposites for Solar Energy Conversion, Storage, and Sensing,” *Acc. Chem. Res.*, vol. 46, no. 10, pp. 2235–2243, 2013.

[24] K. Watanabe, D. Menzel, N. Nilius, and H.-J. Freund, “Photochemistry on Metal Nanoparticles,” *Chem. Rev.*, vol. 106, pp. 4301–4320, 2006.

[25] A. Jimenez-Ruiz, P. Perez-Tejeda, E. Grueso, P. M. Castillo, and R. Prado-Gotor, “Nonfunctionalized Gold Nanoparticles : Synthetic Routes and Synthesis Condition Dependence,” *Chem. - A Eur. J.*, vol. 21, pp. 9596–9609, 2015.

[26] L. Polavarapu and L. M. Liz-Marzán, “Towards low-cost flexible substrates for nanoplasmonic sensing,” *Phys. Chem. Chem. Phys.*, vol. 15, pp. 5288–5300, 2013.

[27] K. A. Willets and R. P. Van Duyne, “Localized Surface Plasmon Resonance Spectroscopy and Sensing,” *Annu. Rev. Phys. Chem.*, vol. 58, pp. 267–297, 2007.

[28] L. M. Liz-Marzán, “Tailoring Surface Plasmons through the Morphology and Assembly of Metal Nanoparticles,” *Langmuir*, no. 22, pp. 32–41, 2006.

[29] A. R. Tao, S. Habas, and P. Yang, “Shape Control of Colloidal Metal Nanocrystals,” *Small*, vol. 4, no. 3, pp. 310–325, 2008.

[30] K. Aslan, J. R. Lakowicz, and C. D. Geddes, “Plasmon light scattering in biology and medicine : new sensing approaches , visions and perspectives,” *Curr. Opin. Chem. Biol.*, vol. 9, pp. 538–544, 2005.

[31] J. Zhang, Y. Fu, M. H. Chowdhury, and J. R. Lakowicz, “Single-Molecule Studies on Fluorescently Labeled Silver Particles: Effects of Particle Size,” *J. Phys. Chem. C*, vol. 112, no. 1, pp. 18–26, 2008.

[32] K. Ray, R. Badugu, and J. R. Lakowicz, “Polyelectrolyte Layer-by-Layer Assembly To Control the Distance between Fluorophores and Plasmonic Nanostructures,” *Chem. Mater.*, vol. 19, pp. 5902–5909, 2007.

[33] L. A. Austin, B. Kang, C.-W. Yen, and M. A. El-Sayed, “Plasmonic Imaging of Human Oral Cancer Cell Communities During Programmed Cell Death by Nuclear Targeting Silver Nanoparticles,” *J. Am. Chem. Soc.*, vol. 133, no. 44, pp. 17594–17597, 2011.

[34] U. E. Steiner, “Fundamentals of Photophysics , Photochemistry , and Photobiology,” in *Photodynamic Therapy: From Theory to Application*, 2014, pp. 22–58.

[35] K.-H. Nguyen, M. Chollet-Krugler, N. Gouault, and S. Tomasi, “UV-protectant metabolites from lichens and their symbiotic partners,” *Nat. Prod. Rep.*, vol. 30, pp. 1490–1508, 2013.

[36] J. A. S. Cavaleiro and K. M. Smith, “Porphyrin synthesis,” *Rev. Port. Química*, vol. 31, no. 29, pp. 29–41, 1989.

[37] R. Giovannetti, “The Use of Spectrophotometry UV-Vis for the Study of Porphyrins,” in *Macro To Nano Spectroscopy*, 2012, pp. 87–108.

[38] L. B. Josefsen and R. W. Boyle, “Photodynamic Therapy and the Development of Metal-Based Photosensitisers,” *Met. Based. Drugs*, vol. 2008, pp. 1–24, 2008.

[39] S. M. Andrade and S. M. B. Costa, “Spectroscopic Studies on the Interaction of a Water Soluble Porphyrin and Two Drug Carrier Proteins,” *Biophys. J.*, vol. 82, no. March, pp. 1607–1619, 2002.

[40] P. Kubát, K. Lang, K. Procházková, and P. Anzenbacher Jr, “Self-Aggregates of Cationic meso -Tetratolylporphyrins in Aqueous Solutions,” *Langmuir*, vol. 19, pp. 422–428, 2003.

[41] N. C. Maiti, S. Mazumdar, and N. Periasamy, “J- and H-Aggregates of Porphyrin - Surfactant Complexes : Time-Resolved Fluorescence and Other Spectroscopic Studies †,” *J. Phys. Chem. B*, vol. 5647, no. 97, pp. 1528–1538, 1998.

[42] F. Würthner, T. E. Kaiser, and C. R. Saha-Möller, “J-Aggregates : From Serendipitous Discovery to Supra- molecular Engineering of Functional Dye Materials Angewandte,” *Angew. Chemie - Int. Ed.*, vol. 50, pp. 3376–3410, 2011.

[43] A. D’Urso, M. E. Fragalà, and R. Purrello, “From self-assembly to noncovalent synthesis of programmable porphyrins’ arrays in aqueous solution,” *Chem. Commun.*, vol. 48, pp. 8165–8176, 2012.

[44] R. Rai, V. Kumar, and S. Pandey, “Aggregation of a model porphyrin within poly(ethylene glycol) (PEG): effect of water,PEG molecular weight, ionic liquids, salts, and temperature,” *Phys. Chem. Chem. Phys.*, vol. 16, pp. 7263–7273, 2014.

[45] S. M. Andrade, P. Raja, V. K. Saini, A. S. Viana, P. Serp, and S. M. B. Costa, “Polyelectrolyte-Assisted Noncovalent Functionalization of Carbon Nanotubes with Ordered Self-Assemblies of a Water-Soluble Porphyrin,” *ChemPhysChem*, vol. 13, no. 16, pp. 3622–3631, 2012.

[46] J. E. Van Lier and J. D. Spikes, “The Chemistry, Photophysics and Photosensitizing Properties of Phthalocyanines,” in *Photosensitizing Compounds: Their Chemistry, Biology and Clinical Use*, 2007, pp. 17–39.

[47] H. Yaku, T. Fujimoto, T. Murashima, D. Miyoshi, and N. Sugimoto, “Phthalocyanines: a new class of G-quadruplex-ligands with many potential applications,” *Chem. Commun.*, vol. 48, pp. 6203–6216, 2012.

[48] W. S. Hummers Jr. and R. E. Offeman, “Preparation of Graphitic Oxide,” *J. Am. Chem. Soc.*, vol. 80, no. 6, pp. 1339–1339, 1958.

[49] J. Turkevich, P. C. Stevenson, and J. Hillier, “A study of the nucleation and growth processes in the synthesis of colloidal gold,” *Discuss. Faraday Soc.*, vol. 11, pp. 55–75, 1951.

[50] “Introduction to Raman Spectroscopy.” [Online]. Available: http://bwtek.com/raman-introduction-to-raman-spectroscopy/. [Accessed: 31-Oct-2016].

[51] P. K. Jain, K. S. Lee, I. H. El-Sayed, and M. A. El-Sayed, “Calculated Absorption and Scattering Properties of Gold Nanoparticles of Different Size, Shape, and Composition: Applications in Biological Imaging and Biomedicine,” *J. Phys. Chem. B*, vol. 110, no. 14, pp. 7238–7248, 2006.

[52] X. Liu, M. Atwater, J. Wang, and Q. Huo, “Extinction coefficient of gold nanoparticles with different sizes and different capping ligands,” *Colloids Surfaces B Biointerfaces*, vol. 58, no. 1, pp. 3–7, 2007.

[53] K. N. Kudin, B. Ozbas, H. C. Schniepp, R. K. Prud, I. A. Aksay, and R. Car, “Raman Spectra of Graphite Oxide and Functionalized Graphene Sheets,” *Nano Lett.*, vol. 8, no. 1, pp. 36–41, 2008.

[54] P. M. R. Paulo and S. M. B. Costa, “Non-covalent dendrimer-porphyrin interactions : the intermediacy of H-aggregates?,” *Photochem. Photobiol. Sci.*, vol. 2, pp. 597–604, 2003.

[55] S. M. Andrade and S. M. B. Costa, “Aggregation Kinetics of Meso -tetrakis (4-sulfonatophenyl) Porphine in the Presence of Proteins : Temperature and Ionic Strength Effects,” *J. Fluoresc.*, vol. 12, no. 1, pp. 77–82, 2002.

[56] R. F. Pasternack, C. Fleming, S. Herring, P. J. Collings, G. Decastro, and E. J. Gibbs, “Aggregation Kinetics of Extended Porphyrin and Cyanine Dye Assemblies,” *Biophys. J.*, vol. 79, no. 1, pp. 550–560, 2000.

[57] C. A. T. Laia and S. M. B. Costa, “Interactions of a Sulfonated Aluminum Phthalocyanine and Cytochrome c in Micellar Systems : Binding and Electron-Transfer Kinetics,” *J. Phys. Chem. B*, vol. 108, pp. 17188–17197, 2004.

[58] R. F. Correia, S. M. Andrade, and M. I. Viseu, “Journal of Photochemistry and Photobiology A : Chemistry Aggregation and disaggregation of anionic aluminum phthalocyanines in cationic pre-micelle and micelle media : A fluorescence study,” *J. Photochem. Photobiol. A Chem.*, vol. 235, pp. 21–28, 2012.

[59] S. M. Andrade, C. J. Bueno-Alejo, V. V Serra, J. M. M. Rodrigues, M. G. P. M. S. Neves, A. S. Viana, and S. M. B. Costa, “Anchoring of Gold Nanoparticles on Graphene Oxide and Noncovalent Interactions with Porphyrinoids,” *ChemNanoMat*, vol. 1, pp. 502–510, 2015.

[60] P. Pang, Y. Zhang, S. Ge, Q. Cai, S. Yao, and C. A. Grimes, “Determination of glucose using bienzyme layered assembly magnetoelastic sensing device,” *Sensors Actuators B Chem.*, vol. 136, pp. 310–314, 2009.

[61] B. Y. Song, K. Qu, C. Zhao, J. Ren, and X. Qu, “Graphene Oxide : Intrinsic Peroxidase Catalytic Activity and Its Application to Glucose Detection,” *Adv. Mater.*, vol. 22, pp. 2206–2210, 2010.

[62] Q. Liu, H. Li, Q. Zhao, R. Zhu, Y. Yang, Q. Jia, B. Bian, and L. Zhuo, “Glucose-sensitive colorimetric sensor based on peroxidase mimics activity of porphyrin-Fe3O4 nanocomposites,” *Mater. Sci. Eng. C*, vol. 41, pp. 142–151, 2014.

Annex

- **Annex 1 - Lifetime analysis tables**

Table A1-1 – Lifetime analysis results for TSPP system with chitosan (pH 3.5) – λ_{exc}=445 nm; λ_{emi}=645 nm

[Chi] (mg/mL)	*A1*	*A2*	*A3*	*τ1/ns*	*τ2/ns*	*τ3/ns*	*f1*	*f2*	*f3*	*χ2*
0	1.00	------	------	3.84	------	------	1.00	------	------	1.10
0.2	0.30	0.51	0.20	3.90	0.33	11.42	0.32	0.05	0.63	1.17
0.4	0.26	0.64	0.10	3.70	0.16	11.01	0.44	0.05	0.51	1.10
0.6	0.20	0.75	0.05	3.71	0.10	11.05	0.55	0.06	0.40	1.04
0.8	0.63	0.26	0.10	3.87	0.67	11.29	0.64	0.05	0.31	1.01
1	0.46	0.48	0.05	3.72	0.23	11.24	0.71	0.05	0.25	0.99

Table A1-2 – Lifetime analysis results for TSPP system with chitosan (pH 6.5) – λ_{exc}=445 nm; λ_{emi}=645 nm

[Chi] (mg/mL)	*A1*	*A2*	*τ1/ns*	*τ2/ns*	*f1*	*f2*	*χ2*
0	1.00	------	9.93	------	1.00	0.00	1.30
0.2	0.26	0.74	5.41	11.59	0.14	0.86	1.11
0.4	0.23	0.77	5.99	11.92	0.13	0.87	1.04
0.6	0.23	0.77	5.78	11.97	0.12	0.88	1.08
0.8	0.17	0.83	5.38	12.07	0.08	0.92	1.10
1	0.17	0.83	5.08	12.09	0.08	0.92	1.17

Table A1-3 - Lifetime analysis results for TSPP system with chitosan and GO (pH 3.5) – λ_{exc}=445 nm; λ_{emi}=650 nm

[GO] (mg/mL)	*A1*	*A2*	*τ1/ns*	*τ2/ns*	*f1*	*f2*	*χ2*
0	0.74	0.26	4.00	1.99	0.85	0.15	1.31
0.005	0.15	0.85	5.38	3.32	0.22	0.78	1.04
0.0075	0.06	0.94	6.49	3.44	0.10	0.90	1.07
0.01	0.66	0.34	4.11	2.21	0.78	0.22	1.11
0.025	0.61	0.39	3.97	1.26	0.83	0.17	1.20
0.05	0.39	0.61	4.21	1.20	0.69	0.31	1.27

Table A1-4 - Lifetime analysis results for TSPP system with chitosan and AuNP (pH 3.5) – λ_{exc}=445 nm; λ_{emi}=650 nm

[AuNP] (pM)	*A1*	*A2*	*A3*	*τ1/ns*	*τ2/ns*	*τ3/ns*	*f1*	*f2*	*f3*	*χ2*
0	0.02	0.24	0.74	11.02	3.62	0.11	0.22	0.72	0.07	1.13
30	0.02	0.22	0.77	10.43	3.59	0.09	0.16	0.77	0.07	1.03
60	0.03	0.64	0.34	10.86	3.67	0.38	0.12	0.84	0.05	1.01
90	0.01	0.30	0.69	10.53	3.61	0.13	0.11	0.82	0.07	1.06
120	0.02	0.73	0.25	11.51	3.74	0.56	0.07	0.88	0.05	1.02
150	0.02	0.66	0.32	10.83	3.69	0.40	0.08	0.88	0.05	1.01

Table A1-5 - Lifetime analysis results for TSPP system with chitosan and AuNP (pH 6.5) – λ_{exc}=445 nm; λ_{emi}=650 nm

[AuNP] (pM)	*A1*	*A2*	*A3*	*τ1/ns*	*τ2/ns*	*τ3/ns*	*f1*	*f2*	*f3*	*χ2*
0	0.77	0.23	---	11.92	5.99	----	0.87	0.13	----	1.04
15	0.12	0.29	0.59	10.85	3.68	0.37	0.49	0.42	0.09	1.15
30	0.09	0.16	0.75	10.68	2.70	0.29	0.58	0.28	0.14	1.21
45	0.18	0.20	0.62	10.04	4.18	0.25	0.65	0.30	0.06	1.23
60	0.63	0.37	------	10.92	4.57	-----	0.80	0.20	0.00	1.12
75	0.63	0.37	------	10.76	4.48	------	0.80	0.20	0.00	1.17

Table A1-6 - Lifetime analysis results for TSPP system with chitosan, GO and AuNP (pH 3.5) – λ_{exc}=445 nm; λ_{emi}=650 nm

[AuNP] (pM)	*A1*	*A2*	*A3*	*τ1/ns*	*τ2/ns*	*τ3/ns*	*f1*	*f2*	*f3*	*χ2*
0	0.02	0.14	0.85	10.67	3.41	0.80	0.14	0.35	0.51	1.21
30	0.01	0.26	0.74	10.42	3.53	0.93	0.04	0.55	0.42	1.19
60	0.03	0.09	0.88	4.22	1.28	0.15	0.33	0.30	0.36	1.30
90	0.02	0.06	0.92	4.09	1.17	0.09	0.35	0.28	0.37	1.26
120	0.03	0.07	0.90	3.97	1.14	0.12	0.38	0.28	0.35	1.24
150	0.02	0.06	0.92	4.04	1.18	0.10	0.34	0.28	0.38	1.18

Table A1-7 - Lifetime analysis results for TSPP system with PEI (pH 3.3) – λ_{exc}=445 nm; λ_{emi}=665 nm

[PEI]	*A1*	*A2*	*A3*	*τ1/ns*	*τ2/ns*	*τ3/ns*	*f1*	*f2*	*f3*	*χ2*
0 μM	1	------	------	3.89	------	------	1.00	-------	------	1.04
8 μM	0.39	0.61	------	7.72	11.42	------	0.30	0.70	------	1.32
31 μM	0.07	0.18	0.75	6.18	10.88	0.11	0.16	0.81	0.03	1.14
54 μM	0.04	0.09	0.86	4.08	10.57	0.06	0.14	0.82	0.05	1.16
77 μM	0.32	0.23	0.45	3.21	10.61	0.29	0.29	0.67	0.04	1.04
100 μM	0.43	0.11	0.46	2.85	10.49	0.25	0.49	0.46	0.05	1.09

Table A1-8 - Lifetime analysis results for TSPP system with PEI (pH 6.4) – λ_{exc}=445 nm; λ_{emi}=660 nm

[PEI]	*A1*	*A2*	*τ1/ns*	*τ2/ns*	*f1*	*f2*	*χ2*
0 μM	0.34	0.66	3.09	10.13	0.14	0.86	1.21
8 μM	0.41	0.59	4.49	9.96	0.24	0.76	1.22
31 μM	0.49	0.51	4.26	9.65	0.30	0.70	1.09
54 μM	0.54	0.46	3.97	9.08	0.34	0.66	1.16
77 μM	0.58	0.42	3.89	8.84	0.38	0.62	1.22
100 μM	0.60	0.40	3.93	8.63	0.41	0.59	1.21

Table A1-9 - Lifetime analysis results for TSPP system with PEI and GO (pH 6.5) – λ_{exc}=445 nm; λ_{emi}=660 nm

[GO] (mg/mL)	*A1*	*A2*	*A3*	*τ1/ns*	*τ2/ns*	*τ3/ns*	*f1*	*f2*	*f3*	*χ2*
0	0.34	0.66	------	3.09	10.13	------	0.14	0.86	------	1.21
0.005	0.47	0.27	0.26	4.80	9.37	1.52	0.44	0.49	0.08	1.20
0.0075	0.48	0.17	0.35	6.03	10.23	2.26	0.54	0.32	0.14	1.08
0.01	0.45	0.25	0.30	5.27	9.59	1.90	0.45	0.44	0.11	1.19
0.025	0.17	0.13	0.70	3.56	8.66	0.16	0.33	0.61	0.06	1.17
0.05	0.09	0.07	0.84	3.28	8.48	0.09	0.30	0.62	0.08	1.17

Table A1-10 - Lifetime analysis results for TSPP system with PEI and AuNP (pH 3.5) – λ_{exc}=445 nm; λ_{emi}=665 nm

[AuNP] (pM)	*A1*	*A2*	*A3*	*τ1/ns*	*τ2/ns*	*τ3/ns*	*f1*	*f2*	*f3*	*χ2*
0	0.38	0.62	------	10.08	2.97	------	0.67	0.33	------	1.17
30	0.16	0.34	0.49	10.20	2.94	0.28	0.59	0.36	0.05	1.13
60	0.16	0.50	0.34	9.94	2.86	0.44	0.50	0.45	0.05	1.07
90	0.25	0.75	------	8.01	2.27	------	0.54	0.46	------	1.17
120	0.11	0.59	0.30	10.19	2.93	0.65	0.37	0.56	0.06	1.18

Table A1-11 - Lifetime analysis results for TSPP system with PEI and AuNP (pH 6.5) – λ_{exc}=445 nm; λ_{emi}=660 nm

[AuNP] (pM)	*A1*	*A2*	*A3*	*τ1/ns*	*τ2/ns*	*τ3/ns*	*f1*	*f2*	*f3*	*χ2*
0	0.34	0.66	------	7.69	3.69	------	0.52	0.48	------	1.27
15	0.37	0.63	------	7.43	3.36	------	0.56	0.44	------	1.15
30	0.38	0.62	------	7.20	3.24	------	0.58	0.42	------	1.17
45	0.37	0.63	------	7.47	3.43	------	0.56	0.44	------	1.24
60	0.58	0.36	0.06	5.86	2.34	11.06	0.69	0.17	0.13	1.16
75	0.38	0.62	------	7.41	3.37	------	0.57	0.43	------	1.27

Table A1-12 - Lifetime analysis results for TSPP system with PEI, GO and AuNP (pH 3.5) – λ_{exc}=445 nm; λ_{emi}=665 nm

[AuNP] (pM)	*A1*	*A2*	*A3*	*τ1/ns*	*τ2/ns*	*τ3/ns*	*f1*	*f2*	*f3*	*χ2*
0	0.02	0.43	0.55	9.99	2.82	0.88	0.11	0.63	0.25	1.18
30	0.01	0.19	0.80	7.49	2.42	0.37	0.09	0.55	0.36	1.29
60	0.01	0.22	0.77	8.80	2.59	0.44	0.07	0.59	0.34	1.32
90	0.01	0.24	0.75	8.40	2.58	0.45	0.07	0.60	0.33	1.20
120	0.01	0.22	0.77	7.78	2.50	0.42	0.08	0.59	0.34	1.28
150	0.01	0.41	0.58	9.70	2.91	0.92	0.05	0.66	0.29	1.28

Table A1-13 - Lifetime analysis results for TSPP system with PEI, GO and AuNP (pH 6.5) – λ_{exc}=445 nm; λ_{emi}=660 nm

[AuNP] (pM)	*A1*	*A2*	*A3*	*τ1/ns*	*τ2/ns*	*τ3/ns*	*f1*	*f2*	*f3*	*χ2*
0	0.11	0.21	0.68	8.54	3.88	0.24	0.48	0.44	0.09	1.11
30	0.12	0.21	0.67	8.24	3.60	0.22	0.52	0.40	0.08	1.25
60	0.05	0.09	0.86	8.31	3.53	0.10	0.50	0.39	0.10	1.29
90	0.04	0.07	0.89	8.09	3.34	0.08	0.54	0.36	0.11	1.17
120	0.06	0.09	0.86	8.03	3.31	0.09	0.56	0.35	0.10	1.22
150	0.03	0.06	0.91	8.19	3.29	0.07	0.53	0.35	0.12	1.17

Table A1-14 - Lifetime analysis results for AlPcS4 system with Chitosan and AuNP– λ_{exc}=594 nm; λ_{emi}=685 nm

[AuNP] (pM)	*A1*	*A2*	*A3*	*τ1/ns*	*τ2/ns*	*τ3/ns*	*f1*	*f2*	*f3*	*χ2*
0	1.00	------	------	5.19	------	------	1.00	------	------	1.29
30	1.00	------	------	5.13	------	------	1.00	------	------	1.22
60	0.70	------	0.30	4.91	------	0.41	0.96	------	0.04	1.13
90	0.67	------	0.33	4.86	------	0.32	0.97	------	0.03	1.11
120	0.82	0.18	------	5.19	2.64	------	0.90	0.10	------	1.05
150	0.77	0.23	------	5.16	2.51	------	0.87	0.13	------	1.15

Table A1-15 - Lifetime analysis results for AlPcS4 system with Chitosan, GO and AuNP– λ_{exc}=594 nm; λ_{emi}=685 nm

[AuNP] (pM)	*A1*	*A2*	*A3*	*τ1*	*τ2*	*τ3*	*f1*	*f2*	*f3*	*χ2*
0	0.51	0.14	0.70	5.48	4.19	0.23	0.82	0.17	0.04	1.05
30	0.19	0.30	0.51	5.73	4.37	0.40	0.42	0.50	0.08	1.05
60	0.12	0.37	0.51	6.07	4.48	0.52	0.28	0.63	0.10	1.12
90	0.03	0.49	0.48	7.68	4.65	0.55	0.08	0.82	0.10	1.00
120	0.04	0.59	0.37	7.75	4.76	0.57	0.10	0.84	0.06	1.08

Table A1-16 - Lifetime analysis results for AlPcS4 system with PEI– λ_{exc}=594 nm; λ_{emi}=685 nm

[PEI] (μM)	*A1*	*A2*	*A3*	*τ1*	*τ2*	*τ3*	*f1*	*f2*	*f3*	*χ2*
0	1.00	------	------	5.13	------	------	1.00	------	------	1.34
8	0.11	0.27	0.61	3.44	1.86	0.38	0.35	0.44	0.21	1.19
31	0.04	0.39	0.57	4.63	2.42	0.59	0.13	0.64	0.23	1.17
54	0.06	0.39	0.55	4.30	2.30	0.58	0.18	0.60	0.22	1.05
77	0.23	0.30	0.48	3.23	1.59	0.43	0.52	0.34	0.14	1.10
100	0.14	0.36	0.49	3.75	2.06	0.57	0.34	0.48	0.18	1.19

Table A1-17 - Lifetime analysis results for AlPcS4 system with PEI, AuNP and GO– λ_{exc}=594 nm; λ_{emi}=685 nm

[AuNP] (pM)	*A1*	*A2*	*A3*	*τ1/ns*	*τ2/ns*	*τ3/ns*	*f1*	*f2*	*f3*	*χ2*
0	0.17	0.38	0.54	4.54	2.52	0.65	0.45	0.46	0.17	1.17
30	0.03	0.41	0.56	5.49	2.71	0.66	0.11	0.67	0.22	1.13
60	0.02	0.42	0.56	6.06	2.82	0.74	0.08	0.68	0.24	1.16
90	0.11	0.38	0.51	4.35	2.39	0.69	0.28	0.52	0.20	1.20
120	0.03	0.41	0.56	5.76	2.85	0.75	0.10	0.66	0.24	1.18
150	0.08	0.40	0.52	5.03	2.63	0.70	0.22	0.58	0.20	1.22

- **Annex 2 - Circular Dichroism Spectra**

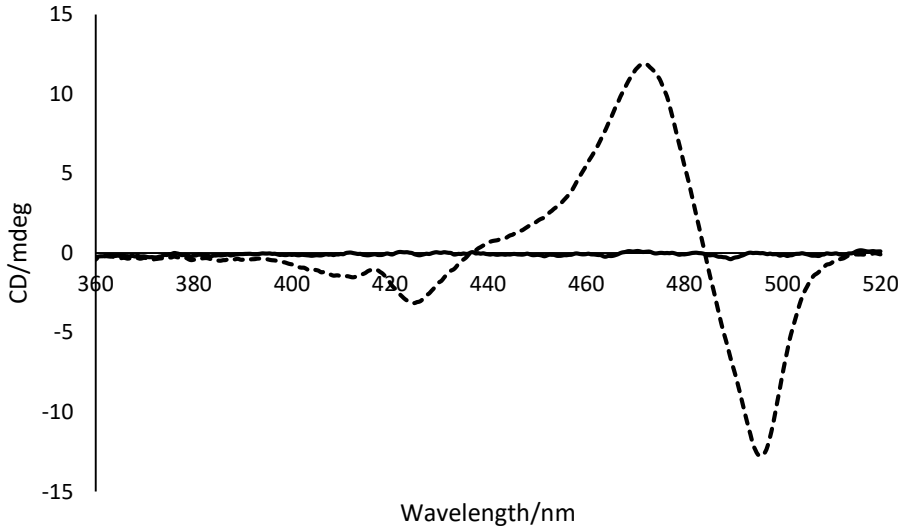

Figure A2-1 – Circular dichroism spectra of TSPP in the absence (full line) and presence of chitosan at which J-aggregates prevail (dotted line)